THEORY AND PRACTICE OF HIGH-ENERGY FEMTOSECOND FIBER LASERS

A Dissertation

Presented to the Faculty of the Graduate School

of Cornell University

in Partial Fulfillment of the Requirements for the Degree of

Doctor of Philosophy

by

Fatih Ömer Ilday

January 2004

THEORY AND PRACTICE OF HIGH-ENERGY FEMTOSECOND FIBER LASERS

Fatih Ömer Ilday, Ph.D.

Cornell University 2004

Ultrafast optics is a rapidly-evolving field encompassing much scientific activity and generating an increasing number of applications. The primary tool of ultrafast optics, solid state lasers producing energetic femtosecond pulses, remain as a complicated, large and expensive equipment.

This thesis presents an experimental and theoretical study of high-energy, femtosecond fiber lasers. The primary emphasis has been the development of practical femtosecond fiber-based sources with performance similar to that of bulk solid state lasers. Since the limitations to performance limitations to pulse energy originate in the strongly-nonlinear nature of the pulse generation dynamics, a thorough understanding of these dynamics has been indispensable. Novel schemes for pulse generation in the presence of strong nonlinearity have been explored.

The concept of nonlinearity management has been suggested as a route to two orders of magnitude improvement in the pulse energy of soliton fiber lasers by introducing an optical medium with (effective) negative cubic nonlinearity. A fiber source based on a medium-energy fiber laser seeding an integrated fiber amplifier has been demonstrated to be an energy-scalable approach for the generation of high-energy pulses. The concept of self-similar pulse evolution within the optical cavity has theoretically been suggested and experimentally demonstrated to avoid

the break-up of pulses due to excessive nonlinearity. With this method, unprecendented pulse energies can in principle be obtained, approaching 1 μJ. As a first step in this direction, a Yb-doped fiber laser has generated 50-fs, 5-nJ pulses, corresponding to the highest peak power obtained from a fiber laser. The pulse energy is currently limited by the saturable absorber mechanism. Finally, an investigation of high-energy pulse dynamics in the presence of a failing saturable absorber has been conducted.

BIOGRAPHICAL SKETCH

Ömer was born in Istanbul in 1976, and by the fifth grade, his nickname had been switched to *fizikçi* (the physicist) from *ressam* (the painter). His interest in physics and mathematics led him to the Physics Department at Boğaziçi University in Istanbul, Turkey (the poetic beauty of its Güney campus did not have any share in his decision) where he obtained a B.S. in theoretical physics in 1998. During his undergraduate studies (conducted in the ugliest building on campus), he was a junior member of the experimental high-energy physics group and he worked on cosmology and a mathematical treatment of musical consonance. The lure of the New World pulled and placed him in Ithaca. At Cornell University, where the physics building is not any better looking, his interest in nonlinear phenomena in complex systems resonated with a new-found appreciation of applied science and nonlinear optics, placing him in the Wise group. After four wonderful years, he is almost unhappy to be leaving. Having realized that femtosecond pulses are not that short after all, he is going to MIT to generate attosecond pulses.

In grateful dedication to my parents, Mübeccel & Doğan.

ACKNOWLEDGEMENTS

First and foremost, I would like to thank Frank Wise, my thesis advisor, for being an excellent advisor and a friend. I hope to have learned from his non-technical skills as well, in particular his communication and management skills. I thank him for listening to my passionate "core-dumps" late in the evenings. I thank his wife, Judy, for enduring the numerous delays I must have caused. Finally, I thank Frank Wise for recognizing that the flow of creative thought is whimsical.

I thank my committee members, Alexander Gaeta and Sandip Tiwari for their guidance and for accepting to serve on my committee.

I thank to all past and present members of the Wise research group that I have overlapped with for their company. To name only a few: It was a pleasure to interact with Kale Beckwitt. Joel Buckley has been a great co-worker and some of the work presented here would not have been completed without him. I thank Lyuba Kuznetsova for being a true professional and a hard-working co-worker. Yi-Fan's probing questions have been pleasurable additions to the daily life in the lab.

I am grateful to the fine people at Clark-MXR, Inc. who have been my collaborators. Bill Clark has not only been an additional motivator for much of this work, but I owe him my still-developing appreciation of industrial research, and the many steps from basic research to the development of a commercial product. Larry Walker has always found the time to respond to equipment crisis and I enjoyed our brain-storming sessions. I have learned about building fiber oscillators from Tom Sosnowski. I thank Philippe Bado, Edesly Canto-Said, Mark Dugan, and Mike Moosley for useful discussions and the invaluable logistical support they provided.

I would like to thank Boris Malomed with whom I have enjoyed several days close-packed with discussions of many aspects of our work.

I would like to acknowledge Valerio Carruba, Aycan Yurtsever, and Deniz Sezer, several of my friends for their company outside the research environment.

The primary support for this work was provided by the National Institutes of Health, with additional funding by Clark-MXR, Inc., and the National Science Foundation. I am grateful for their support without which this work would not have been possible.

TABLE OF CONTENTS

LIST OF FIGURES

Chapter 1

Introduction

Ultrafast optics is a rapidly growing field. Not only the scientific interest in ultrafast optical phenomena is increasing but ultrafast optics is proving to be an important tool for many branches of science. In addition many industrial and medical applications have been demonstrated and their importance can only be expected to rise.

Ultrafast pulse lasers producing intense femtosecond pulses are the main tools of ultrafast optics and as such, they have diverse applications, including time-resolved studies in chemistry, novel imaging techniques in medicine, and optical communications. Thus, the Frontier of ultrafast optics technology is multi-faceted: Current research efforts span a wide spectrum, from generating pulses shorter than two optical cycles, to powerful lasers racing beyond the 100 W limit, and toward extreme control on the pulses with carrier-envelope phase-stabilization. Another facet of the Frontier is the effort to make femtosecond lasers more befitting to wide-spread use. It is this facet of the Frontier to which this thesis strives to contribute.

To date, the dominant platform for femtosecond pulse generation has been the bulk solid state laser technology. These systems, most notably Ti:sapphire lasers, provide the highest peak powers and the shortest pulse, while their reliability has increased considerably within the last decade. However, despite tremendous commercially-motivated effort, these systems are still prohibitively complicated, expensive and unreliable for many applications outside of the research laboratory. Sources that are significantly more compact, more robust, and inexpensive can have

a major impact on the proliferation of ultrafast optics applications. Fiber lasers are very promising in this regard since they can be constructed of inexpensive components with highly-integrated and miniaturized cavities. Fiber lasers have one major drawback: The effective coefficient of nonlinearity for a fiber laser is 10,000 times greater than that of a bulk solid state laser.

This thesis reports theoretical and experimental studies conducted for the goal of developing practical, high-performance, passively mode-locked, fiber-based sources of femtosecond pulses in the near-infrared region. We have striven to improve the performance of fiber lasers to the level of bulk solid state laser technology without trading-off their practical advantages.

Fiber lasers have major inherent advantages: Rare-earth doped fibers can provide up to 40 dB small signal gain, have high saturation energies due to long gain relaxation times (in the ms range) which translates to a high tolerance for linear loss, diode laser pumping *via* fiber which is reliable, efficient and free of misalignment. Finally fiber itself is an excellent guiding medium that can be bent, and stored compactly. Furthermore, the large surface area to volume ratio makes fiber lasers virtually immune to thermal problems. Thus, fiber lasers already offer superior practical features due to these properties. In addition, many of the components are inexpensive since they are produced in large quantities for the optical-fiber communications market. However, it has been a challenge to obtain performance comparable to that of bulk solid-state lasers in terms of the pulse energy and duration. Fiber lasers, prior to the studies reported in this thesis, did not compare favorably to a standard laser based on the bulk solid state technology: The pulse energy was ~ 5 times lower and pulse durations were ~ 2 longer than that of a standard commercial Ti:sapphire laser, corresponding to an order

of magnitude lower peak power. As will be discussed in length in this thesis, all major limitations of fiber lasers can be traced to the strongly-nonlinear nature of the process of pulse generation.

In recognition of the fact that nonlinearity is the main limitation to improving the performance of fiber lasers rather than technological limitations (loss, pump power, *etc.*), this thesis study strives to achieve maximal understanding of the dynamics of short pulse generation in fiber lasers and the use of such knowledge for controlling and/or suppressing the various nonlinear phenomena that dominates an energetic, femtosecond fiber laser. In this thesis, the term "fiber oscillator" is used to denote a laser consisting of a cavity formed predominantly by optical fiber. The term "fiber laser" serves a more general purpose, used to describe a fiber oscillator seeding a fiber amplifier in a highly-integrated geometry, as well as a stand-alone fiber oscillator.

Here, we describe three approaches to generating high-peak power pulses from fiber lasers: the use of *negative* nonlinearities for controlling nonlinearity (nonlinearity management), the development of high-energy fiber oscillators through self-similar pulse shaping, and the development of fiber lasers consisting of a moderate-energy fiber oscillator seeding a powerful fiber amplifier. Studies have been conducted at two commonly-used wavelengths of operation, 1.55 μm and 1.0 μm, using on Er-doped and Yb-doped fibers as the gain medium, respectively. Nd-doped fibers, although promising, have been excluded from this study due to unavailability of high-power single-mode diode lasers for pumping during the time period of this study. The operational wavelength of the Er-doped fiber is interesting because fibers with both anomalous and normal dispersion are available. Furthermore, 1.55 μm corresponds to the primary telecommunications window.

Therefore, the cost and the availability of optical components is highly-favorable in comparison to 1.0 μm. On the other hand, Yb-doped fibers have superior performance and the fact that standard fiber has normal dispersion has advantages from concerning the pulse dynamics. It is the Yb fiber lasers that this thesis is primarily concerned with.

The evolution of femtosecond pulses in the presence of temporal dispersion and nonlinear response of the medium, coupled with the feedback nature of a laser, results in complicated dynamic behavior. Thus, numerous simulations based on realistic models of the pulse generation were performed, assisted by simple analytical models wherever possible. Thanks to the ease of constructing and experimenting on fiber lasers, it was possible to construct and conclude experiments in a matter of days in some instances. A short turn-around time for experiments made it possible to iterate between theory and experiment. On the other hand, the feedback nature of the lasers and the short time scale over which changes occur makes it difficult to perform controlled experiments and to characterize the experimental system fully.

1.1 Organization of the Thesis

The rest of the thesis is organized as follows. Section 1.2 provides a brief introduction to short-pulse propagation. Section 1.3 summarizes various theoretical approaches to pulse formation in lasers and is intended to serve a guide to the existing literature. Section 1.4 briefly summarizes the development fiber lasers and describes their main limitations. Section 1.5 builds on the previous sections to develop a categorization of different pulse shaping mechanisms applicable to femtosecond oscillators.

Chapter 2 describes the concept of nonlinearity management, analogous to dispersion management, for high-energy femtosecond fiber lasers. Application of nonlinearity management to soliton and dispersion-managed fiber oscillators are discussed.

Chapter 3 describes an alternative approach to the generation of high-energy pulses by utilizing a fiber source consisting of a simple, moderate-energy fiber oscillator seeding an all-fiber amplifier. This is an energy-scalable approach and these scaling properties are discussed.

Chapter 4 describes a new mechanism of pulse shaping that is particularly suited to the generation very high energy pulses. The system dynamics are set such that the pulses undergo self-similar evolution as a result of which stable solutions can be scaled up to much higher energies.

Chapter 5 presents the first results utilizing the concepts discussed in Chapter 4 to avoid breaking of the pulse due to nonlinearity. A fiber laser that exceeds the peak power of the previous best fibers laser by ~ 5 is reported. This laser is presently limited in energy due to overdriving the saturable absorber mechanism.

Chapter 6 describes the effect on the pulse dynamics of a non-monotonic saturable absorber. A theoretical model which does not assume small changes per roundtrip is constructed. Period-doubling route to multiple-pulsing is predicted by this model when the SA mechanism is overdriven. Experimental observations confirm this expectation. The implications of this behavior on the understanding of pulse formation in fiber lasers are deep and are discussed in detail.

Finally, we conclude with an overview in Chapter 7. Also contained is a summary of future directions. Appendix A describes the computational aspects of the numerical techniques used in this thesis. Appendix B describes the practice of

constructing high-energy, femtosecond fiber oscillators.

1.2 Propagation of Short Pulses in Optical Media

An equation of motion describing the propagation of short-pulses with a given polarization in an optical medium in the absence of resonant interactions can be derived starting from the wave equation obtainable from Maxwell's equations. Ref. [1] provides an easily-readable summary of the derivation as well as references for the original development. Here, we provide a coarse outline.

In general, the polarizability of any medium is a function of intensity of the electric field. This is the origin of the nonlinear response. The case of temporal pulse can treated by considering a wave packet, in the form of a carrier frequency (corresponding to the central frequency of the wave packet) under a pulse envelope. The treatment is usually simplified by invoking the slowly-varying envelope approximation (SVEA), namely that the envelope varies slowly in comparison to the carrier modulation, which is a good approximations for pulses containing many cycles at the carrier frequency. Transforming to the reference frame of the propagating pulse and making appropriate normalizations, the following equation can be obtained

$$\frac{\partial a(\xi,\tau)}{\partial \xi} + i\frac{\partial \beta\omega}{\partial \omega}a(\xi,\tau) = i\gamma|a(\xi,\tau)|^2 a(\xi,\tau), \tag{1.1}$$

where $a(\xi,\tau)$ is the pulse envelope, $E(\xi,\tau) = u(\xi,\tau)exp(i\omega_c\tau)$ in the reference frame moving with the pulse. $\gamma = \omega_c n_2/(cA_{eff})$ is the coefficient of Kerr nonlinearity, which is typically the dominant nonlinear polarization term. Kerr nonlinearity arises from χ^3, third order susceptibility. A_{eff} is the effective area of spatial confinement, ω_c the carrier frequency, c speed of light in vacuum. $\frac{\partial \beta\omega}{\partial \omega}$ describes the dependence of index of refraction on frequency, and it can be expanded in powers

of ω:

$$\frac{d\beta\omega}{d\omega} = \beta_0 + \beta_1\omega + \frac{1}{2}\beta_2\omega^2 + \frac{1}{6}\omega^3 + ... \tag{1.2}$$

Here, the first term of the expansion is a constant phase shift with no physical consequence. The second term with frequency is the phase velocity and can be absorbed into the definition of the carrier frequency. The third term is referred to as group velocity dispersion (GVD). The fourth term in the expansion is referred to as third order dispersion (TOD). Typically, it is sufficient to consider GVD only but TOD will be seen to play an important role with short pulses within this thesis.

Therefore, keeping only GVD and Kerr nonlinearity, we obtain the (1+1)-dimensional nonlinear Schrödinger equation (NLSE)

$$\frac{\partial a(\xi,\tau)}{\partial \xi} + i\frac{\partial^2}{\partial \tau^2}a(\xi,\tau) = i\gamma|a(\xi,\tau)|^2 a(\xi,\tau). \tag{1.3}$$

NLSE can be integrated using the inverse scattering method and admits soliton solutions [2]. The details will not be discussed here, except within the context of mode-locking theory and the reader is referred to the extensive literature (see, for example Ref. [3, 4, 5]).

When the pulse intensity is very high and the pulse duration corresponds to a few optical cycles, correction terms need to be added to NLSE for an accurate description. These effects include higher order dispersion, Raman-scattering (which causes the pulse spectrum to self-shift to higher wavelengths), and self-steepening (which is a first correction to the SVEA). For a discussion of these effects, see Ref. [1] and references therein. For most of the discussions in this thesis, these higher-order effects will not be significant.

1.3 Mode-locking of Lasers

Mode-locking refers to the phase-locking of the many axial modes of a laser cavity. Passive mode-locking refers to the situation that the dynamics of pulse propagation in the resonant cavity promote the formation of a short pulse from intra-cavity noise without any external agent. This method results in the generation of shortest pulses. All of the studies presented in this thesis utilize passive mode-locking. A nice overview of active and passive mode-locking and its historical development, written by one of its main contributors can be found in Ref. [6].

Passive mode-locking is the establishment of coherence, or phase-locking between the many, initially incoherent modes of the laser cavity. It is an inherently nonlinear phenomena because the phase-locking between the modes is self-promoted as a result of their nonlinear coupling. Thus, passive mode-locking is another example of the broader phenomena of emergence of synchrony in complex nonlinear systems.

Passive mode-locking is much easier to understand if there is a fast saturable absorber. A saturable absorber (SA) imparts nonlinear loss which decreases with increasing intensity. Therefore, in the presence of a saturable absorber, fluctuations in the field distribution inside the cavity (*i.e.*, intra-cavity noise) build up over many roundtrips as the higher intensity results in lower loss. Since the intra-cavity energy is approximately constant, the lowest-loss condition for the laser operation is the formation of a single, short pulse that maximally saturates the absorber. A theory of passive mode-locking with a fast SA has been developed by Haus [7]. This treatment is concerned with pulses that are long enough with intensities low enough for Kerr nonlinearity and dispersive effects can be neglected.

In the case of ultrafast lasers, the shortening of the pulse continues unabated

until the pulse intensity becomes so large that Kerr nonlinearity becomes an important factor and the pulse bandwidth increases to the point that dispersive effects and gain bandwidth start to play a major role. The analytic theory of passive mode-locking with soliton-like pulse shaping and a fast SA has been described in Ref. [8], which is a generalization of Ref. [7].

The solution to the master equation of Ref. [8] is of the form of a hyperbolic secant with a linear frequency chirp

$$u = u_0 sech^{1+\beta\tau/\tau_0}(\tau/\tau_0) \tag{1.4}$$

where β characterizes the linear chirp and τ_0 is the pulse width. Recall that the solution to the master equation of Ref. [7] which neglects dispersion and nonlinearity is of the same $sech(\tau)$ form. In either case, there is a relation the amplitude and the width of the hyperbolic secant pulse has to satisfy. Introducing a linear chirp permits the amplitude and phase modulations to be connected and the optical effects acting on the envelope and the phase of the pulse become interconnected. A necessary condition for stability of the solution is that there is no net gain for small intensities (cw light). Otherwise, the wings of the pulse grow, destabilizing the pulse.

In these treatments, one does not describe in the initiation of mode-locking. It is true that the cw-solution is unstable and since the pulsed solution can be an attractor, it follows that mode-locking can be self-initiated. This expectation is verified with realistic, numerical models of mode-locking starting from a continuous initial field with noise. However, recently, a direct treatment based on a statistical approach has shown that ordering of the modes in the presence of a SA and a slowly-saturating gain medium is a first order phase transition [9]. The same authors have later extended their analysis to include dispersion and Kerr

nonlinearity [10]. This way, the presence of a power threshold for mode-locking is placed on a firm theoretical basis.

Various different approaches have been formulated for understanding pulse formation in solid state and fiber lasers. The reader is referred to Ref. [6] for further information. These approaches make the assumption of small changes from each different effect. However, this assumption of small changes per roundtrip can be drastically violated in fibers lasers where the pulse duration can vary by 50 times and the pulse energy by 20 times in a fiber laser. Furthermore, the different effects, such as Kerr nonlinearity, dispersion, linear and nonlinear gain are assumed to be uniformly distributed over the laser cavity. Such an approach is inadequate for a thorough understanding of pulse evolution in different fiber lasers considering that, for example, the main difference between soliton and stretched-pulse lasers is the non-uniform distribution of dispersion over the cavity. Extensions on these usual assumptions have been made in the form of a perturbative analysis [11].

More realistic descriptions of mode-locking have been provided in the context of the complex Ginzburg-Landau equation (CGLE) (see Ref. [12] for a review various physical phenomena described by the CGLE, including nonlinear waves). One intuitive way of understanding the difference in roles played by the NLSE and the CGLE is to recall that NLSE is a non-dissipative, Hamiltonian equation. Therefore, NLSE cannot have attractor solutions and is thus relevant to propagation of pulses in the absence of loss and gain. Furthermore, Hamiltonian systems cannot pulsating soliton solutions, and if initial conditions are such, solutions nevertheless evolve to stationary solutions. On the other hand CGLE is a dissipative equation which can have attractor solution and is able to describe the formation of pulse solutions starting from arbitrary initial conditions for an appropriate choice of its

parameters.

Several authors have used the CGLE to describe passive mode-locking. The reader may find the introductory paragraphs of Ref. [13] to be a useful resource for a summary of such efforts. Similarly, Ref. [14] contains a thorough review of CGLE-based efforts. However, in all of these cases, the laser cavity is comprised of a single, homogeneous optical medium.

The amplification process in the gain medium is modeled in various levels of realism. In the simplest case frequency-dependence of the gain is ignored. This is only valid if the pulse spectrum is much narrower than the gain bandwidth. A more realistic approach is to assume a parabolic frequency dependence, which is valid as long as the spectral width is several times smaller than the gain bandwidth. Generalizations have been outlined [15] where the gain medium is treated as a two-level atomic system, described by Maxwell-Bloch equations [16]. A complex Lorentzian gain spectrum can be obtained within this formalism, if the homogeneous broadening assumption is made [15, 17]. This generalization is necessary for a quantitative description of pulse generation and propagation in fiber lasers and amplifiers for sub-100 fs pulses. The dynamic saturation of the gain medium can typically be neglected due to extremely long upper state lifetimes of fiber amplifiers (typically ~ 1 ms), and the saturated gain can be expressed as

$$g_s(E_p) = \frac{g_0}{1 + E_p/E_{sat}}, \tag{1.5}$$

where E_p is the pulse energy, g_0 is the small signal gain, and $E_{sat} = E_g \frac{T_R}{T_G}$ with E_g is the gain saturation energy, T_R is the temporal separation between successively pulses, T_G is the upper state lifetime (for example, see [13]).

Due to the complexity of the underlying dynamics and the fact that fiber lasers are typically comprised of several segments of fiber with different optical proper-

ties, a detailed understanding of pulse generation typically requires a numerical solutions. While this is a time-consuming process due to fact that a nonlinear partial differential equation needs to be solved, it is possible to obtain quantitative agreement with the experiments as will be shown in this thesis.

1.4 Limitations of Femtosecond Fiber Lasers

The generic fiber laser is the soliton laser, comprising of a gain fiber providing both anomalous dispersion and nonlinearity, and a fast SA mechanism such as nonlinear polarization evolution (NPE) or a nonlinear optical loop mirror (NOLM). However, soliton fiber lasers [20] are limited in pulse energy to ~ 30 pJ and ~ 300 fs, ultimately due to an instability arising from the period perturbations on the soliton as a result of gain and loss [21].

A major improvement on pulse energy was achieved with the introduction of the stretched-pulse fiber laser [22]. In this laser, two fiber segments with anomalous and normal dispersion form a dispersion map. In close analogy to dispersion management [23] in optical communications, breathing solutions (dispersion-management solitons) are obtained. As a result of the large variations in pulse duration, the average pulse intensity is reduced by an order of magnitude. With such a reduction in the effective nonlinearity, pulse energies have been improved by more than an order of magnitude over the soliton fiber lasers, and the highest pulse energies prior to this thesis study was 2.7 nJ [24]. A stretched-pulse fiber laser routinely produces 1-nJ, 100-fs pulses with very good stability, and some distortion in the pulse shape.

Although higher energies were achieved, the fundamental limitation imposed by excessive nonlinearity was not eliminated: This limitation manifests itself as

a tendency to multiple pulsing as energy is increased. The stretching and compression ratio cannot be increased indefinitely without undesirable effects on the pulse dynamics. Stretched-pulse lasers remain with peak powers about an order of magnitude below that of typical bulk solid state lasers.

From the point of view applications, the lack of higher pulse energies and peak powers are the leading drawback of fiber lasers if they will indeed become an alternative technology to bulk solid solid state lasers.

1.5 A Catalog of Pulse Shaping Schemes in Fiber Lasers

The rich interplay of dispersion and nonlinearity in short-pulse fiber lasers gives rise to many different pulse shaping mechanisms, such as soliton-like pulses, dispersion management, nonlinearity management, and self-similar pulse propagation. Significant advances in the pulse properties, in particular in pulse energy have been achieved by considering various pulse shaping mechanisms beyond the basic case of soliton-like pulse shaping.

In this thesis, several of these mechanisms are proposed and studied for the first time. It would be desirable to place the different mechanisms into a unifying picture and catalog within a general structure. In addition, one may hope to discover other useful, even better mechanisms. In this section, we attempt to provide a complete list of all pulse shaping mechanisms with regards to dispersion and nonlinearity for a two-segment laser cavity.

It should be emphasized that dispersion and nonlinearity typically dominate pulse shaping in femtosecond fiber lasers, but they are not the only mechanisms responsible for pulse stabilization. Hence, the enumeration presented here will overlook mechanisms such as bandwidth-limited operation of highly-chirped pulses

under normal dispersion. However, the consideration of dispersion and nonlinearity alone is necessary to keep the task manageable. The restriction to two different segments is motivated by practical constraints on the complication of a laser cavity.

Here, the main goal is to identify the main features of a given pulse shaping scheme, as determined by the combined effects of dispersion and nonlinearity. Once promising schemes are identified, realistic corrections can be considered. A laser cavity is represent by a two-by-two matrix,

$$\begin{bmatrix} D_1 & D_2 \\ NL_1 & NL_2 \end{bmatrix} \tag{1.6}$$

where D_1 and D_2 are the GVD coefficients of the first and the second optical segments (the first and the second columns, respectively) comprising the cavity. Similarly, NL_1 and NL_2 are the effective nonlinearity coefficients of the two optical segments. We allow the elements of the matrix to take on values of 1, -1, and 0 only, representing a large positive, a large negative, or a negligibly small value. A negative nonlinearity coefficient corresponds to self-defocussing nonlinearity as described in Chapter 2. For example, a generic soliton laser would be represented by

$$\begin{bmatrix} -1 & -1 \\ 1 & 1 \end{bmatrix} \tag{1.7}$$

In this case the two columns are identical since the cavity is formed mainly by one segment with anomalous GVD and positive nonlinearity. A stretched-pulse laser (supporting dispersion-managed solitons) would be represented by

$$\begin{bmatrix} 1 & -1 \\ 1 & 1 \end{bmatrix} \tag{1.8}$$

Even though the net cavity dispersion can be normal, we set the GVD coefficients

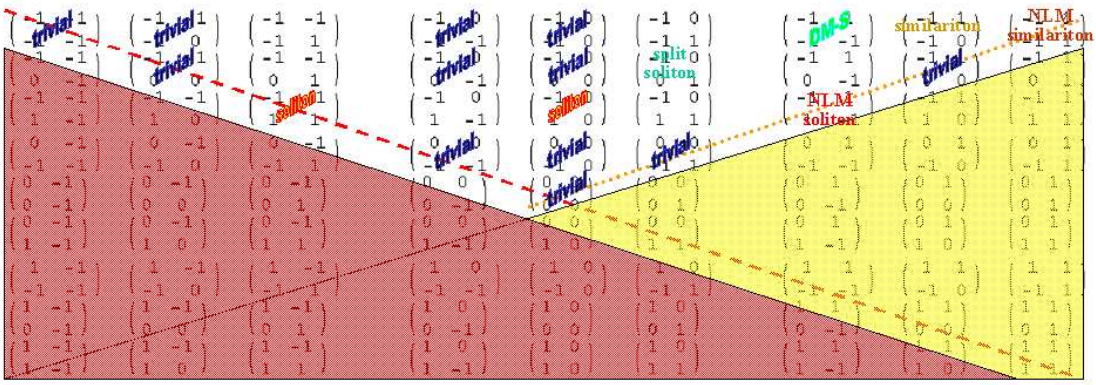

Figure 1.1: A complete list of two-segment soliton-like pulse shaping schemes.

to 1 and -1; equal magnitudes need to be interpreted as an equality within an order of magnitude.

A complete list of two-segment pulse shaping schemes can then be constructed under these assumptions (Fig. 1.1). Although there are as many as 81 different combinations, many of them are physically equivalent through a reordering of the columns or an overall multiplication by -1. The identifiable schemes are labeled. Schemes which don't result in pulsed operation as a result of a balance of dispersion and nonlinearity are labeled as *trivial*. Schemes that remain unexplored are left without a label.

Within this list, the familiar schemes are solitons (labeled as *soliton*), dispersion-managed solitons (labeled as *DM-S*), self-similar pulse evolution (labeled as *similariton*, discussed in Chapter 4), nonlinearity-managed solitons (labeled as *NLM soliton*, discussed in Chapter 2), split-step solitons [25] (labeled as *split soliton*). The combination of nonlinearity management and self-similar pulse formation is worthy of mention (labeled as *NLM similariton*). Self-similarity and nonlinearity management are two concepts that promise large improvements in the maximum pulse energy obtainable from a fiber laser. The combination of these two ap-

proaches can be synergical, however this possibility has not been explored in detail during this thesis study.

BIBLIOGRAPHY

[1] G. P. Agrawal, *Nonlinear Fiber Optics, 2nd Ed.* (Academic, New York, 1995).

[2] V. E. Zakharov, and A. B. Shabat, Sov. Phys. JETP **34** 62 (1972).

[3] P. G. Drazin, and R. S. Johnson, *Solitons: an Introduction* (University Press, Cambridge, 1989).

[4] N. N. Akhmediev, *Solitons: Nonlinear Pulses and Beams* (Chapman & Hall, London, 1997).

[5] A. Hasegawa, *Optical Solitons* (Springer-Verlag, New York, 1989).

[6] H. A. Haus, IEEE J. Selec. Top. Quan. Electron. **6**, 1173 (2000).

[7] H. A. Haus, J. Appl. Phys. **46**, 3049 (1975).

[8] O. E. Martinez, R. L. Fork, and J. P. Gordon, Opt. Lett. **9**, 156 (1984).

[9] A. Gordon, and B. Fischer, Phys. Rev. Lett. **89**, 103901 (2002).

[10] A. Gordon, and B. Fischer, Opt. Commun. **223**, 151 (2003).

[11] C. Spielmann, P. F. Curley, T. Brabec, adn F. Krausz, IEEE J. Quan. Electron. **30**, 1100 (1994).

[12] I. S. Aranson, L. Kramer, Rev. Mod. Phys. **74** 99 (2002).

[13] A. K. Komarov, K. P. Komarov, Phys. Rev. E **62** R7607 (2000).

[14] N. Akhmediev, J. M. Soto-Crespo, and G. Town, Phys. Rev. E **63** 056602 (2001).

[15] S. Chi, C.-W. Chang, S. Wen, Opt. Commun. **106** 193 (1994).

[16] L. Allen, and J. H. Eberly, Optical Resonance and Two-Level Atoms (Dover, New York, 1975).

[17] L. W. Liou, G. P. Agrawal, Opt. Commun. **145** 385 (1998).

[18] M. Hofer, M. E. Fermann, F. Harberl, M. H. Ober, and A. J. Schmidt, Opt. Lett. **16**, 502 (1991).

[19] N. J. Doran and D. Wood, Opt. Lett. **13**, 56 (1988).

[20] For example, see K. Tamura, C. R. Doerr, H. A. Haus, and E. P. Ippen, IEEE Phot. Tech. Lett. **6**, 697 (1994).

[21] S. M. J. Kelly, Elec. Lett. **28**, 806-807 (1992).

[22] K. Tamura, E. P. Ippen, H. A. Haus, L. E. Nelson, Opt. Lett. **18**, 1080 (1993).

[23] N. J. Smith, N. J. Doran, W. Forysiak, and F. M. Knox, J. Lightwave Technol. **15**, 1808-1822 (1997), and references therein.

[24] L. E. Nelson, S. B. Fleischer, G. Lenz, and E. P. Ippen, Opt. Lett. **21**, 1759 (1996).

[25] R. Driben, B. A. Malomed, Opt. Commun. **185** 439 (2000).

Chapter 2

Nonlinearity Management: A Route to High-Energy Soliton Fiber Lasers[1]

This chapter describes a proposal to use negative (self-defocusing) nonlinearities to control nonlinear phase shifts in soliton fiber lasers toward the goal of high-energy pulse generation. By analogy to dispersion management, this scheme is referred to as nonlinearity management. We first describe a map which can be regarded as a combination of nonlinearity management and dispersion management. The map is designed to support solitons in two segments of alternating sign of nonlinearity and dispersion. Analytical and numerical calculations demonstrate that this map can be essentially free of spectral sideband generation. By suppressing the spectral sidebands, pulse energies 100 times greater than those of existing soliton fiber lasers should be possible.

We also discuss the less ideal case of direct reduction of average nonlinearity by use of self-defocusing nonlinearity segments, without optimizing dispersion. The second scheme has the advantage of easier implementation. Practical implementations with existing materials are discussed.

2.1 Introduction

Fiber lasers have emerged as attractive alternatives to solid state lasers for generation of femtosecond pulses at near-infrared wavelengths. Fiber lasers possess considerable advantages over solid state lasers, most notably the simplicity of op-

[1]Most of the results presented in this chapter have been published in Ref. [1]

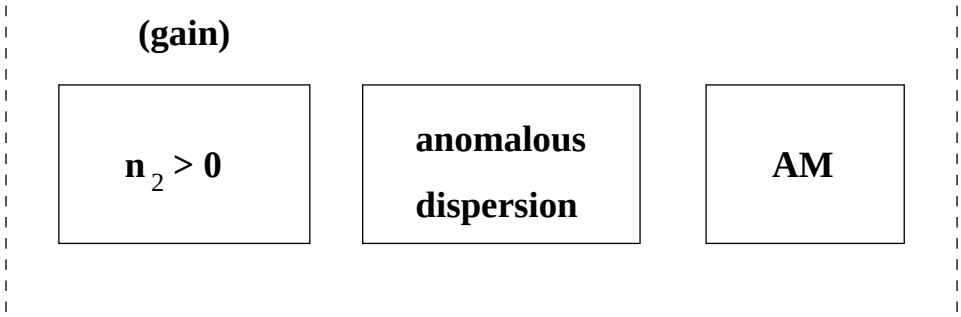

Figure 2.1: Schematic of a generic soliton laser consisting of segments with self-focusing nonlinearity, anomalous dispersion and amplitude modulation (AM).

eration. The high stability compared to solid state lasers, combined with their compact size, offers the possibility of wide-spread application. The drawbacks of fiber lasers are insufficient environmental stability for use outside the research laboratory, and lack of high-pulse energies directly from an oscillator. The obstacles to generation of higher-energy and shorter pulses can be traced back to accumulation of excessive nonlinear phase shift. Previous approaches to this problem have been based on an indirect reduction of effective nonlinearity. We consider direct management of nonlinearity in fiber lasers, which can be realistically considered with the demonstration that nonlinear phase shifts of either sign can be generated with femtosecond pulses [2, 3]. Similar approaches in telecommunications have been theoretically considered previously [4, 5].

A schematic drawing of a soliton laser is depicted in Fig. 2.1. Amplitude modulation (AM) produced by a real or artificial saturable absorber (SA) is necessary for the initial formation of a soliton-like pulse, and to stabilize the pulse against perturbations. We refer to an "artificial" SA if there is no real absorption; nonlinear transmittance is obtained through a nonlinear phase shift. An example of

an artificial SA is nonlinear polarization evolution (NPE) [6]. Gain fiber with self-focusing nonlinearity and anomalous dispersion can support solitons. Several gain materials are available for use at near-infrared frequencies. The most common dopants are Er, Yb and Nd. Among these, only Er-doped fiber benefits from the availability of anomalous dispersion in ordinary fiber.

The best reported results with Er fiber soliton lasers are several-hundred femtosecond pulses with energies of tens of picojoules. The most important obstacle to generation of shorter and/or higher energy pulses is the perturbation that arises from variations of pulse energy over the cavity period due to loss (including output coupling) and gain. This perturbation manifests itself in the formation of discrete sidebands in the spectrum and is known as spectral sideband generation (SSG). A first-order treatment shows that the offset of the frequencies of the sidebands from the center of the spectrum are given by $\Delta\omega_n \sim \pm 1/\tau_p\sqrt{8nz_s/z_c - 1}$, where n is the order of the sideband [7, 8]. Here z_c is the cavity length, $z_s = \pi/2\ (\tau_p^2/\beta'')$ is the soliton period, β'' is the group velocity dispersion (GVD), and τ_p is the pulse width. It is experimentally found that z_c/z_s must be limited to < 3 to avoid instability [9]. Thus, SSG places a lower limit to pulse width. In the soliton regime, $E_p\tau_p = 2\ (\beta''/\gamma)$ (E_p is the pulse energy, and γ is the Kerr nonlinearity), so this limitation becomes an upper boundary to pulse energy for given fiber nonlinearity.

In order to achieve higher pulse energies or shorter pulses, two possibilities emerge: the use of a shorter cavity or the reduction of the Kerr nonlinearity. There are limitations to a shorter cavity, one of which is imposed by the minimum length of fiber necessary for adequate gain. Additionally, a laser with a shorter cavity is more likely to be plagued by Q-switching. Reduction of nonlinearity is therefore, the preferable alternative for most situations. For femtosecond-pulse fiber lasers,

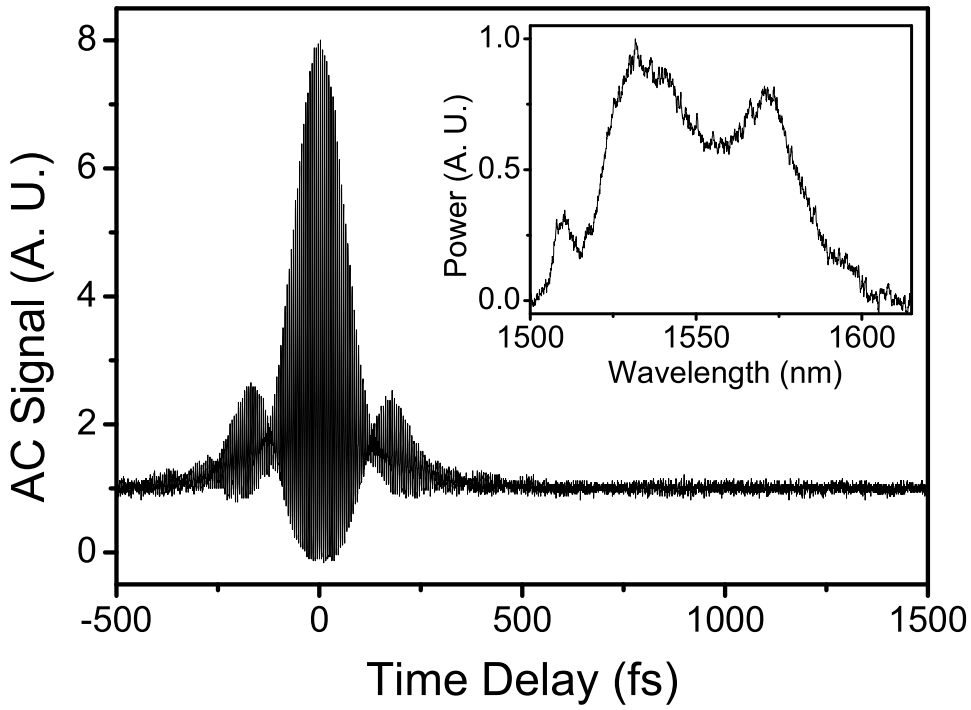

Figure 2.2: Typical autocorrelation of the stretched-pulse laser in our laboratory. Inset: The corresponding spectrum.

this has been addressed most effectively by the stretched-pulse laser [10]. The stretched-pulse laser essentially implements dispersion management (DM), which has been very successful in optical communications [11]. As a result, SSG is suppressed [12]. Pulse stretching has resulted in the generation of 100-fs pulses of $\sim 2.7\, nJ$ energy [13]. In this approach, the effects of nonlinearity are reduced indirectly, through the effects of dispersion.

There are limitations to the stretched-pulse approach. Highly-chirped, picosecond pulses are switched out of the laser and these are compressed externally, in a dispersive delay line. The need for an external compression stage is an inconvenience for applications. Although effective nonlinearity is reduced and higher energies are achieved, it is clear that the fundamental limitation imposed by excessive nonlinearity is not eliminated: This limitation manifests itself as a tendency to multiple pulsing as energy is increased. The stretching and compression ratio cannot be increased indefinitely without undesirable effects on the pulse dynamics. Increasing the dispersion contrast by using higher dispersion fiber in both sections of the dispersion map is limited by available fiber parameters, and it is clear that increasing the total positive dispersion will result in larger deviations from a linear chirp. Increased nonlinearity of the chirp limits compression and distorts the pulse shape. A typical interferometric autocorrelation and spectrum produced by a stretched-pulse laser in our laboratory is shown in Fig. 2.2, and similar results have been reported previously [14]. The structures in the spectrum and time profile can be undesirable for many ultrafast applications, as well as amplification. Furthermore, DM is only possible for Er-doped fiber around $\sim 1.55\, \mu m$. Fiber lasers are needed at shorter wavelengths, where only normal dispersion is available. Novel microstructured fiber may provide anomalous dispersion. However,

due to small effective areas, these fibers have increased nonlinear effects, which would be a limitation to high-energy pulse generation.

In this report, we propose direct management of nonlinearity by use of negative (self-defocusing) nonlinear phase shifts. In Sect. 2, we describe the concept for a fiber laser that is essentially free of spectral sidebands. This is achieved by utilizing dispersion and nonlinearities of both signs. In Sect. 3, we consider the use of negative nonlinearities without optimizing dispersion. This is a less ideal scheme, but one that will be easier to implement. In Sect. 4, we discuss practical implementation of nonlinearity management in fiber lasers. Section 5 summarizes our main conclusions.

2.2 Nonlinearity- and Dispersion-Managed Solitons

The use of negative nonlinearities is a degree of freedom that has not been previously explored in short-pulse fiber laser design. Let us consider a general dispersion and nonlinearity map described by the nonlinear Schrodinger equation (NLSE) written in normalized units:

$$\frac{du}{dz} - i\frac{1}{2}D(z)\frac{d^2u}{dt^2} = i\Gamma(z)|u|^2u \tag{2.1}$$

where $D(z)$ and $\Gamma(z)$ can take the values -1 to $+1$ across the map. Although one can consider arbitrary variations, in practice, it is realistic only to consider piece-wise constant maps composed of a small number of segments. In particular, we will consider the following simple map:

$$D(z) = \Gamma(z) = \begin{cases} +1 & \text{for } 0 < z < \xi z_c; \\ -1 & \text{for } \xi z_c < z < z_c. \end{cases}$$

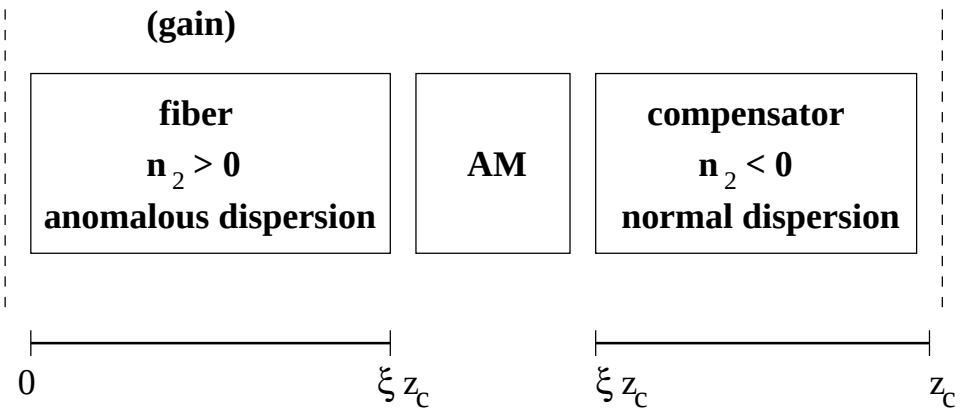

Figure 2.3: Block diagram of the proposed laser consisting of fiber, compensator and SA. We envision a ring cavity for the increased ease of self-starting. The sequence of the components in the diagram are the same as in the simulations.

where $\xi : 0 < \xi < 1$ and determines the relative strength of the two segments. The conceptual model of a laser based on this map is illustrated in Fig. 2.3. Both segments support formation of a soliton with identical parameters. However, the signs of the dispersion and nonlinearity operators are reversed. Hence, it is expected that the solution for the fundamental soliton becomes:

$$u = \ sech(t) \ \ exp(i\delta(z)/2) \tag{2.2}$$

where $\delta(z) = D(z) = \Gamma(z)$. For the special case of $\xi = 1/2$, the effects of each segment are exactly compensated by the following segment. Indeed, any input field is an eigensolution. We call this scheme "full compensation".

In a real system the implementation cannot be ideal and there will be departures from a full compensation. An equally attractive approach is to implement the map such that $\xi \neq 1/2$, which we denote as "partial compensation". In this case, the map has a reduced effective length, defined as $z_{c,eff} = |2\xi - 1|z_c$. The phase shift accumulated by the soliton will be proportional to the difference of normalized

lengths of the two segments, as opposed to the total length. This has important consequences for SSG: The sidebands are expected to move toward larger frequency offsets from the center of the spectrum. Adapting a simple model of SSG similar to that of Ref.[7], we introduce lumped loss (e.g. output coupling) at the end of the map, balanced by linear gain throughout the map:

$$\frac{du}{dz} - i\frac{1}{2}D(z)\frac{d^2u}{dt^2} = i\Gamma(z)|u|^2u + g\ u, \tag{2.3}$$

where $D(z)$ and $\Gamma(z)$ are defined as before. The lumped loss at the end of the second segment is described by $u \rightarrow u\ exp(-gz_c)$. With the transformation $u \rightarrow A(z)\ u$ it can be shown that the energy variation due to loss and gain is equivalent to a variation in the effective nonlinearity experienced by the soliton, with $A(z)$ characterizing this variation. With simple algebraic manipulation, Eqn. 2.3 takes the form:

$$m(z)\frac{du}{dz} - i\frac{1}{2}\frac{d^2u}{dt^2} = iA^2(z)|u|^2u, \tag{2.4}$$

where $m(z) = -1/D(z) = -1/\Gamma(z)$. Using the scaling properties of NLSE, the non-perturbed solution can be expressed as

$$u = \eta\ sech(\eta(t - \omega z))\ exp[i\delta(z)(\omega t - kz)], \tag{2.5}$$

where $k = (\omega^2 - \eta^2)/2$. We look for a solution of this form for Eqn. 2.5, and replace $A^2(z)$ with its Fourier series expansion. A first-order expansion for small perturbations shows that resonances occur for $\int_0^{z_c} k\delta(z)dz = 2\pi n$. The integral equals the difference between the total phase accumulated by the perturbed soliton and the dispersive waves, and is proportional to the effective map length, $z_{c,eff}$. Hence, the frequencies at which the sidebands are formed become a function of a (smaller) effective map length, not the total map length. The sideband frequency

offsets are given by

$$\Delta\omega_n \sim \pm 1/\tau_p \sqrt{8nz_s/(z_c|2\xi - 1|) - 1}. \tag{2.6}$$

The sidebands can be pushed out to large offsets, where there is little energy, by choosing ξ close to 1/2. Thus, SSG is effectively suppressed. This is the main result of this section.

We used numerical simulations to evaluate this concept in detail. Since we envision the application of these ideas to femtosecond fiber lasers, the simulations were done assuming a fiber laser based on the proposed map. We consider a ring laser design for increased ease of self-starting. The first segment consists of gain fiber with finite gain bandwidth. The compensating segment has normal dispersion and self-defocusing nonlinearity, and it is labeled the "compensator." In order to illustrate the concept, normalized units were used in the simulations. Implementation with realistic parameters is discussed later in the text. The length of the compensator ($(1 - \xi)z_c$) was increased, starting from zero, while shortening the fiber such that the total cavity length was kept constant at $z_c = 10$. For every simulation, a control simulation was run corresponding to a laser consisting only of gain fiber with physical length equal to $z_{c,eff}$. The dispersion and nonlinearity of the fiber and the compensator are chosen such that the characteristic dispersion and nonlinear lengths $L_D = \tau_p^2/\beta'' = 1$ and $L_{NL} = 1/(\gamma P_p) = 1$ (P_p is the peak power). Gain is modeled as distributed over the length of the fiber and saturating with total intra-cavity energy (E) with a Gaussian frequency dependence: $g(E, \omega) = g_0\ (1 - E/E_{sat})\ exp(-(\omega - \omega_0)^2/\Omega_{bw}^2)$. Here E_{sat} is the gain saturation energy, ω_0 is the carrier frequency and Ω_{bw} is the gain bandwidth. Small signal gain is approximately 30 dB and E_{sat} is set to the energy of a fundamental soliton in normalized units. If the normalized pulse duration is assumed to be 100-fs in

physical units, the gain bandwidth corresponds to $\sim 50\ nm$. SA and output coupling (linear loss, in general) are modeled as a transmission function of the form $u \rightarrow u\ [(1-\alpha-\beta)+\alpha\ sin^2(\pi I/I_{sat})]$. Here I denotes the instantaneous intensity, and I_{sat} is the saturation intensity, which is set to the peak intensity of the soliton unless stated otherwise. $\beta = 10\%$ is the output coupling, and $\alpha = 10\%$ is the modulation depth. Thus, the round-trip loss of the laser for cw light is 20%. We note that the exact value of linear loss is not crucial if the gain is strong enough, since the nonlinearity of the subsequent segment can be set to offset a decrease in energy.

We begin by considering partial compensation for varying $z_{c,eff}$. All the simulated cases resulted in self-starting stable solitary pulses (the build-up of the pulse from noise for $z_{c,eff} = 1$ is illustrated in Fig. 2.4). The departure of the sidebands from the center of the spectrum with increasing compensation ratio is illustrated in Fig. 2.5(a), and offset of the first sidebands is plotted in comparison to control simulations in Fig. 2.5(b). For the highest compensation that was simulated ($z_{c,eff} = 0.1$), the pulse energy is increased by a factor of 100 in the proposed scheme, while the offset of the first sideband is equivalent to that in the uncompensated soliton laser.

For full compensation (corresponding to vanishing $z_{c,eff}$), the enhancement in energy is smaller than for $z_{c,eff} = 0.1$. Spectral sidebands are eliminated at an order of magnitude higher energies compared to the ordinary soliton laser. The proposed laser produces pulses with a time profile virtually indistinguishable from that of the soliton laser with 10 times higher pulse energy (Fig. 2.6). The energy can be increased to larger values. However, deviations from ideal compensation due to non-instantaneous recovery of the loss begin to distort the pulse. On the

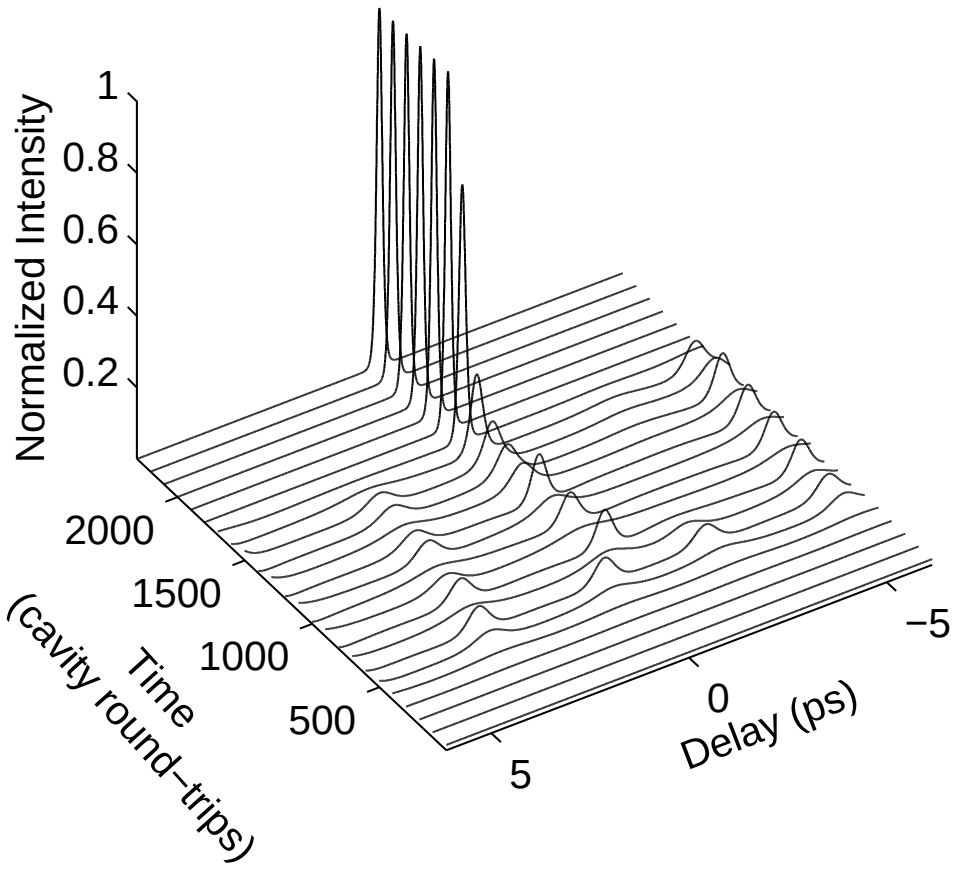

Figure 2.4: The build-up of a solitary pulse from intra-cavity noise is plotted for the proposed laser with $z_{c,eff} = 1$.

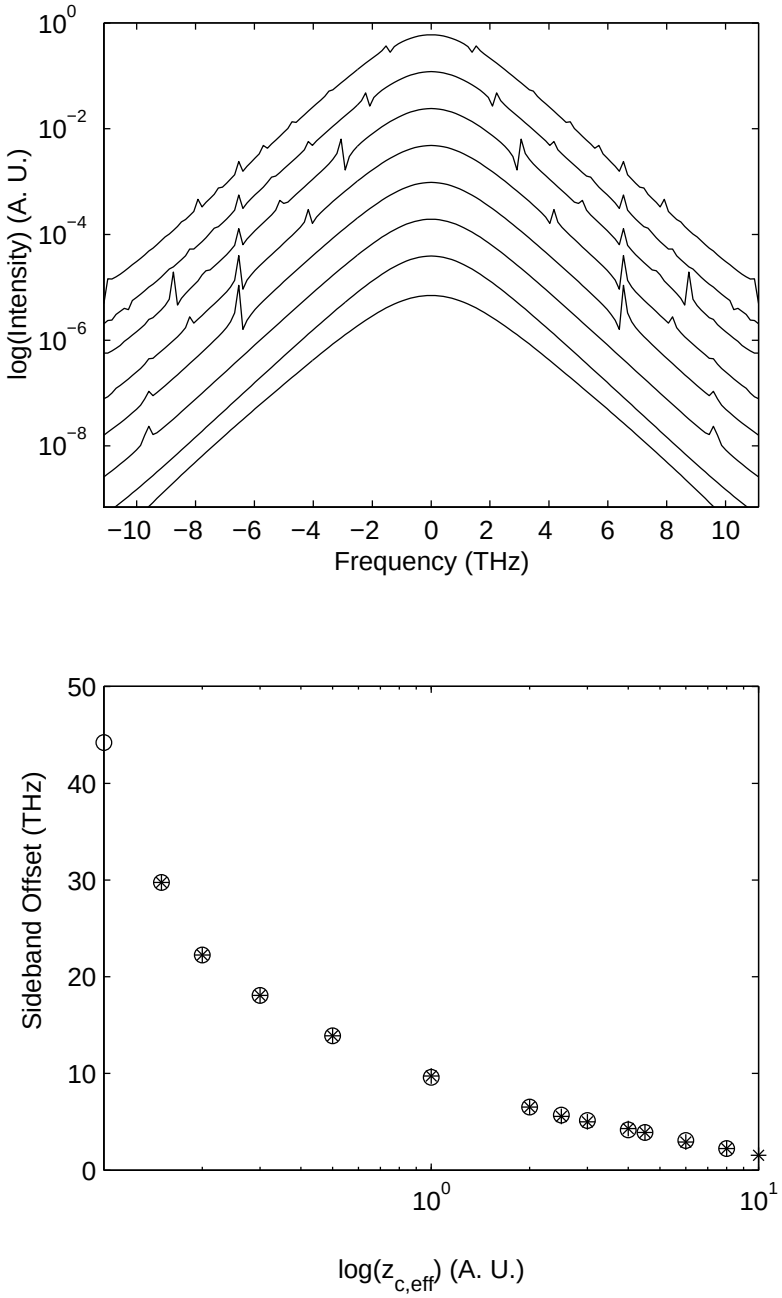

Figure 2.5: Upper panel: Spectra (as offset from the carrier frequency) for effective map lengths of (top to bottom): $z_{c,eff}$ = 10, 8, 6, 4, 2, 1, 0.5, 0.1. Lower panel: Frequency offset of the first sidebands for the proposed laser and the control simulation are plotted.

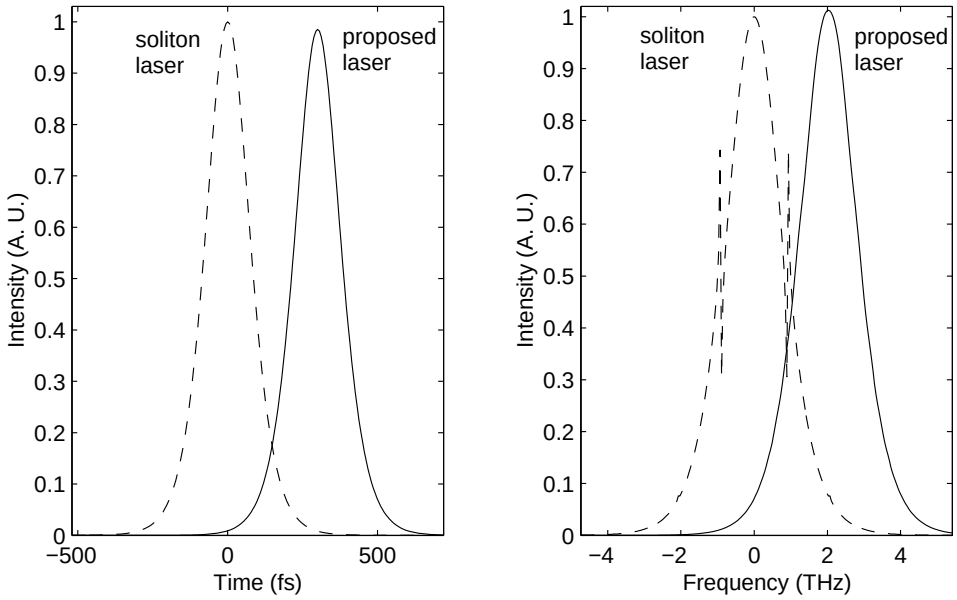

Figure 2.6: Results of simulations for full compensation ($\xi = 1/2$): SSG is eliminated and similar pulse duration is achieved at 10 times higher energy than in the soliton laser. The traces are displaced horizontally for clarity.

other hand, full compensation has a remarkable feature. It constitutes a mode-locking mechanism that is not dominated by soliton effects, but by the SA: The peak intensity of the pulse is determined by the saturation intensity of the SA. The reduced influence of solitary effects explains the result mentioned above, namely, that full compensation does not scale to as high energies as partial compensation. If the saturation intensity of the SA is set to a value that does not correspond to the fundamental soliton (intra-cavity energy is constant), breathing pulses result. If the gain bandwidth is much larger than the pulse bandwidth, the peak intensity of the pulse increases linearly with the saturation intensity of the SA. This linear increase saturates as the pulse bandwidth becomes comparable to the gain bandwidth.

The consequences of an ideal compensation of the effects of the fiber are ob-

vious from an elementary consideration of the NLSE . On the other hand, the benefits that we expect from this approach pertain to reduction of the effects of perturbations. In the presence of perturbations, the compensation is inherently not ideal. Thus, it was not clear *a priori* that these expectations would prevail in a real fiber laser. We see from numerical simulations that self-starting solitary pulse formation at high energies is possible. To summarize the substantial benefits of this approach:

(1) The idealized system with full compensation is essentially independent of pulse shape and energy. As a consequence of this, SSG is not present even for higher power fiber lasers, and SA dominates pulse dynamics.

(2) For a more realistic implementation, we consider partial compensation. Compensation such that $z_{c,eff} < 1$ practically eliminates SSG.

2.3 Nonlinearity Management Without Dispersion Optimization

The use of nonlinearity and dispersion of either sign to create a fiber-compensator pair is very promising. However, the desired parameters, particularly sufficient dispersion of correct sign for the negative-nonlinearity segment, may not be possible or practical to achieve for many applications. In this section, we briefly consider alternative approaches that are less ideal but that can provide significant advantages.

It will be difficult to compensate the GVD of more than several meters of fiber. It is, however, possible to produce large negative nonlinear phase shifts. This leads us to consider nonlinearity management without fine control of dispersion.

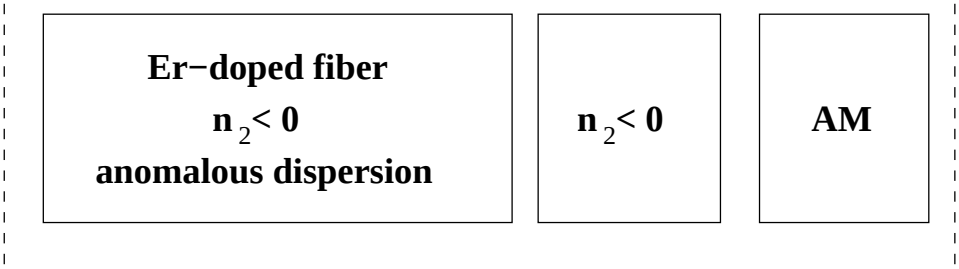

Figure 2.7: Schematic of a fiber laser with reduced average nonlinearity.

Reduction of average nonlinearity should permit formation of higher-energy pulses.

Numerical simulations were performed to investigate this expectation. A soliton fiber laser was chosen over a stretched-pulse laser since it is better understood quantitatively. The simulated laser is depicted schematically in Fig. 2.7. The model used in the simulations is the same as described in the previous section. However, the compensating segment provides only negative nonlinear phase shifts and it has negligible dispersion. A simulation without the compensating segment serves as the baseline. Relative to this, gain saturation energy was increased to two, three, and four times that of a fundamental soliton, respectively. The magnitude of the compensating nonlinearity was increased accordingly, such that the increase in pulse energy was balanced by the decrease in the average nonlinearity. The intensity profiles of the resulting pulses are shown in Fig. 2.8. Increasing the energy by a factor of two is managed well by decreasing the average nonlinearity. However, for a three-fold increase, the resulting pulse sheds radiation visible as small intensity fluctuations away from the pulse. When the energy is increased to four times the original value, the pulse breaks into two, resulting in irregular double-pulsing.

The order in which nonlinearity and dispersion act on the pulse matters. From

a physical point of view, this limitation means that the pulse in the first segment should not be severely distorted before it reaches the compensating segment. From the numerous simulations performed, we see that, as a rule of thumb, a total nonlinear phase shift of $\sim \pi$ is the maximum that can be compensated without dispersion optimization. Further increases in energy can be achieved without pulse break-up and multiple-pulse formation by introducing additional compensating segments at equi-distant positions in the cavity. Unfortunately, the benefits of such an approach will be proportional to the number of compensating segments. The use of more than two compensating segments seems impractical. In summary, the reduction of average nonlinearity by the addition of compensating materials is promising for soliton and DM fiber lasers, but in practice, improvement appears to be limited to a several-fold increase in pulse energy.

As another example, we briefly consider the use of negative nonlinearities for the design of fiber lasers at $\lambda < 1.3\ \mu m$. An all-fiber, high-energy femtosecond laser in the $1.0 - 1.3\ \mu m$ region is highly desirable for applications, such as medical imaging. However, at these wavelengths, ordinary fiber has normal dispersion. Anomalous dispersion can be obtained with prism pairs or diffraction gratings, but these offset the primary advantages of fiber lasers. Microstructured fibers offer anomalous dispersion through the use of large waveguide dispersion to offset the material dispersion, and may be useful for soliton pulse shaping. An alternative approach is to form solitons with $n_2 < 0$ and positive GVD. This approach has already been demonstrated experimentally for a bulk solid state laser [2]. Numerical simulations using existing material properties show that generation of 100-fs pulses with more than 100-pJ energy is feasible with this approach.

In conclusion, reduction of average nonlinearity offers limited but significant

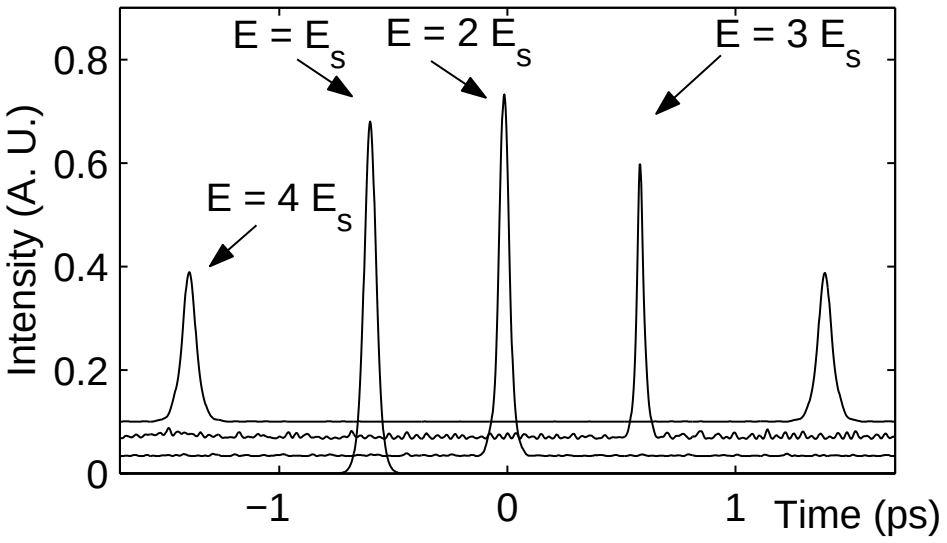

Figure 2.8: Results of numerical simulations of a soliton fiber laser showing the intensity profiles with increasing pulse energy and nonlinearity compensation. The intensity profiles are normalized, and displaced vertically and horizontally for clarity.

improvement over existing soliton and stretched-pulse lasers and is considerably easier to implement than the fiber-compensator pair. We have considered the addition of one segment with $n_2 < 0$ of negligible dispersion. It is likely that one can achieve better results through optimization of the map by the use of more than one type of fiber and careful consideration of the ordering of the segments.

2.4 Implementation of Nonlinearity Management

The experimental implementation of nonlinearity management relies on the presence of suitable materials with negative (self-defocusing) Kerr nonlinearity. Semiconductors have large self-defocusing refractive nonlinearity (~ 1000 times that of fused silica) for $h\nu > 0.7\, E_{bandgap}$. However, the negative nonlinearity is associated with strong two-photon absorption (TPA), which is a nonlinear loss. Large TPA becomes detrimental for short-pulse formation at rather low intensities since the modulation depth of the SA is limited. Thus, these materials are unattractive for high-energy fiber laser design. An alternative to semiconductors is the effective negative nonlinearity produced by cascaded quadratic processes [15]. Liu *et al.* have shown that $\Delta\Phi^{NL} \sim \pi$ can be impressed on femtosecond pulses with small ($< 1\%$) loss to second harmonic generation by use of the cascade processes at large phase mismatch [2, 3].

Consider the construction of a fiber laser based on this concept, with Er-doped fiber as the gain medium for $\sim 1550\, nm$. Fiber with anomalous dispersion of several ps^2/km and small third-order dispersion is available. Several crystals can be used as the quadratic medium. In particular, periodically poled lithium niobate (PPLN) in waveguide geometry is promising [16]. Dispersion of PPLN for type-I phase matching is $\sim 100\, ps^2/km$ at $1550\, nm$. Thus, the dispersion of 1 m-long

gain fiber can be compensated with a PPLN waveguide a few cm in length. With a 70-mm-long waveguide, we estimate that the nonlinear phase accumulation of fiber $\sim 10\ m$ in length can be compensated at ΔkL large enough to avoid the detrimental effects of GVM for 100-fs pulses. Thus, dispersion, rather than nonlinearity, will be the limiting factor in the construction of a compensator. Similarly, for the construction of a soliton-supporting Nd- or Yb-doped fiber laser at $\sim 1\ \mu m$, the use of cascaded processes in a PPLN waveguide appears to be promising. According to our calculations, it should be possible to balance the nonlinearity of gain fiber $\sim 10\ m$ in length at phase-mismatches necessary to support $\sim$ 100-fs pulses. It is clear that the implementation of the approaches considered here will require the solution of challenging material problems. Nevertheless, we see that it is possible to form a compensator via cascaded processes in existing and available materials.

A fast SA is necessary for femtosecond pulse formation. Nonlinear polarization evolution (NPE) or the use of a nonlinear optical loop mirror requires the use of fiber at least several meters long to accumulate the nonlinear phase needed for sufficient modulation depth. This requirement imposes a challenging minimum length of fiber to be compensated. Additionally, due to the interferometric nature of these techniques, there is a maximum energy for a given pulse shape, beyond which loss increases with increasing pulse energy. This is referred to as the saturation of NPE. For this purpose, NPE produced by the use of cascaded quadratic nonlinearities [17] should be advantageous, because it can be implemented in a several-cm-long frequency-doubling crystal. Saturation of NPE can be avoided since the saturation energy can be set to high values through the choice of phase-mismatch and crystal parameters. NPE works equally well with negative or positive nonlinear phase shifts. Therefore, it may be possible to accomplish AM in the compensator itself.

In a real implementation, in addition to the perturbations on the pulse inherent to the operation of a pulsed laser, precise matching of the fiber and the compensator may be difficult. We tested the robustness of the proposed laser by intentionally mismatching the parameters in the numerical simulations. Mismatches of 10% in either parameter are easily tolerated even for a high degree of compensation (corresponding to $z_{c,eff} = 1$) (Fig. 2.9). The resulting pulse shape does not change appreciably, and the sideband frequency offset from the center of the spectrum decreases by only a few percent. Finally, we would like to note that it is possible to consider hybrid approaches for which the average dispersion of the fiber section is decreased by the use of dispersion-compensating fiber, as in DM systems. A potential advantage of such an approach is that obtaining sufficient dispersion in the compensator is likely to be a greater limitation than nonlinearity. As long as the combined effect of the two fibers is a good approximation to a single fiber of uniform dispersion equal to their average dispersion, the degradation in the laser operation will be small. In summary, despite the difficulties that need to be confronted for a practical application of nonlinearity management, we see that existing materials already offer some promise.

2.5 Conclusion

In conclusion, we propose the use of negative nonlinearity as a new degree of freedom in the design of short-pulse fiber lasers. We describe a nonlinearity- and dispersion-managed map and demonstrate that it is essentially free of spectral sideband generation. This approach permits the pulse energy in a soliton fiber laser to be increased by two orders of magnitude. Implementation by the use of existing materials appears to be feasible, but challenging. As another application

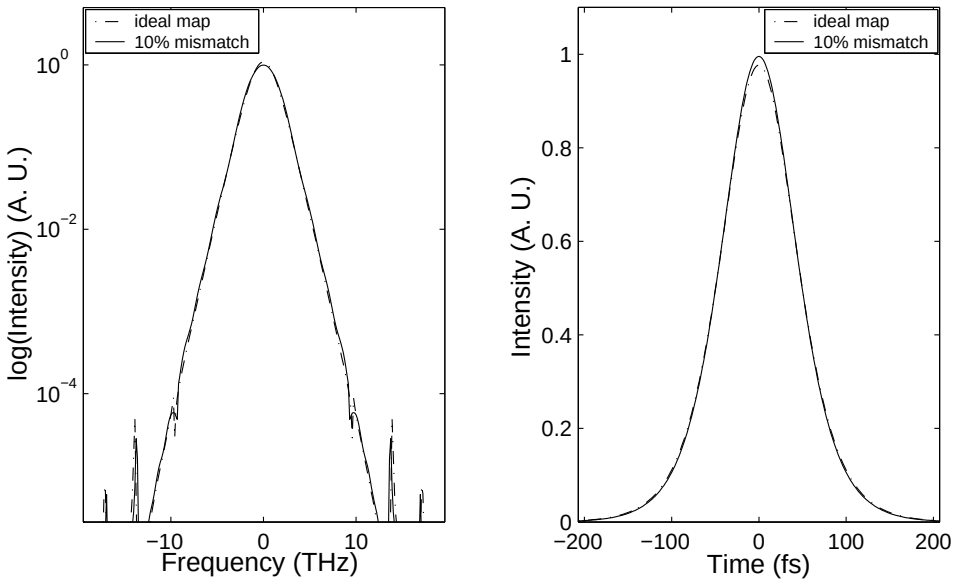

Figure 2.9: Intensity profile and spectrum (as offset from the carrier frequency) of the proposed laser with $z_{c,eff} = 0.1$ is compared to the same laser with 10% mismatch in the nonlinearity coefficient of the compensating segment.

of nonlinearity management, we consider the less ideal, but easier-to-implement approach of reducing average Kerr nonlinearity by the inclusion of a negative nonlinearity segment into the cavity. This approach offers significant benefits but is limited due to non-commutation of self-phase modulation and group velocity dispersion. Work is in progress for experimental implementation. Although we focus on applications to high-energy or shorter pulse formation from fiber lasers, the concept is general and applies to passive propagation of short pulses in optical fiber. Consequently, nonlinearity management is likely to be useful in soliton communications, as a way to avoid spectral sidebands and excessive nonlinear phase shifts.

BIBLIOGRAPHY

[1] F. Ö. Ilday, and F. W. Wise, J. Opt. Soc. Am. B **19**,470 (2002).

[2] L. J. Qian, X. Liu, and F. W. Wise, Opt. Let. **24**, 166 (1999).

[3] X. Liu, L. Qian, and F. W. Wise, Opt. Let. **24**, 1777 (1999).

[4] C. Pare, A. Villeneuve, and P.-A. Belanger, Opt. Let. **21**, 459 (1996).

[5] C. Pare, A. Villeneuve, and S. LaRochelle, Opt. Comm. **160**, 130 (1999).

[6] M. Hofer, M. E. Fermann, F. Haberl, M. H. Ober, and A. J. Schmidt, Opt. Let. **16**, 502 (1991).

[7] S. M. J. Kelly, Elec. Lett. **28**, 806 (1992).

[8] B. A. Malomed, Opt. Comm. **61**, 192 (1987).

[9] K. Tamura, C. R. Doerr, H. A. Haus, and E. P. Ippen, IEEE Photon. Tech. Lett. **6**, 697 (1994).

[10] K. Tamura, E. P. Ippen, H. A. Haus, and L. E. Nelson, Opt. Let. **18**, 1080 (1993).

[11] N. J. Smith, N. J. Doran, W. Forysiak, and F. M. Knox, J. Lightwave Technol. **15**, 1808 (1997), and references therein.

[12] D. J. Jones, Y. Chen, H. A. Haus, and E. P. Ippen, Opt. Let. **23**, 1535 (1998).

[13] G. Lenz, K. Tamura, H. A. Haus, and E. P. Ippen, Opt. Let. **20**, 1289 (1995).

[14] L. E. Nelson, S. B. Fleischer, G. Lenz, and E. P. Ippen, Opt. Let. **21**, 1759 (1996).

[15] R. DeSalvo, D. J. Hagan, M. Sheik-Bahae, G. Stegeman, E. W. Van Stryland, and H. Vanherzeele, Opt. Lett. **17**, 28 (1992).

[16] R. Schiek, M. L. Sundheimer, D. Y. Kim, Y. Baek, G. I. Stegeman, H. Seibert, and W. Sohler, Opt. Let. **19** 1949 (1994).

[17] X. Liu, F. Ö. Ilday, K. Beckwitt, and F. W. Wise, Opt. Let. **25**, 1394 (2000).

Chapter 3

High-Power, Femtosecond Pulses from a Fiber-Based Source[1]

In this chapter, we describe the second approach that we pursue toward generatioin of high-energy pulses: We report the amplification of femtosecond pulses at 1.03 μm in standard Yb-doped single-mode fiber. Pulse energy of 8 nJ and average power of 400 mW are obtained, limited by available pump power. These are the highest pulse energy and average power obtained from an integrated, single-mode fiber amplifier. After dechirping, 120 fs, 6 nJ pulses are obtained. A practical, fiber-based source with performance comparable to that of a bulk solid state laser is thus demonstrated, and scaling to substantially higher powers will be possible.

3.1 Introduction

There is rapidly growing, application-driven interest in ultrafast lasers. The development of efficient, compact and highly-stable femtosecond lasers and amplifiers promises to have a major impact on the use of ultrafast optics outside the laser research laboratory. Fiber lasers offer a number of practical advantages over bulk solid-state lasers, including compact size, better stability and freedom from misalignment. However, maximum pulse energies are around 1 nJ, limited by the inherent fiber nonlinearity. This is in contrast to $5-10$ nJ pulse energies available from bulk solid-state lasers and demanded by many applications. Thus, amplification is necessary to generate pulses with energies that can equal and surpass those

[1]Most of the results presented in this chapter have been published in Ref. [1]

of bulk solid state lasers.

There is great interest in practical short-pulse sources at wavelengths between 1.0 and 1.3 μm. In particular, biological applications such as optical coherence tomographies, multi-photon microscopy and laser-assisted eye surgery benefit from tissue transparency in this wavelength range. Aside from bulk solid-state lasers, a source of 8-nJ, femtosecond pulses based on amplification in Yb-doped fiber has been demonstrated [2]. The performance is good, but the setup is complicated: Pulses are generated with a fiber oscillator at 1.5 μm, Raman-shifted to 2.1 μm, converted to 1 μm through second-harmonic generation, and finally amplified in double-clad fiber pumped by a multimode diode laser. is an attractive gain medium for high-energy, femtosecond pulse generation owing to its high efficiency and broad emission spectrum at 1 μm. Furthermore, amplification in the presence of normal dispersion avoids pulse breakup induced by soliton effects at high energies [3]. This feature has been exploited in parabolic amplification, which permits accumulation of large nonlinear phase shifts [4, 5]. Practical, all-fiber chirped-pulse amplifiers at 1.5 μm have attracted much attention, but pulses shorter than 400 fs could not be obtained, and the maximum pulse energy after dechirping was limited to $\sim$ 3 nJ [6]. Currently, there is much excitement surrounding fiber amplifiers with tens of watt average power or up to millijoule pulse energies[7]. These amplifiers utilize multimode fibers and double-clad geometry for pumping with multimode diodes. Double-clad pumping technique requires the use of longer fibers which increases the strength of the nonlinear effects. Multimode fibers are typically used to offset the nonlinear effects. These techniques represent a significant deviation from the simplicity of standard single-mode fibers (SMF) and thus offset some of the advantages of fiber. The fiber-equivalent of bulk solid state lasers using only

readily-available components could have broad impact.

Two relevant, enabling advances have recently occurred: The first is the development of high-energy Yb fiber lasers. The first reliable and compact femtosecond Yb fiber lasers were limited to $\sim$ 60 pJ[8]. Ideally, an amplifier should be fiber-coupled to the oscillator for simplicity and freedom from misalignment. To prevent instabilities and to ensure high-quality seed pulses, only a small fraction ($< 10\%$) of the pulse energy can be diverted into the amplifier. Recently, we have demonstrated a Yb fiber laser[9] with pulse energy in excess of 1 nJ, which can be used to reliably seed an amplifier using a small fraction of its pulse energy. The second advance is the development of pump lasers: 980-nm diode lasers that deliver more than 500 mW in single-mode fibers have become commercially available. The use of single-mode diodes permits the construction of an all-fiber amplifier.

Here we explore the limitations to a femtosecond pulse source using standard SMF only. A simple and compact source delivering 6-nJ and 120-fs pulses at 1.03 μm with a repetition rate of 50-MHz is demonstrated through the use of a short gain fiber. These are the highest pulse energy and average power obtained through amplification in standard SMF to our knowledge. Overall, we obtain close to an order of magnitude increase in peak power, as well as a $\sim$ 3-fold increase in average power compared to previous all-fiber devices [6]. The setup consists of a Yb fiber amplifier seeded by a fiber oscillator. The use of single-mode fiber and pump diodes permits a high level of integration and excellent stability. Except for wavelength tunability, this approach offers and will eventually surpass the performance of a standard Ti:sapphire laser.

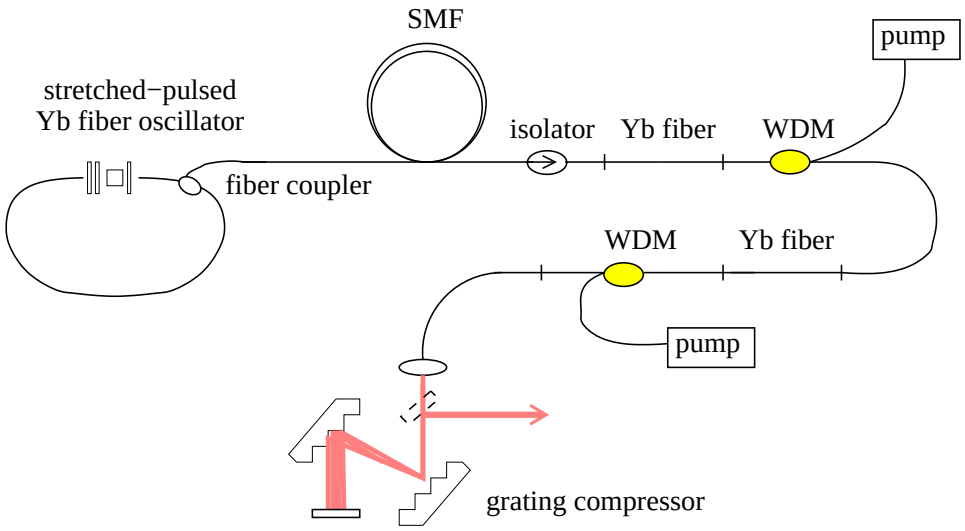

Figure 3.1: Experimental setup of the amplified laser.

3.2 Experimental and theoretical results

The experimental setup is shown in Fig. 3.1. A stretched-pulsed Yb fiber oscillator seeds the amplifier with 100-fs pulses. Ideally, the seed pulses should be clean and unstructured for highest-quality amplification. Therefore, the oscillator was designed to operate at small, anomalous dispersion (-0.02 ps^2). The pulses are directed into the amplifier via a $\sim 7\%$ fiber coupler placed after the gain fiber in the oscillator. The coupled energy is ~ 0.1 nJ. The pulses are then dispersively stretched to ~ 15 ps in 20 m-long single-mode fiber (SMF) to minimize nonlinear effects [10] and amplified in highly-doped Yb fiber (23,600 ppm doping, NA $=$ 0.12, core diameter 6 μm). The Yb fiber consists of two ~ 20 cm-long segments and is pumped by two 980-nm diode lasers providing 1 W total power through wavelength-division multiplexed (WDM) couplers. The pulse energy after amplification is 8 nJ, corresponding to 400 mW average power. A single segment of Yb fiber can be used if a 1 W diode laser is available or if the pump light from the

two diode lasers can be efficiently combined.

The experimental results are compared with numerical simulations. Propagation in each fiber segment is modeled using an extended nonlinear Schrodinger equation that accounts for GVD, third order dispersion (TOD), Kerr nonlinearity with Raman contribution, and gain in the Yb fiber. The gain saturates with total energy and has a parabolic frequency dependence with a bandwidth of 40 nm. These simulations indicate that consideration of Kerr nonlinearity, GVD and gain saturation are sufficient for a qualitative understanding of the amplification process. Raman scattering is found to be negligible. Quantitative agreement can be obtained with the inclusion of gain bandwidth and an effective frequency-filter imposed by the WDM couplers. The results of simulations are summarized in Fig. 3.2. Amplification is simulated for various pulse energies corresponding to stretching in 10 m and 20 m of SMF. Peak power is maximized with optimal dechirping (linear losses are ignored). As the pulse energy increases, broader spectra are obtained, which produce pulses with smaller full-width at half maximum duration. This is balanced by distortion of the pulse shape; a larger fraction of the energy resides in the wings of the pulse. As a result, an approximately linear dependence of peak power on pulse energy is obtained. The need for a minimum length of SMF to avoid distortion is evident; a square-like spectrum develops at 8 nJ with 10 m of SMF, whereas clean pulses are obtained with 20 m of SMF. The experimental spectra for 8-nJ pulse energy agrees well with the results of simulations (Fig. 3.2). The simulations also demonstrate that at least an order of magnitude higher pulse energies can be accomodated by stretching the seed pulses in a longer segment of SMF. The pulse shape is not degraded despite larger uncompensated TOD (mostly from the grating compressor), gain narrowing, and Raman scattering.

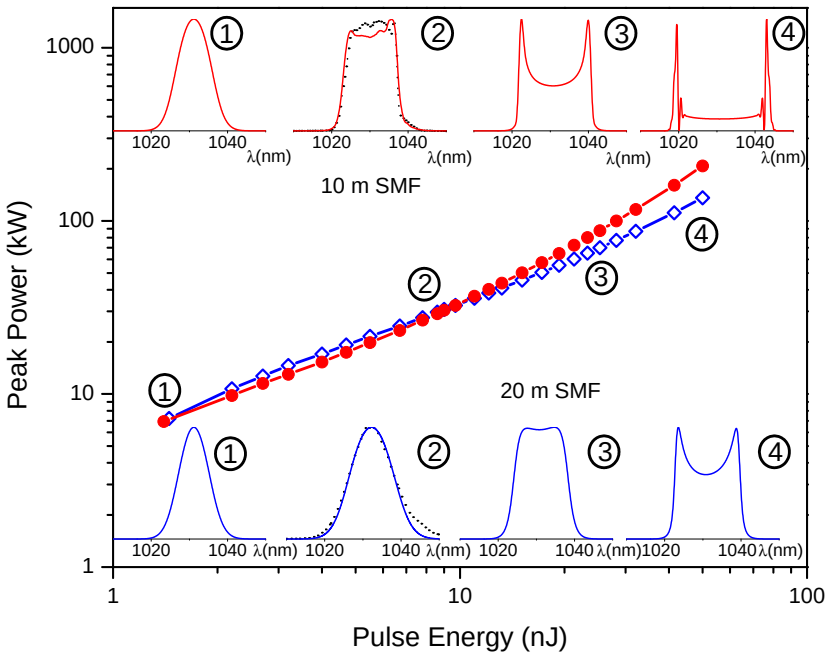

Figure 3.2: Peak power of amplified and dechirped pulses as a function of pulse energy with stretching in 10 m (closed symbols) and 20 m (open symbols) of SMF. Insets: Calculated pulse spectra (1), (2), (3), and (4) are for pulse energies of 1.4 nJ, 8 nJ, 25 nJ, and 50 nJ, respectively. Note the agreement between calculated spectra with experimental results for 8-nJ pulse energy.

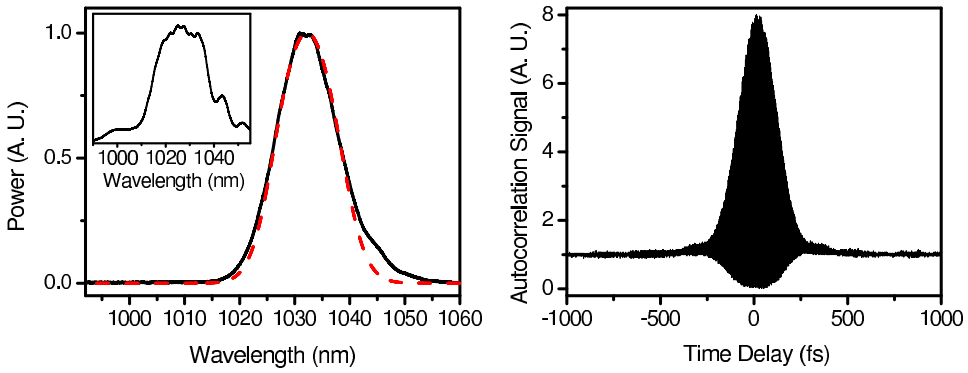

Figure 3.3: (a) Experimental (solid line) and calculated (dashed line) spectra of the amplified pulses. Inset: Spectrum of the pulses from the oscillator. (b) Interferometric autocorrelation of the dechirped pulses.

The spectra of the seed and the amplified pulses are presented in Fig. 3.3(a), along with the results of numerical simulations. The amplified pulses are subsequently dechirped in a grating compressor. After dechirping, the pulse energy is reduced to $\sim$ 6 nJ owing to loss at the gratings. Interferometric autocorrelation of the dechirped pulses is shown in Fig. 3.3(b). The calculated pulse duration is 125 fs, assuming a sech^2 pulse shape. The intensity and phase profiles were inferred by the use of a pulse retrieval algorithm based on fitting the measured interferometric autocorrelation and spectrum[11]. The corresponding pulse width is 115 fs which is close to that of the constant-phase transform of the pulse spectrum. The benefits of normal dispersion are evident; in the presence of anomalous dispersion, the stretched pulses ($\sim$ 0.6 kW peak power) would be significantly reshaped as a nonlinear phase shift in excess of π is accumulated towards the end of the gain fiber and in the 1-m-long SMF of the WDM coupler.

Since the amplifier is completely integrated, the overall stability is identical to that of the oscillator. The grating compressor is decoupled from the nonlin-

ear dynamics and does not degrade the stability. Uninterrupted operation can be maintained for at least several weeks. The setup is inexpensive in comparison to a bulk solid-state laser, more stable, and easy to duplicate since only standard components are used. Performance comparable to that reported in Ref.[1] is obtained in a much simpler device. The current setup occupies < 0.05 m^3 volume and could be made smaller.

3.3 Conclusion

In conclusion, we have demonstrated amplification of femtosecond pulses from a Yb fiber laser up to 8 nJ (400 mW average power) in single-mode Yb fiber diode-pumped through fiber couplers. Following dechirping, 120-fs, 6 nJ pulses are delivered. We obtain performance similar to that of a bulk solid-state laser by use of a scheme that employs single-mode fiber and diodes only. Equally significantly, this approach can be scaled to higher energies as more powerful pump diodes become available. Energies of 20 nJ at 50 MHz repetition rate can reasonably be expected in the next few years. An all-fiber Yb laser would allow a further level of integration. Recently, 100 fs and 1 nJ pulses have been obtained from a Yb fiber laser that employs a photonic crystal fiber for dispersion control[12]. With this approach, an all-fiber laser can ultimately be constructed of polarization-maintaining fiber and serve as the basis of environmentally stable pulse generation.

BIBLIOGRAPHY

[1] F. Ö. Ilday, H. Lim, J. R. Buckley, and F. W. Wise, Opt. Lett. **28**, 1362 (2003).

[2] M. E. Fermann, A. Galvanauskas, M. L. Stock, K. K. Wong, and D. Harter, Opt. Lett. **24**, 1428 (1999).

[3] D. Anderson, M. Desaix, M. Karlsson, M. Lisak, and M. L. Quiroga-Teixerio, J. Opt. Soc. Am. B **10**, 1185 (1993).

[4] M. E. Fermann, V. I. Kruglov, B. C. Thornsen, J. M. Dudley, and J. D. Harvey, Phys. Rev. Lett. **84**, 6010 (2000).

[5] J. Limpert, T.Schreiber, T. Clausnitzer, K. Zöllner, H.-J. Fuchs, E.-B. Kley, H. Zeller, A. Tünnermann, Opt. Express **10**, 628 (2002).

[6] A. Galvanauskas, M. E. Fermann, and D. Harter, Opt. Lett. **19**, 1201 (1994).

[7] For example, J. Limpert, A. Liem, T. Gabler, H. Zellmer, A. Tünnermann, S. Unger, S. Jetschke, and H. R. Müller, Opt. Lett. **26**, 1849 (2001) and A. Galvanauskas, IEEE J. Selec. Topics Quantum Electron. **7**, 504 (2001).

[8] L. Lefort, J. H. V. Price, D. J. Richardson, G. J. Spühler, R. Paschotta, U. Keller, A. R. Fry, and J. Weston, Opt. Lett. **27**, 291 (2002).

[9] H. Lim, F. Ö. Ilday, F. W. Wise, Opt. Lett. **28** 1 (2003).

[10] D. Strickland and G. Mourou, Opt. Commun. **56**, 219 (1985).

[11] J. W. Nicholson, J. Jasapara, W. Rudolph, F. G. Omenetto, and A. J. Taylor, Opt. Lett. **24**, 1774 (1999).

[12] H. Lim, F. Ö. Ilday, F. W. Wise, Opt. Express **10** 1497 (2002).

Chapter 4

Self-similarly Evolving Parabolic Pulses in a Fiber Laser

In this chapter, we describe the third approach described in this thesis toward the generation of high-energy pulses. The possibility of a fiber laser supporting ultrashort, parabolic pulses propagating self-similarly is demonstrated theoretically and experimentally. Observation of the self-similar pulses in the laser for over 10^{14} cavity periods implies exact stability. In addition to constituting another example of self-similarity arising in nonlinear optics, these results are distinguished from previous reports with the degree of stability. This regime of operation constitutes a new type of pulse shaping applicable to short-pulse lasers which in principle allows scaling to unprecedented pulse energies, removing a fundamental barrier arising from soliton properties.

4.1 Introduction

Self-similarity is a recurring theme in the description of many mathematical and natural phenomena. The emergence of self-similarity in complicated, nonlinear phenomena can be particularly informative about the internal dynamics: Self-similarity arises after the the fine details of initial and/or boundary conditions have faded away, but the system is still far from ultimate state [1]. Furthermore, the presence of self-similarity implies an inherent spatial and/or temporal order which can be exploited in the mathematical treatment of the governing equations to apply reduction of symmetry techniques, effectively reducing the dimensionality

of the system [2]. Self-similar phenomena have been previously reported in nonlinear optics, albeit in a limited number of instances. One example is the theoretical demonstration of self-similar propagation of short pulses with a parabolic intensity profile in optical fibers with normal dispersion and in the presence of a strong nonlinearity [3]. Recently, parabolic pulses have been shown to propagate self-similarly in an optical fiber amplifier with constant gain and normal dispersion theoretically with the technique of symmetry reduction, and experimentally [4]. Later, these results have been generalized to an arbitrary dependency of gain on the propagation distance [5]. Previous experimental observations of self-similar phenomena in nonlinear optics were naturally limited to a small number of characteristic lengths due to practical limitations such as the total fiber amplifier length and achievable total gain. More importantly, we are not aware of any experimental observation of self-similarity in ultrafast optics where the system entailed strong feedback.

In this letter, we demonstrate the first laser to our knowledge to support a pulse that propagate self-similarly in optical fiber which comprises most of the cavity. The pulse assumes a parabolic intensity profile with a linear chirp, and is stable indefinitely. These results constitute experimental observation of self-similar pulse evolution in a system with strong feedback and large fluctuations from other effects that contribute to pulse-shaping. This regime of operation constitutes a new type of pulse shaping, distinct from the well-known soliton [7] and dispersion-managed soliton [8] regimes. From a laser engineering point of view, establishing the possibility of self-similar pulse shaping is exciting since such a laser can, in principle, can be scaled to support unprecedented pulse energies. There is much interest in obtaining high-energy, femtosecond pulses from fiber lasers since fiber lasers have excellent practical features and can potentially become a standard tool

in nonlinear optics.

The operation of lasers producing ultra-short (femtosecond duration) pulses is dominated by an interplay between dispersion and nonlinearity, in the form of soliton dynamics [9]. These pulses are not exact solitons, because the laser cavity constitutes a dissipative system. Hence, their basic features can be understood within the formalism of a complex Ginzburg-Landau equation [6]. Soliton-like dynamics are particularly strong in fiber lasers with cavity lengths corresponding to several soliton periods. The laser cavity comprises of an amplifier fiber with anomalous dispersion and a mechanism for obtaining saturable absorber. The latter is responsible for initiation of pulsed operation from intra-cavity noise, and subsequent stabilization of the pulse. In the steady state, a short pulse propagates in the cavity indefinitely, undergoing small changes in shape, size, and duration, maintaining a balance between dispersion and nonlinearity. Soliton fiber lasers are limited to low pulse energies (100 pJ or less) [7]. At higher energies, the nonlinear effects become excessive, causing wave-breaking [10], which leads to a transition to multiple-pulsing (more than one pulse circulates in the cavity). The pulse can tolerate only a small amount of net nonlinear phase shift ($\Phi^{NL} << \pi$) within one roundtrip before instabilities occur.

Fiber lasers comprising of segments of anomalous (soliton-supporting) and normal (non-soliton-supporting) dispersion have been developed [11], implementing the concept of dispersion management(DM) [12] from optical telecommunications, and supporting the analog of DM solitons. This pulse shaping method has led to the generation of shorter pulses with an order of magnitude higher energy [13].

4.2 Theoretical Results

The propagation of both solitons and DM solitons in non-dissipative environment can be stable for arbitrary lengths. Solitons propagate unchanged, and DM solitons undergo breathing a periodicity matching that of the dispersion map. Therefore, their periodicity is a necessary (not a sufficient) condition for existence within a laser cavity.

In contrast to soliton and DM solitons, parabolic pulses that propagate self-similarly are asymptotic solutions to the governing equation. As such, the evolution of their properties (e.g., the pulse duration) is monotonic. Such a non-static solution cannot satisfy periodic boundary conditions. Additional mechanism is required to completely undo the changes that occur within a cavity period. Another issue must be addressed before self-similarly evolving parabolic pulses can be supported in a laser: The pulses in a laser will, in general, evolve to fill available gain bandwidth. However, self-similar propagation of intense pulses are disrupted if the spectrum of the pulse is clamped by bandwidth limiting effects [14].

Numerical simulations exhibit stable pulse formation over a wide range of parameters. The results of these simulations are compared to a laser supporting DM solitons. The simulations demonstrate that the cavity designed to implement self-similar propagation does not improve the maximum pulse energy in comparison to the stretched-pulse laser when the intra-cavity GVD is anomalous ($\beta_{\text{net}} \lesssim 0$). However, for increasing $\beta_{\text{net}} > 0$ (normal dispersion) the maximum pulse energy diverges dramatically for the two cases (see Fig. 4.1). Qualitatively, if the anomalous-GVD section of the laser has negligible Kerr nonlinearity, the pulse evolves to a parabolic shape that maintains a monotonic chirp even in the presence of strong nonlinearity. The inset of Fig. 4.1 illustrates that the stretching ratio for the laser

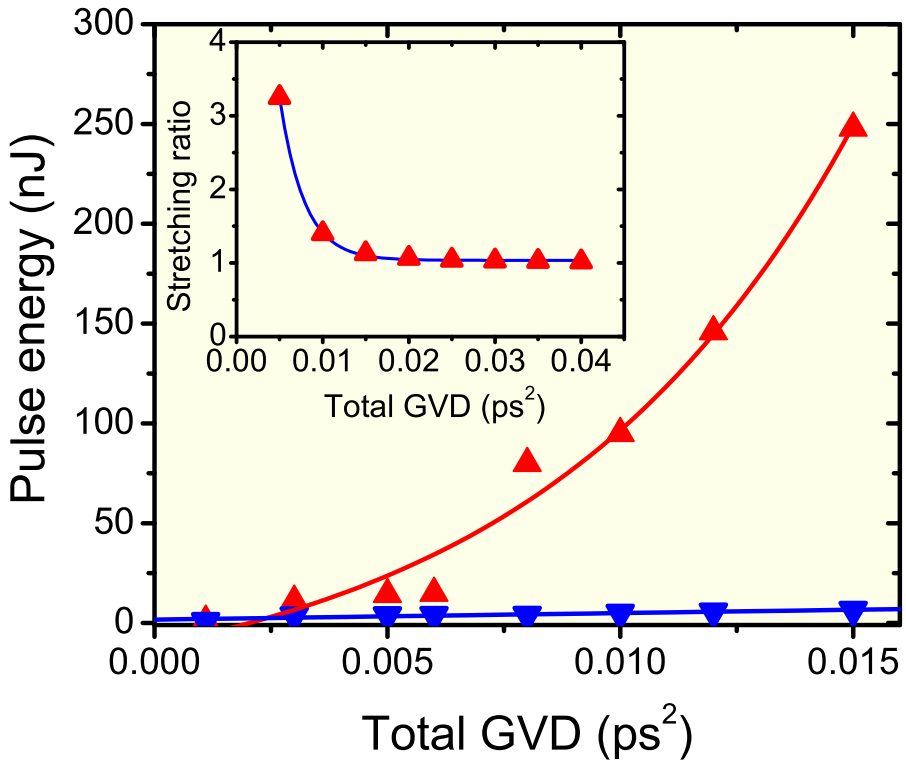

Figure 4.1: Calculated maximum pulse energy vs. total dispersion for the self-similar and stretched-pulse schemes.

with self-similar pulse evolution decreases exponentially at fixed pulse energy as the intra-cavity GVD is increased. Thus, the energy-scaling can be thought of as tolerating (an exponential) increase in pulse energy that maintains a fixed stretching ratio with increasing GVD. The pulse evolution along the cavity is illustrated in a contour plot (Fig. 4.2).

Consider the following conceptual model for a fiber laser that tackles both of these issues: A long stretch of single-mode fiber (SMF) with normal dispersion forms the bulk of the cavity. Amplification is provided by a Yb-doped fiber set to the shortest length possible to provide adequate gain. The pulse experiences negligible dispersion and nonlinearity during amplification, effectively decoupling bandwidth filtering from the self-similar evolution that takes place in the SMF. The gain fiber is followed by a SA mechanism that initiates mode-locking and stabilizes the pulse against small perturbations. The final element is a group delay module that provides anomalous dispersion with negligible nonlinearity. Here, self-similar evolution is confined to the SMF which is the dominant source of nonlinearity. Finally, the gratings compensate for most of the chirp accumulated during self-similar propagation in the SMF. Since the parabolic pulses evolve self-similarly and maintain a (positive) linear chirp, removing the excess bandwidth by filtering in the gain medium and the excess chirp with the anomalous dispersion from the gratings, it is plausible that all changes can be undone at the end of one roundtrip.

Although the scheme described above is suggestive, it is not clear *a priori* that it should work. Lasers are feedback systems, requiring an exact fit of any conceived solution to the constraints imposed by the cavity (periodic boundary conditions). Furthermore, the solution should be a global attractor, for it to be accessible since mode-locked operation should ideally self-initiates from intra-cavity noise.

To address these question, we have constructed a numerical model of the laser, assuming parameters corresponding to the experimental setup which will be discussed below. The cavity is comprised of three main sections. A long segment of SMF ($\sim$ 4 m-long), connected to a gain fiber ($\sim$ 20 cm-long), and a grating-pair to provide anomalous group velocity dispersion (GVD). Propagation within each section is modeled with an extended nonlinear Schrodinger equation

$$\frac{\partial A(\xi,\tau)}{\partial \xi} + i\beta_2 \frac{\partial^2}{\partial \tau^2} A(\xi,\tau) = i\gamma |A(\xi,\tau)|^2 A(\xi,\tau) + g(E_{pulse}) A(\xi,\tau), \tag{4.1}$$

where ξ is propagation coordinate, and τ is time scaled to the pulse width, $\beta_2 = 23 fs^2/mm$ is the GVD, and $\gamma = 0.0047(Wm)^{-1}$ is the effective coefficient of cubic nonlinearity for the fiber section. γ is set to zero for the section providing anomalous GVD, the magnitude of which is adjusted to achieve a desired total dispersion of the cavity. The pulse energy is given by $E_{pulse} = \int_{-T_R/2}^{T_R/2} |A(\xi,\tau)|^2 d\tau$ and $T_R \sim 30$ ns is the cavity roundtrip time, determined by the choice of the fiber lengths. $g(E_{pulse})$ is the net gain which is non-zero only for the amplifier fiber. The gain saturates with total energy according to

$$g(E_{pulse}) = \frac{g_{0,\omega}}{1 + E_{pulse}/E_{sat}}, \tag{4.2}$$

where $g_{0,\omega} \sim 30$ dB is the small signal gain with a parabolic frequency dependence, and a bandwidth of $\sim$ 40 nm is assumed. The effective gain saturation energy, E_{sat}, is set to 0.5 nJ. The SA is assumed to be monotonically-saturating, placed at the end of the fiber section, and it is modeled with a transfer function describing its transmittance

$$T = 1 - \frac{l_0}{1 + P(\tau)/P_{sat}}, \tag{4.3}$$

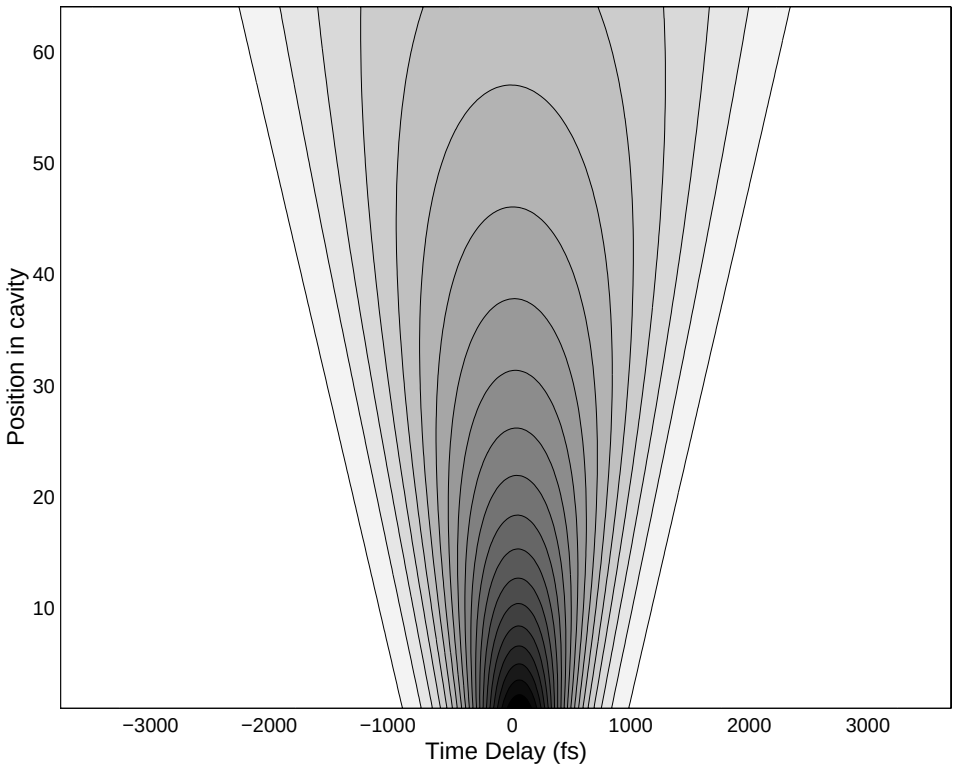

Figure 4.2: Calculated contour plot of the similariton evolution within the cavity.

where T is the transmittance, $l_0 = 0.2$ is the unsaturated loss, $P(\tau)$ is the instantaneous pulse power at the end of the fiber section and $P_{sat} = 2000$ W is the saturation power. The pulse amplitude is scaled down by a factor of ~ 10 after the SA to account for other lumped linear losses as incurred in the experimental setup as described below.

Numerical simulations exhibit stable pulse formation over a wide range of parameters. The results of these simulations are compared to a laser supporting DM solitons. The simulations demonstrate that the cavity designed to implement self-similar propagation does not improve the maximum pulse energy in comparison to the stretched-pulse laser when the intra-cavity GVD is anomalous ($\beta_{\text{net}} \lesssim 0$). However, for increasing $\beta_{\text{net}} > 0$ (normal dispersion) the maximum pulse energy di-

verges dramatically for the two cases (see Fig. 4.1). Qualitatively, if the anomalous-GVD section of the laser has negligible cubic nonlinearity, the pulse evolves to a parabolic shape that maintains a monotonic chirp even in the presence of strong nonlinearity. The inset of Fig. 4.1 illustrates that the stretching ratio for the laser with self-similar pulse evolution decreases exponentially at fixed pulse energy as the intra-cavity GVD is increased. Thus, the energy-scaling can be thought of as tolerating (an exponential) increase in pulse energy that maintains a fixed stretching ratio with increasing GVD. The pulse evolution along the cavity is illustrated in a contour plot (Fig. 4.2).

The numerical simulations strongly suggest that parabolic pulses can exist in such a fiber laser. Furthermore, these simulations predict at least two orders of magnitude improvement in pulse energy over existing lasers at large, normal intra-cavity dispersion. We emphasize that the predicted increases in energy may not be achieved experimentally due to competing effects such as overdriving the SA mechanism. If an interferometric SA such as nonlinear polarization evolution (NPE)[15] is used, there is a trade-off between avoiding overdriving the NPE and ease of self-starting.

4.3 Experimental Results

We have constructed a Yb:fiber laser for experimental confirmation (Fig. 4.3. A ring-geometry is chosen for self-initiation of mode-locking [17]. Here, the Yb fiber can be as short as 23 cm long because of its high doping concentration (23,600 ppm). The short Yb fiber permits decoupling of gain filtering from nonlinear pulse shaping. Pump light is delivered by a wavelength-division multiplexing (WDM) coupler. The pump diode delivers 550 mW into single-mode fiber. The linear

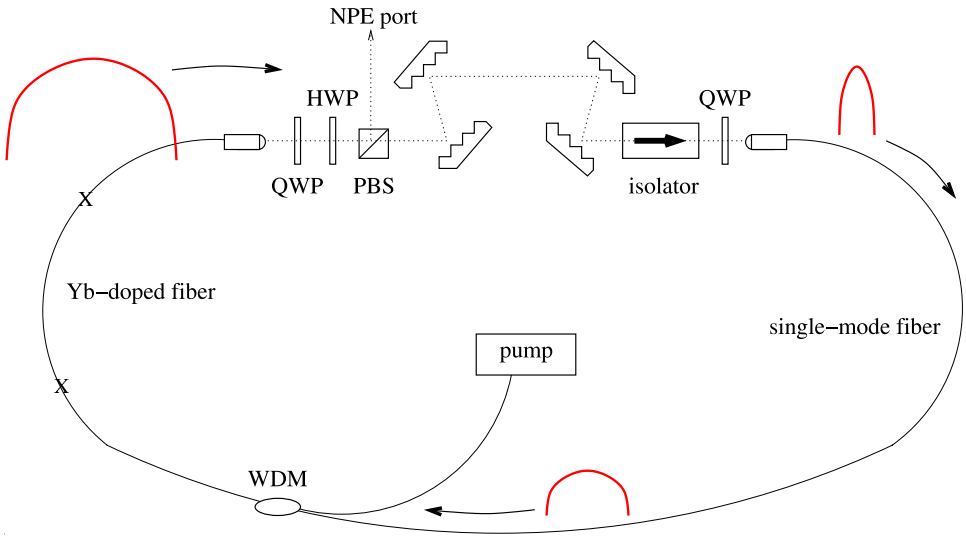

Figure 4.3: Experimental setup: The pulse evolution is indicated.

anomalous-GVD segment is implemented with a pair of diffraction gratings. NPE is implemented as the SA. Mode-locked operation is initiated and stabilized by NPE, and the output is taken from the NPE rejection port. β_{net} of the cavity can be varied by adjusting the grating spacing. Single-pulse operation was verified by monitoring the pulse train with a fast detector ($\sim$ 0.5 ns resolution) and long-range (200 ps) autocorrelation.

The laser mode-locks easily upon the adjustment of the wave-plates for the NPE action. The pulse energy is approximately 2 nJ. Experimental spectrum obtained at $\beta_{\text{net}} > 0.01ps^2$ is presented in Fig. 4.4(a), in comparison the spectrum determined from numerical simulations. The simulations correspond to experimental conditions apart from a much higher pulse energy of 20 nJ. The experiments are performed at low pulse energies to avoid over-driving NPE and minimize the effect of NPE on the self-similar pulse shaping. Separate work is under way to overcome the limitations of NPE. A signature of the self-similar regime is the spectrum,

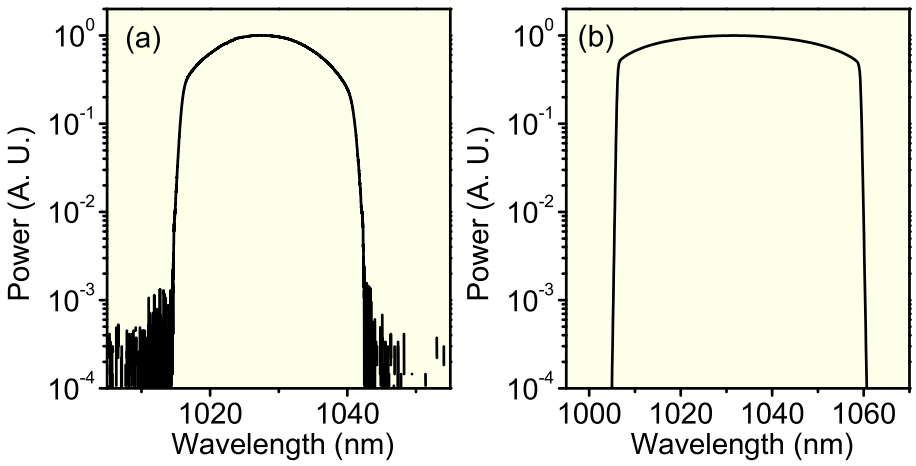

Figure 4.4: (a) Experimentally measured pulse spectrum. (b) Spectrum of the simulated pulses.

which develops the unique shape predicted numerically. This shape is in contrast to that of DM solitons where the spectral shape is approximately a Gaussian [16].

The pulse is extracted from the cavity at a position where it is expected to have maximum positive chirp. Intensity autocorrelation measurement reveals that the pulse duration is $\sim$ 2 ps. After dechirping the pulse with anomalous dispersion in a grating compressor external to the cavity, the inferred full-width at half maximum (FWHM) of the pulse is 70 fs (Fig. 4.5), corresponding to an initial stretching factor of $\sim$ 30. The dechirped pulse duration is close to that of the temporal profile obtained from a Fourier transform of the experimental spectrum, assuming a zero phase. Thus, the chirp of the extracted pulse is inferred to be essentially linear, and the small deviation can be attributed to the presence of third-order dispersion from the gratings. The interferometric autocorrelation of the dechirped pulses shows small amount of secondary structure (inset of Fig. 4.5).

The amount of dispersion required to fully dechirp the pulses is -0.170 ps^2. The

magnitude of dispersion imparted by the gratings within the cavity is -0.150 ps^2 which is not sufficient to completely dechirp the pulse before it is coupled into the SMF. The pulse duration at the beginning of the SMF can be estimated to be approximately 250 fs. Thus, the overall stretching and compression ratio *within* the cavity is ~ 8. The pulse temporally stretches and compresses monotonically in the segments of normal and anomalous dispersion, respectively and maintains a net positive chirp throughout the entire cavity, as expected theoretically. The temporal behavior is in contrast to DM solitons which are stretched and compressed twice per roundtrip and maintain negative and positive chirp for equal portions of propagation time. This change in periodicity of stretching and compression is another signature of the self-similar evolution. Another well-known mode of pulsed operation is pulse shaping through bandwidth filtering in the presence of large normal dispersion. The pulse maintains a positive chirp at all times in this mode of operation as well. However, in this mode the temporal profile is essentially unchanged during propagation. Self-similar operation is distinguished from this mode by the large stretching-compression ratio.

Further support for self-similar nature of the pulse evolution comes from cross-correlation of the chirped and dechirped pulses. Due to the large compression ratio, the dechirped pulse can be approximated as a delta function with respect to the chirped-pulses, exposing the chirped pulse shape from the cross-correlation trace. Figure 4.6 compares the cross-correlation trace to the temporal profile of the chirped pulses obtained from the numerical simulation. Note that good agreement is obtained with the expected parabolic intensity profile.

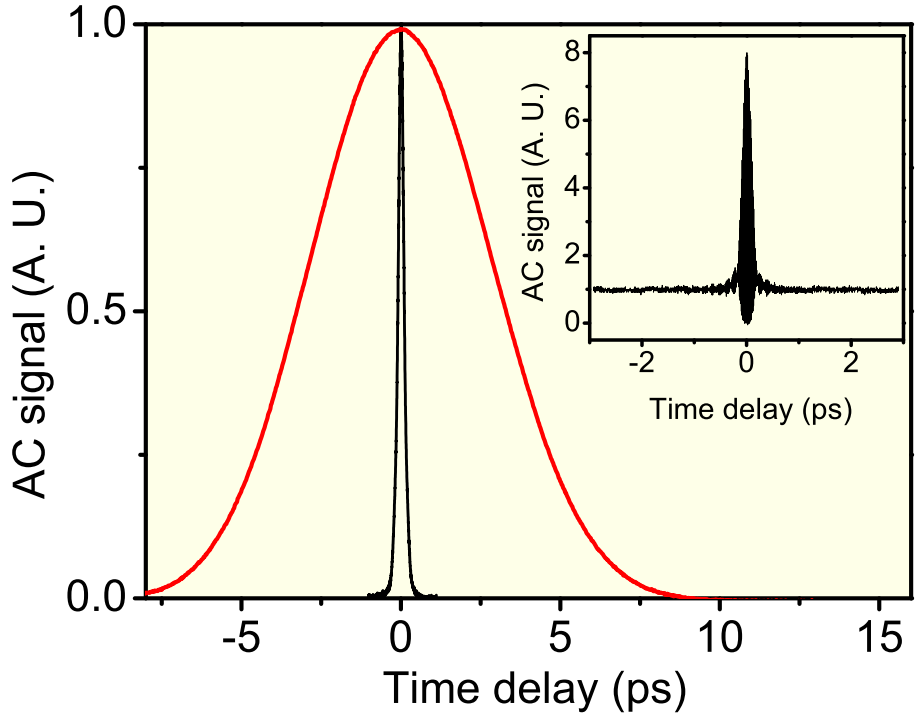

Figure 4.5: Intensity autocorrelation of the chirped and the dechirped pulses. Inset: Interferometric autocorrelation of the dechirped pulses.

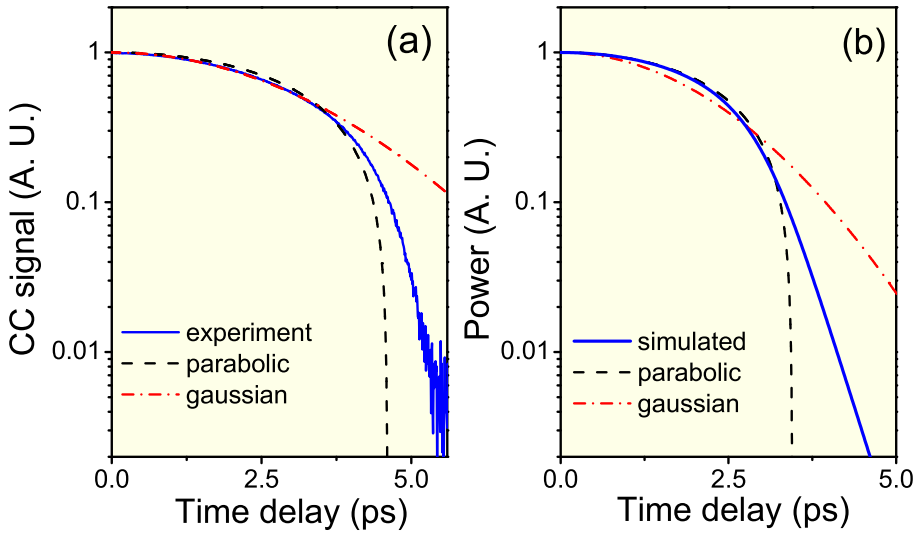

Figure 4.6: (a) Experimentally measured cross-correlation of the chirped and dechirped pulses. (b) Temporal intensity profile of the simulated pulses. Parabolic (dashed lines) and Gaussian (dash-dotted lines) fits are indicated.

4.4 Conclusion

In conclusion, we have shown that self-similarly evolving parabolic pulses with a linear chirp can exist in a fiber laser under appropriate conditions. Experimental observations agree well with the numerical simulations, and this agreement allows us to conclude that pulse energies $\sim$ 100 times larger than those of existing lasers should be possible in the future. This represents a new regime of pulse generation, characterized by monotonic evolution of the pulse in the nonlinear medium, a peculiar spectral shape with sharply decaying wings, and ability to withstand large nonlinearities. We believe that these are the first steps and further developments will be possible. The concept of self-similarity may be the route to the generation of the most energetic femtosecond pulses from a laser, eliminating the limitations of cubic nonlinearity for a generation of femtosecond lasers. The key factor here would be to overcome the limitation posed by overdriving the SA.

BIBLIOGRAPHY

[1] G. I. Barenblatt, *Scaling, Self-similarity, and Intermediate Asymptotics* (Cambridge University, 1996), and P. L. Sachdev, *Self-similarity and Beyond: Exact Solutions of Nonlinear Problems* (CRC, New York 2000).

[2] For example, W. F. Ames, *Nonlinear Partial Differential Equations* (Academic, New York, 1967).

[3] D. Anderson, M. Desaix, M. Karlsson, M. Lisak, and M. L. Quiroga-Teixeiro, J. Opt. Soc. Am. B **10**, 1185 (1993).

[4] M. E. Fermann, V. I. Kruglov, B. C. Thomsen, J. M. Dudley, and J. D. Harvey, Phys. Rev. Lett. **84**, 6010 (2000)

[5] V. I. Kruglov, A. C. Peacock, J. M. Dudley, and J. D. Harvey, Opt. Lett. **25**, 1753 (2000).

[6] For example, N. Akhmediev, J. M. Soto-Crespo, and G. Town, Phys. Rev. E **63**, 056602 (2001), and references therein.

[7] For example, see K. Tamura, C. R. Doerr, H. A. Haus, and E. P. Ippen, IEEE Phot. Tech. Lett. **6**, 697 (1994).

[8] K. Tamura, L. E. Nelson, H. A. Haus, E. P. Ippen, Appl. Phys. Lett. **64** 149 (1994).

[9] H. A. Haus, J. G. Fujimoto, and E. P. Ippen, IEEE J. Quantum Electron., **28**, 2086 (1992).

[10] D. Anderson, M. Desaix, M. Lisak, and M. L. Quiroga-Teixeiro, Opt. Lett. **9**, 1358 (1992).

[11] K. Tamura, J. Jacobson, H.A. Haus, E.P. Ippen, and J.G. Fujimoto, Opt. Lett. **18**, 1080 (1993).

[12] N. J. Smith, N. J. Doran, W. Forysiak, and F. M. Knox, J. Lightwave Technol. **15**, 1808 (1997), and references therein.

[13] L. E. Nelson, S. B. Fleischer, G. Lenz, and E. P. Ippen, Opt. Lett. **21**, 1759 (1996).

[14] A. C. Peacock, R. J. Kruhlak, J. D. Harvey, and J. M. Dudley, Opt. Comm. **206**, 171 (2002).

[15] M. Hofer, M. E. Fermann, F. Harberl, M. H. Ober, and A. J. Schmidt, Opt. Lett. **16**, 502 (1991).

[16] K. Tamura, L. E. Nelson, H. A. Haus, and E. P. Ippen, Appl. Phys. Lett. **64**, 149 (1994).

[17] K. Tamura, J Jacobson, E.P. Ippen, H.A. Haus, and J.G. Fujimoto, Opt. Lett. **18**, 220 (1993).

Chapter 5

50-fs, 5-nJ Pulses at 1.03 μm from a Wave-breaking-free Fiber Laser[1]

This chapter reports the application of the concepts described in the previous chapter to the construction of a high-energy fiber oscillator. We report the generation of 6 nJ chirped pulses from a mode-locked Yb fiber laser at 1.03 μm. A linear anomalous-dispersion segment suppresses wave-breaking effects of soliton-like pulse shaping at high energies. The dechirped pulse duration is 50 fs and the energy is reduced to 5 nJ after dechirping. This laser produces twice the pulse energy and average power, and approximately 5 times the peak power, of the previous modelocked fiber lasers with highest pulse energy, average power and peak power. It is the first fiber laser that directly offers performance similar to solid-state lasers such as Ti:sapphire.

5.1 Introduction

Short-pulse fiber lasers can have wide-spread application as practical alternatives to bulk solid-state lasers, offering compact size, better stability and freedom from misalignment. However, fiber lasers have generated pulses with energies significantly lower than solid-state lasers due to the inherent fiber nonlinearity.

The dynamics of femtosecond pulse formation is dominated by an interplay between anomalous group-velocity dispersion (GVD) and positive Kerr nonlinearity of the fiber [2]. Fiber lasers can be constructed entirely of anomalous-GVD fiber

[1]Most of the results presented in this chapter have been published in Ref. [1]

to operate in the soliton regime, or with segments providing normal-GVD and anomalous-GVD to operate in the stretched-pulse regime[3]. At 1 μm, standard fiber has normal dispersion only. Thus, Nd- and Yb-doped fiber lasers at 1 μm have been constructed with prisms or diffraction gratings to provide the necessary anomalous GVD. Recently, a Yb fiber laser that employs a photonic crystal fiber (PCF) for dispersion control has generated 100 fs and 1 nJ pulses [4]. The highly nonlinear PCF can be expected to present a formidable barrier to higher energies. Stretched-pulse erbium-doped fiber lasers have generated $\sim$ 100 fs, 2.7 nJ pulses, which are the highest pulse energy and peak power from a femtosecond fiber laser [5]. Significant energy resides in the wings of the pulse, which extend to $\sim$ 1 ps. Generation of 50 fs and 1 nJ pulses from a Nd fiber laser has been reported[6]; these pulses have approximately the same peak power as the 2.7-nJ laser. A Yb fiber laser generated 50 fs and 0.7 nJ pulses[7]. The highest average power generated directly from a femtosecond fiber laser is $\sim$ 100 mW [13, 7].

5.2 Theoretical Background

The stretched-pulse technique successfully reduces, but does not eliminate, the effects of nonlinearity through dispersion management. Direct management of nonlinearity has been proposed for substantial increases in pulse energy [8], but has not been demonstrated experimentally. Nonlinearity can limit pulse energy through two mechanisms: (i) Excess energy can result in wave-breaking through the combined effects of dispersion and nonlinearity. (ii) The artificial saturable absorber (SA) can be overdriven at high peak powers, which leads to multiple-pulsing. The former limitation is the more fundamental of the two, which motivates us to explore it.

Here, we recognize the importance of minimizing the Kerr nonlinearity in the anomalous-GVD segment of a stretched-pulse laser designated for maximum pulse energy. We first consider the differences between the extreme cases of nonlinear and completely linear segments of anomalous GVD. The availability of highly-doped Yb fiber enables partial decoupling of gain filtering from the nonlinear pulse shaping. Extensive numerical simulations demonstrate that the limitation to pulse energy through wave-breaking can be suppressed with a linear anomalous-GVD segment and a short gain fiber. We exploit this approach to demonstrate a fiber laser that maximizes the pulse energy and the peak power.

Although it is well-known that soliton-like effects in the anomalous-GVD fiber need to be minimized for best pulse quality[9], it has not been fully-explored experimentally, nor have its implications for the pulse shaping been investigated. We focus on a cavity design similar to that of [6] in order to allow direct comparison to experiment. The oscillator is modeled as comprised of three sections: A section of single-mode fiber (SMF), followed by a short gain section, and a final section with anomalous GVD. Diffraction gratings or a hypothetical fiber (with mode area equal to that of the SMF) provide anomalous GVD for the linear and the nonlinear cases, respectively. For increased computational speed, the SA is modeled with a transfer function, the exact form of which was found not to be important. Pulse propagation is described by an extended nonlinear Schrodinger equation that accounts for the effects of GVD, Kerr nonlinearity and gain for the Yb-doped fiber. Gain in the Yb-doped fiber is modeled as saturating with total energy and has a parabolic frequency dependence with a bandwidth of 40 nm.

The qualitative features of stretched-pulse operation are determined primarily by the total GVD (β_{net}) and to a lesser extent by the length of the normal- and

anomalous-GVD sections. If the gain fiber is sufficiently short, most of the nonlinear shaping occurs in the SMF, decoupled from the bandwidth filtering in the gain fiber. Numerically-simulated cavities with linear and nonlinear segments of anomalous-GVD produce stable pulses with similar energies for $\beta_{\text{net}} \lesssim 0$. However, for increasing $\beta_{\text{net}} > 0$ (normal dispersion) the maximum pulse energy diverges for the two cases. Qualitatively, if the anomalous-GVD section of the laser has negligible Kerr nonlinearity, the pulse evolves to a shape that maintains a monotonic chirp even in the presence of strong nonlinearity [11]. A higher pulse energy generates increased bandwidth, which in turn leads to larger pulse stretching. Increased stretching reduces the peak power, so nonlinear and dispersive effects balance. For instance, at $\beta_{\text{net}} = 0.012$ ps^2 wave-breaking can be avoided at a pulse energy ~ 25 times higher than that of a laser with a nonlinear anomalous-GVD section. A quantitative discussion is beyond the scope of this study and will be presented elsewhere. We emphasize that the predicted increases in energy may not be achieved experimentally due to competing effects such as overdriving the artificial SA. If an interferometric SA such as nonlinear polarization evolution (NPE)[12] is used, there is a trade-off between avoiding overdriving the NPE and ease of self-starting.

5.3 Experimental Results

Following this approach, we built a Yb fiber laser (Fig. 5.1). A unidirectional ring geometry was chosen for self-starting operation [10]. The pump light is delivered by a wavelength-division multiplexing (WDM) coupler. The Yb fiber is only 23 cm long because of its high doping concentration (23,600 ppm). The pump diode delivers 550 mW into single-mode fiber. Mode-locked operation is initiated and stabilized by NPE, and the output is taken from the NPE rejection port [13].

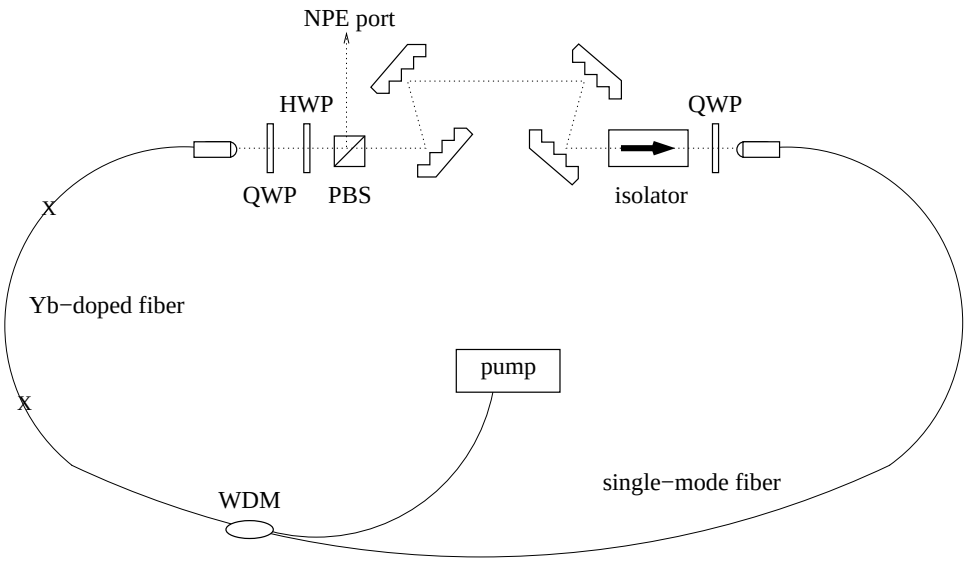

Figure 5.1: Experimental setup. HWP: half-wave plate, QWP: quarter-wave plate, PBS: polarizing beam splitter.

Following the free space section, there is a segment of SMF. β_{net} of the cavity can be varied by adjusting the grating spacing. The laser produces positively-chirped pulses which are dechirped with a grating pair external to the cavity. Single-pulse operation was verified by monitoring the pulse train with a fast detector (~ 0.5 ns resolution) and long-range (200 ps) autocorrelation.

The length of the SMF and β_{net} were varied systematically to optimize pulse energy and peak power. The SMF was initially chosen to be 3.5 m long (50 MHz repetition rate). The pulse energy could be increased while β_{net} was reduced from an initial value of -0.020 ps^2. At $\beta_{\text{net}} = 0.001 \pm 0.002$ ps^2, the pulse energy reached 4.5 nJ, limited by the pump power. The dechirped pulse duration was 70 fs.

In order to determine the maximum pulse energy, the repetition rate was lowered to 40 MHz by increasing the length of the SMF by 1 m. For the same β_{net}, pulse energy could not exceed 4.1 nJ. Therefore, β_{net} was increased. The

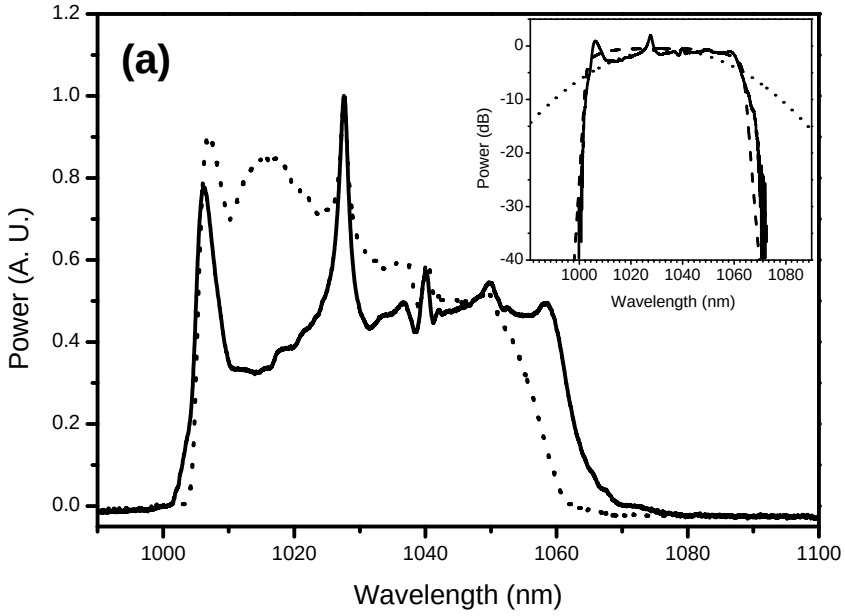

Figure 5.2: Spectra of the pulse from the NPE rejection port (solid line) and of the pulses from a reflection off a diffraction grating (dashed line). Inset: Experimental (solid line), calculated (dashed line) spectra and a gaussian fit (dotted line) plotted on logarithmic scale.

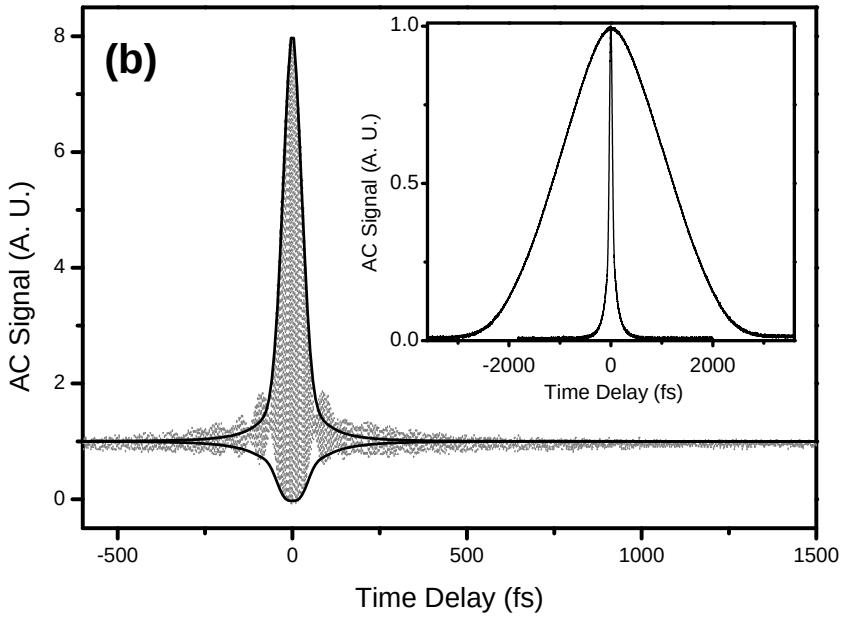

Figure 5.3: Experimental (full trace) and calculated (envelopes only) interferometric autocorrelations of the dechirped pulses. Inset: Intensity autocorrelation of the pulses directly from the oscillator in comparison to that of the dechirped pulses.

maximum pulse energy of $\sim$ 6 nJ (235 mW average power) was obtained at $\beta_{\text{net}} = 0.004 \pm 0.002$ ps^2. The corresponding power spectra from the NPE port and a beam reflected from the first grating are shown in Fig. 5.2. The pulse energy exiting the Yb fiber was determined to be $\sim$ 7.5 nJ and the energy of the pulse coupled into the SMF was estimated as $\sim$ 0.3 nJ. With this information, accurate numerical simulations using experimentally-determined parameters could be performed. The spectrum produced by the numerical simulations agrees with the experimental spectrum (inset of Fig. 5.1). The wings of the spectrum decay faster than those of a gaussian pulse, which describes the pulse shape for a typical stretched-pulse laser with a nonlinear anomalous-GVD section [14].

The interferometric autocorrelation of the dechirped pulses is presented in Fig. 5.3 along with the autocorrelation of the simulated pulses. The inferred pulse duration is 50 fs. Comparison of the intensity autocorrelations before and after dechirping reveals a compression factor of 30 (inset of Fig. 5.3). The dechirped pulse energy is 5 nJ, owing to loss at the grating compressor. Overall, the pulse energy and average power obtained directly from the laser are improved by factors of 2.0 and 2.3, respectively, in comparison to [4]. The peak power is ~ 80 kW, improved by ~ 5 times over previous top-performance fiber lasers[13, 6]. In addition, the laser is more practical than the previous top-performance lasers because it is diode-pumped with a WDM coupler.

The pulse energy was limited not by pump power, but by the onset of double-pulsing. According to our calculations, at least an order of magnitude higher pulse energies should be possible by increasing β_{net}. Experimentally, mode-locking becomes difficult for $\beta_{\text{net}} > 0.004$ ps^2. Increasing the SMF length by 2 m did not enable operation at larger β_{net}. We conclude that the pulse energy is currently limited at 6 nJ and we attribute the difficulty to modelock at larger β_{net} to failure of the NPE action.

5.4 Conclusion

In conclusion, we have demonstrated a Yb fiber laser that generates the highest pulse energy, peak power and average power of any modelocked fiber laser. Its efficiency is 43%, which is the highest of any short-pulse laser, to our knowledge. The improvements in pulse energy and peak power are possible through the avoidance of soliton-like effects in the anomalous-GVD segment and by partially decoupling gain filtering from nonlinear pulse shaping. Preliminary observations and calcu-

lations indicate that this device may be a first step toward a laser that supports self-similar pulses[15, 16, 17]. Work is in progress regarding this exciting possibility. The stability of the laser is similar to that of the all-fiber stretched-pulse Er lasers in our laboratory. We attribute the high stability to diode-pumping with a WDM and the existence of fewer modelocking regimes due to the linearity of the anomalous-GVD section. Fiber lasers with bulk components can thus be viewed as a class of devices that offers performance comparable to bulk solid state lasers with nearly all of the advantages of stability and compactness of "all-fiber" lasers.

BIBLIOGRAPHY

[1] F. Ö. Ilday, H. Lim, J. R. Buckley, and F. W. Wise, Opt. Lett. **28** (2003).

[2] H. A. Haus, J. G. Fujimoto, and E. P. Ippen, IEEE J. Quantum Electron. **28**, 2086 (1992).

[3] K. Tamura, J. Jacobson, H.A. Haus, E.P. Ippen, and J.G. Fujimoto, Opt. Lett. **18**, 1080 (1993).

[4] H. Lim, F. Ö. Ilday, and F. W. Wise, Opt. Express **10**, 1497 (2002), http://www.opticsexpress.org.

[5] L. E. Nelson, S. B. Fleischer, G. Lenz, and E. P. Ippen, Opt. Lett. **21**, 1759 (1996).

[6] M. H. Ober, M. Hofer, and M. E. Fermann, Opt. Lett. **18**, 367 (1993).

[7] H. Lim, F. Ö. Ilday, and F. W. Wise, Opt. Lett. **28**, 660 (2003).

[8] F. Ö. Ilday, and F. W. Wise, J. Opt. Soc. Am. B **19**, 470 (2002).

[9] For example, see K. Tamura, E. P. Ippen, and H. A. Haus, Appl. Phys. Lett. **67**, 158 (1995).

[10] K. Tamura, J Jacobson, E.P. Ippen, H.A. Haus, and J.G. Fujimoto, Opt. Lett. **18**, 220 (1993).

[11] D. Anderson, M. Desaix, M. Lisak, and M. L. Quiroga-Teixeiro, Opt. Lett. **9**, 1358 (1992).

[12] M. Hofer, M. E. Fermann, F. Harberl, M. H. Ober, and A. J. Schmidt, Opt. Lett. **16**, 502 (1991).

[13] K. Tamura, C.R. Doerr, L.E. Nelson, H.A. Haus, and E.P. Ippen, Opt. Lett. **19**, 46 (1994).

[14] K. Tamura, L. E. Nelson, H. A. Haus, and E. P. Ippen, Appl. Phys. Lett. **64**, 149 (1994).

[15] D. Anderson, M. Desaix, M. Karlsson, M. Lisak, and M. L. Quiroga-Teixeiro, J. Opt. Soc. Am. B **10**, 1185 (1993).

[16] M. E. Fermann, V. I. Kruglov, B. C. Thomsen, J. M. Dudley, and J. D. Harvey, Phys. Rev. Lett. **84**, 6010 (2000)

[17] V. I. Kruglov, A. C. Peacock, J. M. Dudley, and J. D. Harvey, Opt. Lett. **25**, 1753 (2000).

[18] F. Ö. Ilday, J. R. Buckley, H. Lim, F. W. Wise, and W. G. Clark, Opt. Lett. **28** 1635 (2003).

Chapter 6

Period-doubling Route to Multiple-pulsing

6.1 Introduction

In this chapter, we present a new approach for describing high-energy operation of soliton-like laser with a fast artificial saturable absorber (SA) that has a multi-modal dependence of transmittance on pulse energy. Multi-modal transmittance is typical of fast SA since these mechanisms are based on the conversion of relative nonlinear phase differences between two modes to amplitude modulation through interference. In the previous chapters, the focus was on maintaining the stability of a pulse at the highest possible energies against wave-breaking, and the limitation to pulse energy arising from soliton-like pulse shaping have been described in detail. The utilization of self-similarity and nonlinearity management in principle remove this limitation, suggesting that unprecedented pulse energies can be obtained. However, the potential for two orders of magnitude improvement in pulse energy as promised by nonlinearity management and self-similar pulse shaping (and possibly more, through a proper unification of the two separate, but compatible approaches) will not fully materialize unless over-driving the SA is prevented. Therefore, a detailed understanding of transition to multiple-pulsing through over-driving the SA can be invaluable.

Here, we present a theoretical and experimental study of over-driving the SA of an energetic, soliton-like fiber laser. The SA has a sinusoidal dependence of transmittance on intensity: The loss initially saturates with increasing intensity,

promoting pulse formation, but this trend is reversed at much higher intensities, finally destabilizing the pulse. The theoretical expectations are experimentally confirmed, with profound implications on the dynamics of a fiber oscillator.

In addition to the direct relevance to constructing high-energy fiber lasers, we note the ease with which various features characteristic of nonlinear dynamical systems can be observed repeatably in fiber lasers. This suggests that fiber oscillators can be an attractive experimental platform for studying various phenomena in nonlinear dynamical systems with a simple, inexpensive system.

6.2 Overdriving the Saturable Absorber

Over-driving of the saturable absorber (SA) mechanism as a limitation to pulse energy in fiber oscillators has its origins in that fast saturable absorbers with a large modulation depth and suitable for use in fiber lasers are all interferometric in origin [1]. The most commonly used techniques are nonlinear polarization evolution (NPE) [2], nonlinear optical loop mirrors (NOLM) [3], and their variants. In each case, the pulse energy is distributed to two modes with unequally. Thus, the two modes acquire a relative nonlinear phase shift upon propagation in a nonlinear medium (typically a fiber). The magnitude of the phase difference is then proportional to the pulse energy. The phase difference is converted into amplitude modulation by a proper superposition of the two modes. In the case of NPE, this is accomplished through a linear polarizer acting on right- and left-circular polarization modes. In the case of a NOLM, the two modes are pulses counter-propagating through a fiber loop, and conversion to amplitude modulation takes place at a fiber coupler that serves as the entry and exit port of the fiber loop. As a result of their interferometric nature, these techniques are sinusoidal functions

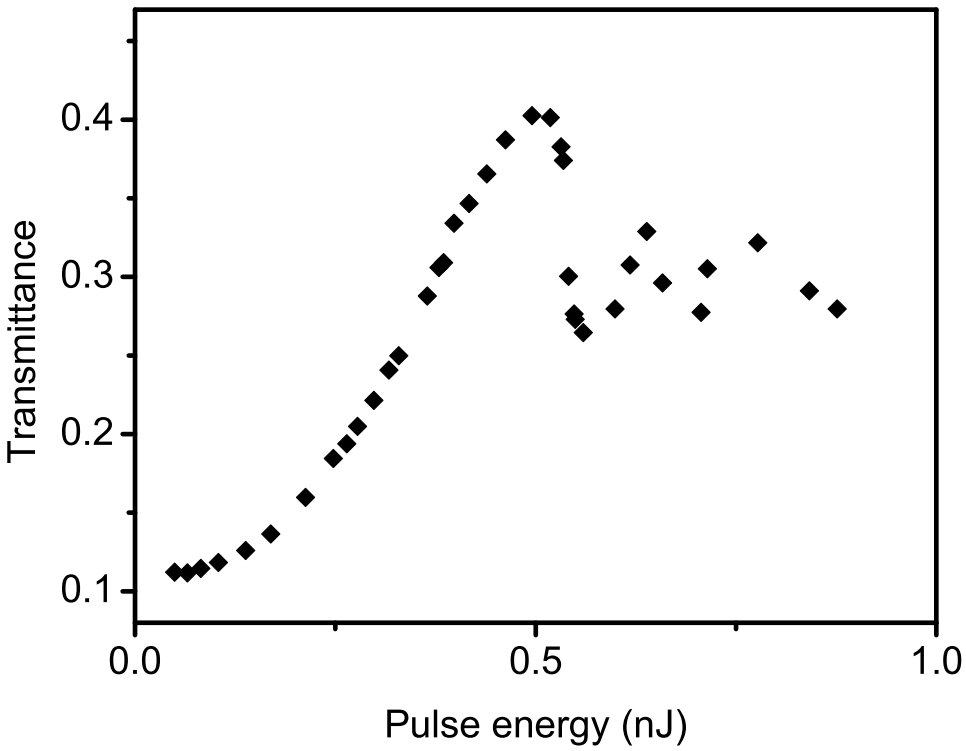

Figure 6.1: Experimentally-measured transmittance of a typical NOLM for operation at 1550 nm.

of the pulse energy. Hence, the loss of the SA begins to diminishes and finally increases as the pulse energy is increased. Figure 6.1 illustrates experimentally measured transmittance of a NOLM.

We define the peak intensity (or energy, for given pulse shape) corresponding to the point of maximum transmittance through the SA to the over-driving intensity/energy. Beyond this value transmittance begins to decrease, promoting lower peak intensity for the pulse. The over-driving energy can be increased with proper linear biasing (Fig. 6.2), or by decreasing the energy difference between the interfering modes. However, these changes result in decreasing transmittance for increasing intensity, or an overall reduction of the transmittance at low intensities,

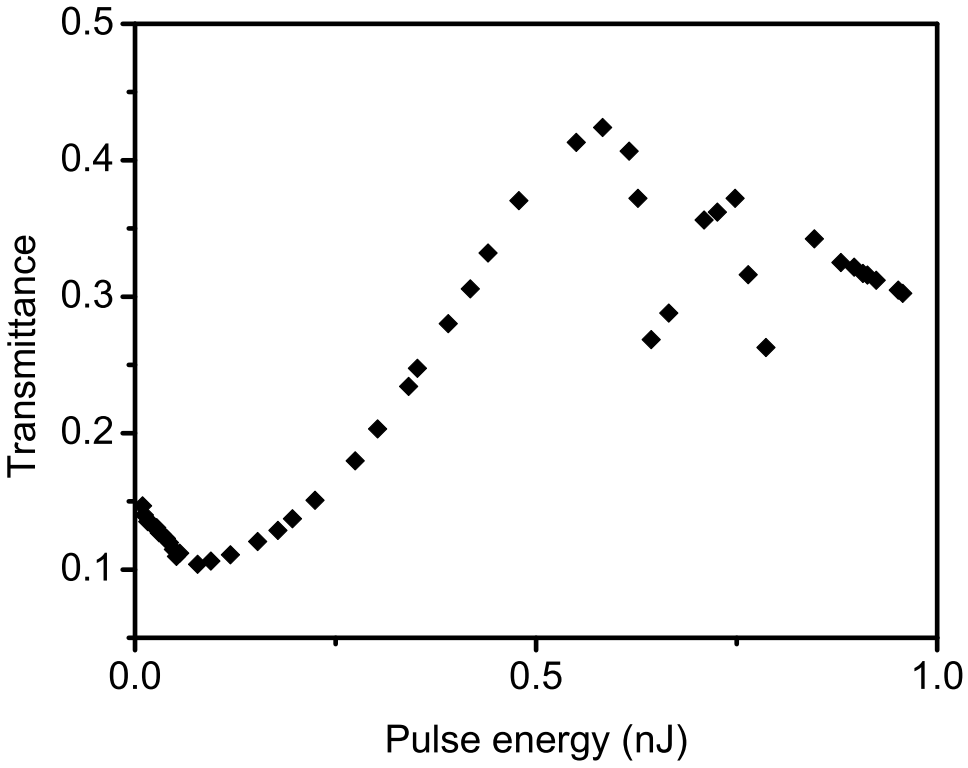

Figure 6.2: Experimentally-measured transmittance of a typical NOLM for operation at 1550 nm, biased for operation at higher pulse energies.

respectively. Either way, initiation of mode-locking from intra-cavity noise becomes difficult, if not impossible. Self-starting operation is an essential feature for practical utility, rendering these approaches unacceptable for most applications.

6.3 Theoretical Model

In this section we develop a basic model for a soliton-like laser mode-locked with a non-monotonic, fast saturable absorber exhibiting multiple transmission maxima. We will use this model to obtain an equation for the pulse energy evolution. The model will be loosely based on soliton fiber lasers, but many of the results should apply to other types of lasers, in particular to dispersion-managed and self-similar

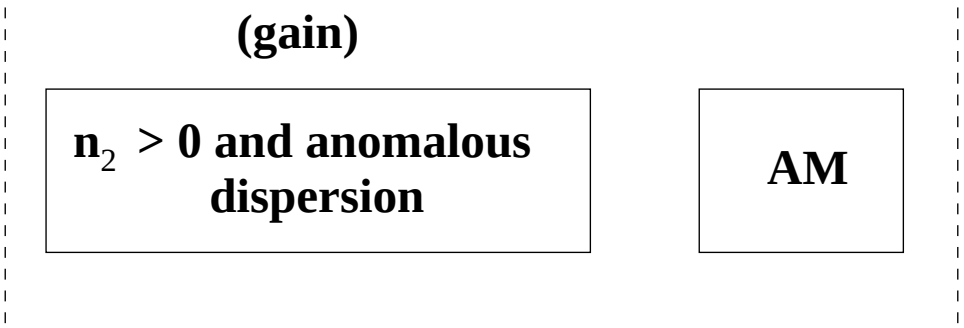

Figure 6.3: Block diagram of a generic soliton-like laser consisting of an optical medium with positive Kerr nonlinearity, anomalous GVD, and gain and a fast SA.

fiber lasers. A block diagram of the model laser cavity is presented in Fig.6.3.

For simplicity, we consider the optical medium to be a single-mode fiber providing uniformly-distributed Kerr nonlinearity ($n_2 > 0$) and anomalous GVD. Generalization of this approach to a dispersion-managed scheme where at least two segments of fiber with normal and anomalous GVD should be possible based on the formalism developed by the MIT group [6].

Pulse propagation through the fiber segment is modeled with the nonlinear Schrödinger equation:

$$T_R \frac{\partial}{\partial T} a(T,t) = -iD_s \frac{\partial^2 a(T,t)}{\partial t^2} + i\delta |a(T,t)|^2 a(T,t) + (g - l_0 - D_g \frac{\partial^2}{\partial t^2}) a(T,t). \quad (6.1)$$

Here, $a(T,t)$ is the slowly-varying pulse envelope, t is a time scale in the order of the pulse duration. The propagation direction is parametrized by $T = z/c$, a time scale in the order of the cavity roundtrip time T_R, instead of the usual z in analogy to the master equation for mode-locking developed by Haus [4]. D_s is the intra-cavity GVD, $D_g = g/\Omega_g^2$ is the gain dispersion. Ω_g^2 is the half-width at half maximum (FWHM) gain bandwidth. The coefficient for self-phase modulation (SPM) arising from the Kerr nonlinearity is $\delta = (2\pi)/(\lambda_0 A_{eff}) n_2 L_{eff}$, where n_2

is intensity-dependent refractive index, A_{eff} and L_{eff} are the effective mode area and path length of the fiber segment, respectively, and λ_0 is the center wavelength of the pulse. g is the gain coefficient and l_0 is the linear intra-cavity loss, including loss due to output coupling.

We assume a gain medium with relaxation time much longer than T_R and a large saturation energy which is a good approximation for the case of Er- and Yb-doped fibers serving as the gain media. Therefore, the gain is saturated by a series of pulses (multiple cavity roundtrips), determined primarily by the average intra-cavity power. The dynamic gain saturation within the duration of an individual pulse is ignored. Hence, the gain obeys the average-rate equation

$$T_R \frac{\partial g(T,E)}{\partial T} = -(g(T,E) - g_0)\frac{T_R}{T_G} - g(T,E)\frac{E_p}{E_g}. \tag{6.2}$$

Here, g_0 is the small signal gain, E_g is the saturation energy of the gain medium, T_G is the gain relaxation time. The pulse energy, E_p, is given by

$$E_p = \int_{-T_R/2}^{T_R/2} |a(T,t)|^2 dt. \tag{6.3}$$

The treatment outlined so far is similar to Haus' the master equation, with the only notable exception being the absence of the self-amplitude modulation term, corresponding to the SA. Instead, we treat the SA action as a lumped effect following propagation in the fiber segment. The main difference of this treatment from the master equation and similar treatments is that we do *not* make the assumption that nonlinear losses resulting from the SA is small. All methods of SA action in fiber lasers act on the pulse in a discrete manner at a well-defined location in the cavity, as opposed to the approximately uniformly-distributed Kerr-lensing effect relevant to bulk solid state lasers. Changes in the pulse energy can be extremely large, Ref. [5] reports a fiber laser incorporating NPE as the SA and transmitting

only 20% of the incident pulse energy. We have observed transmittance values as a low as 5% through the NPE port in an Er-doped fiber laser constructed in our laboratory. Although part of the loss in these cases is linear output coupling, the modulation depth is still very large, in order of 50%, as the indicated by the measurements made exterior to the cavity (for example, see Fig. 6.1). NPE is chosen as the SA mechanism because it is the most commonly-used technique. However, the methods and the results described here can easily be generalized to apply other techniques such as NOLMs.

In soliton lasers, the dominant pulse-shaping mechanism is the soliton formation [4, 7]. One can make a stronger statement in this direction for fiber lasers, considering that a femtosecond fiber laser typically incorporates at least several soliton periods within one roundtrip. This is the main assumption of this treatment, that the combined effects of dispersion and Kerr nonlinearity determine the pulse shape. In the steady-state the pulse shape within the fiber segment can be expressed as

$$a(T,t) = \sqrt{E_p}u(t)exp(i\theta(T)). \tag{6.4}$$

For a soliton laser, the pulse shape is given by

$$u(t) = \sqrt{\frac{1}{2\tau}}sech(\frac{t}{\tau}), \tag{6.5}$$

and the phase shift acquired by the soliton is

$$\theta(t) = \frac{D_s}{\tau^2}\frac{T}{T_R}. \tag{6.6}$$

Here, τ is the pulse width and is related to the FWHM pulse width by $\tau_{FWHM} = 1.76\tau$. Since the existence of a soliton is through the balance of the dispersive effects with the Kerr nonlinearity, the width and the energy of a soliton are related

by

$$\tau = \frac{4|D_s|}{\delta E_p}. \tag{6.7}$$

In the case of pulse shape being maintained as a soliton, the transmittance of NPE can be expressed as a transfer function. For long, square pulses the transmittance, T, of NPE has been shown [8] to be of the form

$$T = E_{out}/E_{in} = \frac{1}{2}(1 - q\cos(\pi I/I_{sw} + \phi_0)), \tag{6.8}$$

where E_{in}, E_{out} are the incident and the transmitted energies, respectively, q is a parameter characterization the modulation depth, ϕ_0 accounts for a linear bias, and I_{sw} is the switching intensity beyond which the transmittance begins to decrease for the case of $\phi_0 = 0$.

The pulse shape after being modified by the NPE action is given by

$$a(T,t)_{NPE} = \frac{1}{2}\sqrt{E_p}\{1 - q\cos[\pi\frac{E_p}{2\tau}\frac{1}{I_{sw}}sech(t/\tau) + \phi_0]\}, \tag{6.9}$$

for the case of a soliton as the incident pulse shape. In general, NPE can significantly alter the shape of the soliton, but all information of this modification will be erased by the soliton dynamics by the end of another pass through the fiber segment. Numerical simulations indicate that this assumption retains its validity for strong strong dynamics (at least several soliton periods within one roundtrip) even for quite deep modulation ($q \sim 0.5$).

It is necessary to allow for large changes in pulse energy, E_p and the gain to be able to compensate for it because deep modulation by the SA is permitted. It can be shown formally that increase of E_p during propagation through the gain fiber is equivalent to a ramping up of the SPM, δ. A similar scenario occurs in optical communications when the slow decrease in pulse energy upon propagation in the fiber link is compensated by a gain module. The effects of a non-constant pulse

energy on the soliton propagation have been analyzed [9]. For pulses that are not excessively short, the soliton adapts to the changes adiabatically. It is a reasonable approximation, then, that the pulse shape will continue to be determined by the soliton dynamics even in the presence of large energy fluctuations.

In the case of fiber lasers as described previously in this thesis, even this assumption is not necessary since the gain fiber is much shorter in length in comparison to the total length of the fiber segment (typically a 20 cm-long Yb fiber is part of a 4 m-long fiber segment). Hence, the SPM and the dispersion experienced by the pulse within the gain fiber is negligible compared to the rest of the cavity and the amplification processes can be considered to be occurring abruptly (lumped amplification).

Finally, the following picture emerges for the evolution of the pulse according to this model. The ordering of the three functions, soliton pulse shaping, amplification, and NPE action, respectively is chosen to correspond to that of actual fiber lasers, but the exact order only effects some of the details of pulse evolution. Propagation through the fiber segment corresponds to that of a soliton,

$$T_R \frac{\partial}{\partial T} a(T,t) = -iD_s \frac{\partial^2 a(T,t)}{\partial t^2} + i\delta |a(T,t)|^2 a(T,t). \tag{6.10}$$

In the steady state, the launched field, $a(0,t)$ is assumed to be sufficiently to close a soliton solution that it will be shaped into one, with some E_p and τ upon propagation. We have ignored losses due to bandwidth filtering which are small for fiber lasers with pulse duration more than 100 fs. The emerging soliton will be amplified in the short gain fiber

$$a(L_{eff},t) = a(L_{eff} - L_{gain},t)\sqrt{g(T,E)L_{gain}}, \tag{6.11}$$

where $L_{gain} << L_{eff}$, and SPM and dispersion in the gain fiber is ignored. $g(T,E)$

is given by Eqn. 6.2. After amplification, the pulse is subjected to NPE action as described by Eqn. 6.9.

In what follows, we consider the evolution of the pulse energy. The treatment is similar to that of Ref. [10, 11]. Because amplification is now decoupled from the soliton propagation, it is trivial to recognize that the pulse shaping in the undoped fiber does not alter the pulse energy. Transmittance through NPE can be shown to alter the pulse energy according to the following *each roundtrip*

$$E_{p,out} = \frac{1}{2} E_{p,in} \int_{-T_R/2}^{+T_R/2} u^2(t)(1 - q\cos(\pi \frac{E_{p,in}}{2\tau I_{sw}} u^2(t) + \phi_0)dt. \tag{6.12}$$

$E_{p,in}$ and $E_{p,out}$ are the incident and the transmittance pulse energies, respectively. The pulse energy after amplification is given by

$$E_{p,out} = E_{p,in} g(T, E_{p,in})/l_0, \tag{6.13}$$

where $E_{p,in}$ and $E_{p,out}$ are the pulse energies before and after amplification, respectively. The linear loss, l_0 is imparted following amplification. In experimental systems, linear loss stems predominantly from coupling in and out of fiber and output coupling. The gain, $g(T, E_{p,in})$ varies on a time scale of several roundtrips, T_R and according to the incident pulse energy.

Eqn. 6.12, together with Eqn. 6.13 completely specify the evolution of the pulse energy in a soliton fiber laser mode-locked with NPE. Large changes in pulse energy due to NPE and gain are allowed and the main assumption made is that soliton dynamics are strong and robust enough that the information of modifications on the pulse shape by NPE is erased within one roundtrip.

6.4 Period-doubling in Fiber Oscillators

In this section, the dynamics of the pulse energy evolution is studied. The primary focus will be on the dynamics in the presence of deep modulation by the NPE action. In this case, large changes in pulse energy occur within each roundtrip and the gain will respond accordingly. The temporal gain dynamics is on the time scale of many roundtrips and as such it will not be able to provide dynamic response to these changes. Furthermore, our interest is in the steady state, even though that the steady state may correspond to a periodicity of more than one roundtrip, as will be shown below. The steady stationary value of the gain on a time scale of T_R is

$$-(g_s(E_p) - g_0)\frac{T_R}{T_G} - g_s(E_p)\frac{E_p}{E_g} = 0. \tag{6.14}$$

Eqn. 6.14 requires

$$g_s(E_p) = \frac{g_{net,0}}{1 + \frac{E_p}{E_{sat}}}, \tag{6.15}$$

where $g_{net,0} = g_0/l_0$, and $E_{sat} = E_g\frac{T_R}{T_G}$ has been introduced for brevity of notation.

Transmittance through NPE, $T(E_{p,in}) = E_{p,out}/E_{p,in}$ can be calculated from Eq. 6.12. While an exact evaluation of the integral is not possible, the integral can be easily evaluated numerically. Figure 6.4 displays transmittance for $q = 0.50$ as a function of the soliton energy in arbitrary units. The general form of the transmittance is a slowly-decaying sinusoidal. For most of what follows, the neighborhood of the first transmission peak is of main interest. Therefore, for simplicity, the transmitted pulse energy can be approximated as

$$E_{p,out} = \frac{1}{2}E_{p,in}[1 - q'\cos(\pi\frac{E_{p,in}}{E_{sw}} + \phi_0)]. \tag{6.16}$$

Here q', order of q, is a modified parameter for the modulation depth and E_{sw},

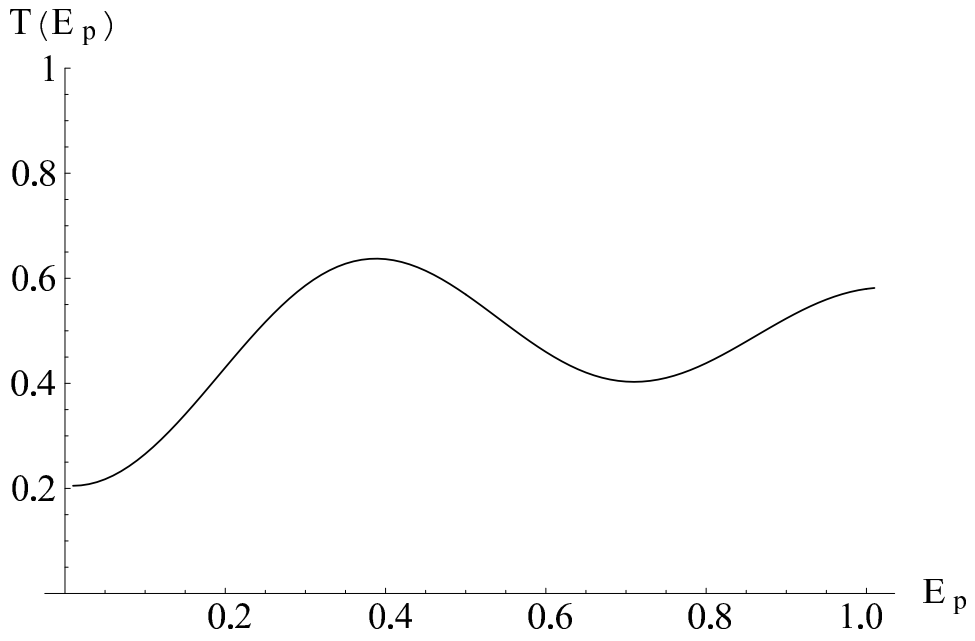

Figure 6.4: Numerically-evaluated transmittance of NPE for a soliton as a function of pulse energy for $q = 0.50$. The energy scale is arbitrarily chosen.

order of $1/(2\tau I_{sw})$, characterizes the soliton energy corresponding to the first transmission peak.

The evolution equation for the pulse energy can be determined from Eq. 6.16 and Eq. 6.15. Let $E_{p,n}$ denote the soliton energy at the conclusion of roundtrip n. Then, assuming commutation for the gain and NPE actions for simplicity of the expression (an exact calculation does not alter the main results to be presented below), a difference equation describing the energy evolution for successive roundtrips is obtained

$$E_{n+1} = \frac{1}{2}\frac{g_{net,0}}{1 + E_n/E_{sat}}[1 - q'\cos(\pi E_n + \phi_0)]E_n \tag{6.17}$$

where the subscript p has been dropped for simplicity and the energy has been normalized to E_{sw} without loss of generality by the transformation $E_n \rightarrow E_n.E_{sw}$.

Eq. 6.17 represents a four-parameter ($g_{net,0}$, E_{sat}, q', and ϕ_0) family of nonlinear

difference equations. The saturating gain ensures that E_n remains finite for $n \to \infty$. However, the non-monotonic part corresponding to the nonlinear loss of NPE heralds complicated dynamics. A formal solution is not possible for the general case, consequently we evaluate Eq. 6.17 numerically.

For the rest of this section, we focus on the case of zero linear bias for the NPE action ($\phi_0 = 0$). The net gain, $g_{net,0}$, is a parameter that determines the self-starting condition and the rate of change in pulse energy. Therefore, we set $g_{net,0} = 3.5$ for most of what follows, which is a reasonable choice for fiber lasers. These choices reduce the free parameters to two, the modulation depth q' and the gain saturation energy, E_{sat}. The latter one is the parameter that is most conveniently controlled in the experiments by adjusting the pump power delivered to the gain fiber. Thus, it is natural to investigate the dependence of the steady state pulse energy on E_{sat} for different modulation depths.

For a small modulation depth of $q' = 0.1$, the steady-state solution to Eq. 6.17 is shown in Fig. 6.5. The transmittance of NPE is also plotted for comparison. At this low modulation depth operation slightly beyond the first peak of transmission is possible. For higher pump powers (increasing E_{sat}), the steady-state solution moves to the vicinity of the second peak. At even higher pump powers (not shown) the system finally destabilizes and the pulse energy does not converge. However, the modulation depth is too low for it to correspond to actual fiber lasers. A low modulation depth results in two problems, initiation of mode-locking from intra-cavity noise is more difficult and the parameter range for stable operation is significantly contracted. For instance, ideally $g_{net,0}$ has to assume a lower value for this modulation depth: Even for vanishing pulse energy, there is net gain ($E_{n+1}/E_n > 0$), which means that the continuous-wave solution is stable and mode-

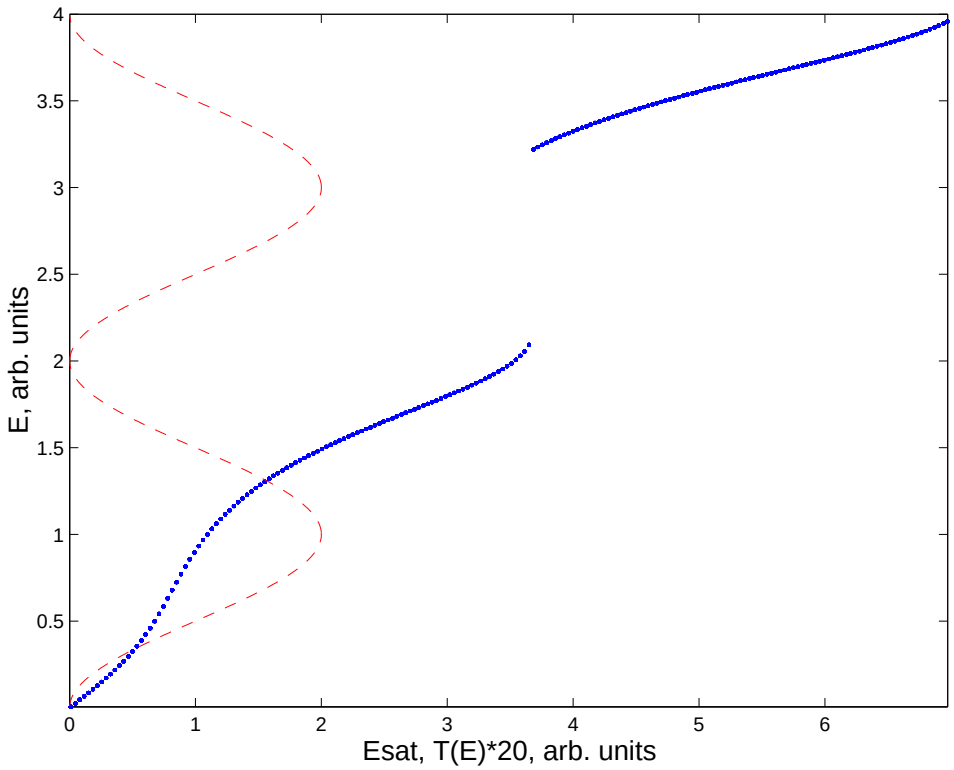

Figure 6.5: The steady-state pulse energy (E) as a function of E_{sat} (corresponding to pump power) for $q' = 0.1$. Also shown is the NPE transmittance curve for the pulse energy on the vertical axis.

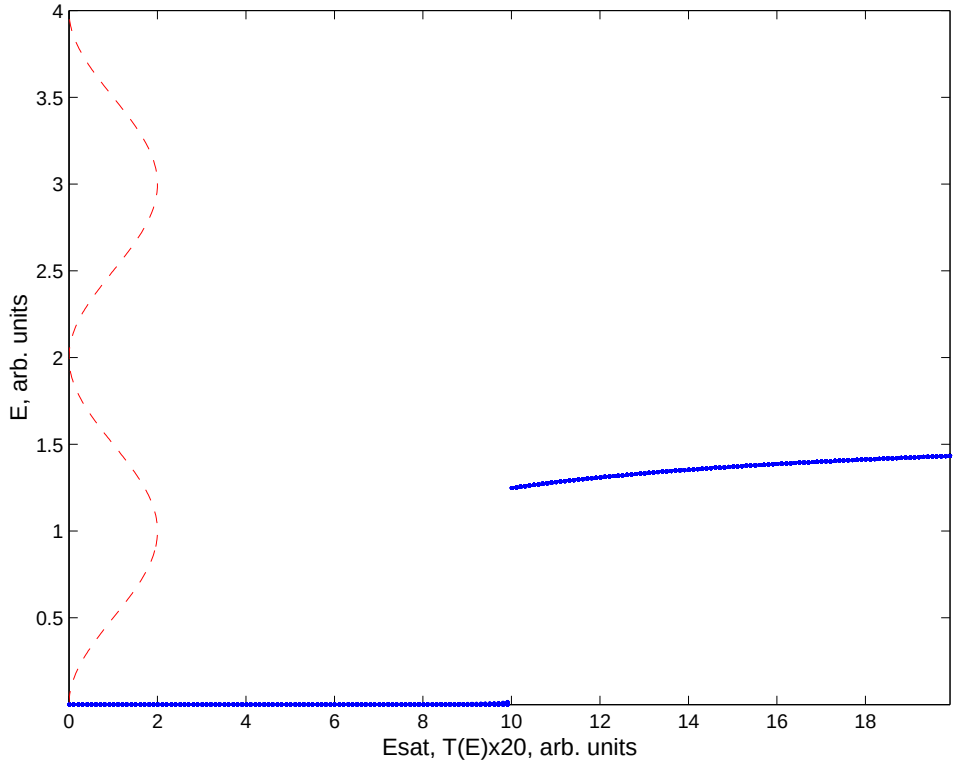

Figure 6.6: The steady-state pulse energy (E) as a function of E_{sat} (corresponding to pump power) for $q' = 0.1$ and $g_{net,0} = 2.1$. Also shown is the NPE transmittance curve for the pulse energy on the vertical axis.

locking would never start from noise. But, if $g_{net,0}$ is reduced then the threshold for stable mode-locking increases dramatically, a highly-undesirable condition for the laser from a practical point of view (Fig. 6.6).

It should be noted that initiation of mode-locking by itself cannot be treated within the context of this model, since a soliton-like solution has already been assumed in the derivation of the equation of motion. As a result, the $E_{p,0} \sim 0.5$ is taken as the initial condition. However, the model inherently reflects the existence of a threshold for mode-locking: If the nonlinear gain from NPE is too small soliton solutions will not be sustainable and the pulse energy will diminish to zero.

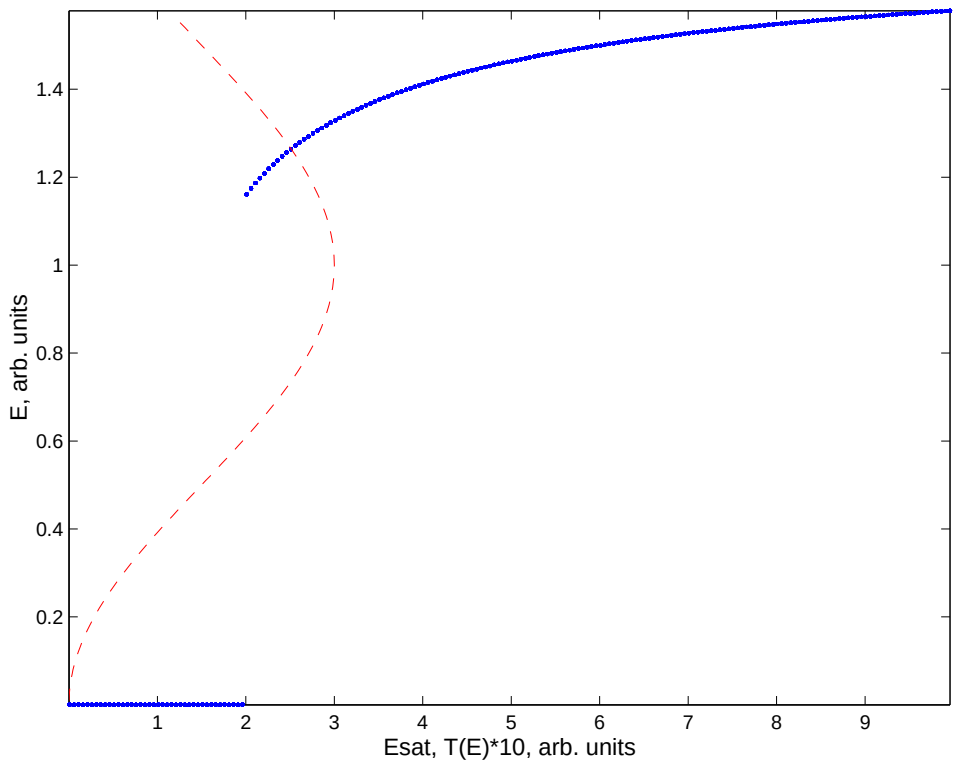

Figure 6.7: The bifurcation diagram for a modulation depth of 0.3. The final state of pulse energy (E) is plotted as a function of the gain saturation energy. Super-imposed on the bifurcation diagram is the transmittance corresponding to the pulse energy of the vertical axis for comparison.

For a modulation depth of $q' = 0.3$ and $g_{net,0} = 2.5$, the general behavior is similar (Fig. 6.7). The main difference is that self-starting operation is lot more likely to be achieved. Nevertheless, large values of E_{sat} (corresponding to a high pump power) are needed, resulting in inefficient operation (low slope-efficiency). Even $q' = 0.3$ corresponds to fairly weak amplitude modulation by NPE for fiber lasers and thus the parameter space of stable, self-starting operation remains contracted.

Increasing the modulation depth to 0.45, we observe an interesting phenomena (Fig. 6.8): The steady-state pulse energy begins to alternate between two dis-

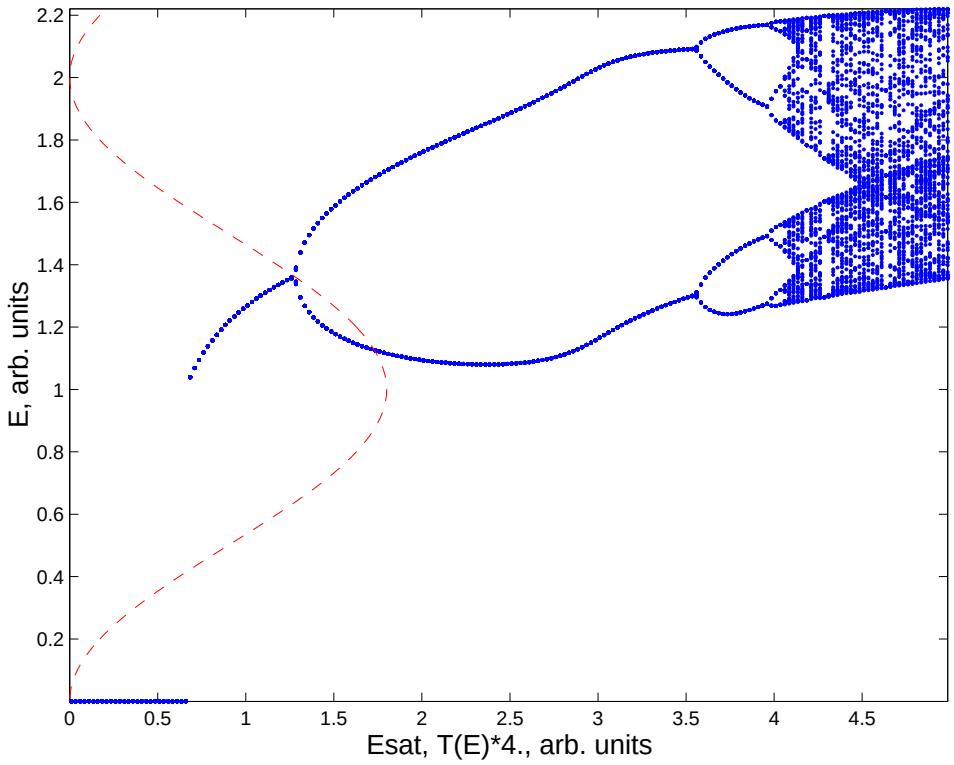

Figure 6.8: The bifurcation diagram for a modulation depth of 0.45. The final state of pulse energy (E) is plotted as a function of the gain saturation energy. Super-imposed on the bifurcation diagram is the transmittance corresponding to the pulse energy of the vertical axis for comparison.

tinct values as E_{sat} is increased. The laser remains completely stable, but with a periodicity of $2T_R$. As E_{sat} is further increased, the system progresses through a familiar period-doubling route to chaos [12]. This is hardly surprising since Eq. 6.17 contains all the ingredients for the period-doubling route to chaos: A nonlinear difference equation incorporating a function with at least one (infinitely many, in our case) maxima.

Larger modulation depths of 0.6 and 0.85 exhibit similar behavior, but the onset of period-doubling and the threshold for mode-locking approach each other.

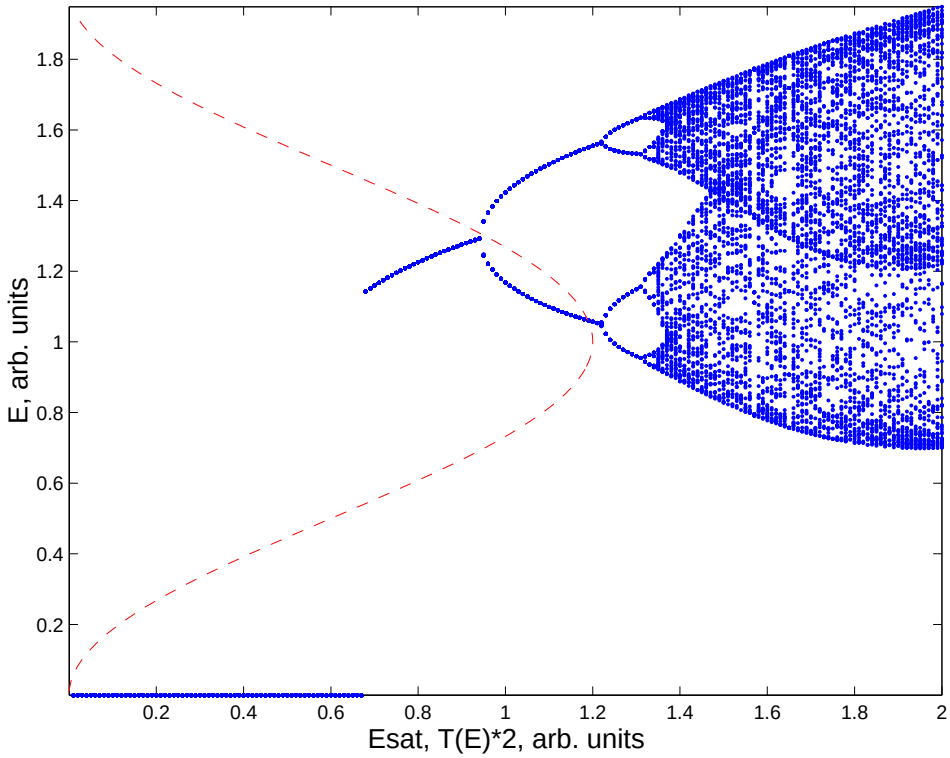

Figure 6.9: The bifurcation diagram for a modulation depth of 0.6. The final state of pulse energy (E) is plotted as a function of the gain saturation energy. Super-imposed on the bifurcation diagram is the transmittance corresponding to the pulse energy of the vertical axis for comparison.

For the latter case, the minimum E_{sat} is larger than the value corresponding to the first period-doubling bifurcation. However, $q' = 0.85$ is unrealistically high even for fiber lasers and we estimate that q' ranges from 0.4 to 0.65 in real fiber lasers.

In summary, for a choice realistic parameters, our model predicts a destabilization of mode-locking with increasing pulse energies (experimentally controllable by the pump power) by the period-doubling route to chaos. A related question is whether the occurrence of the period-doubling bifurcations should follow the Feigenbaum progression. Unimodal maps (maps with one maximum) have been

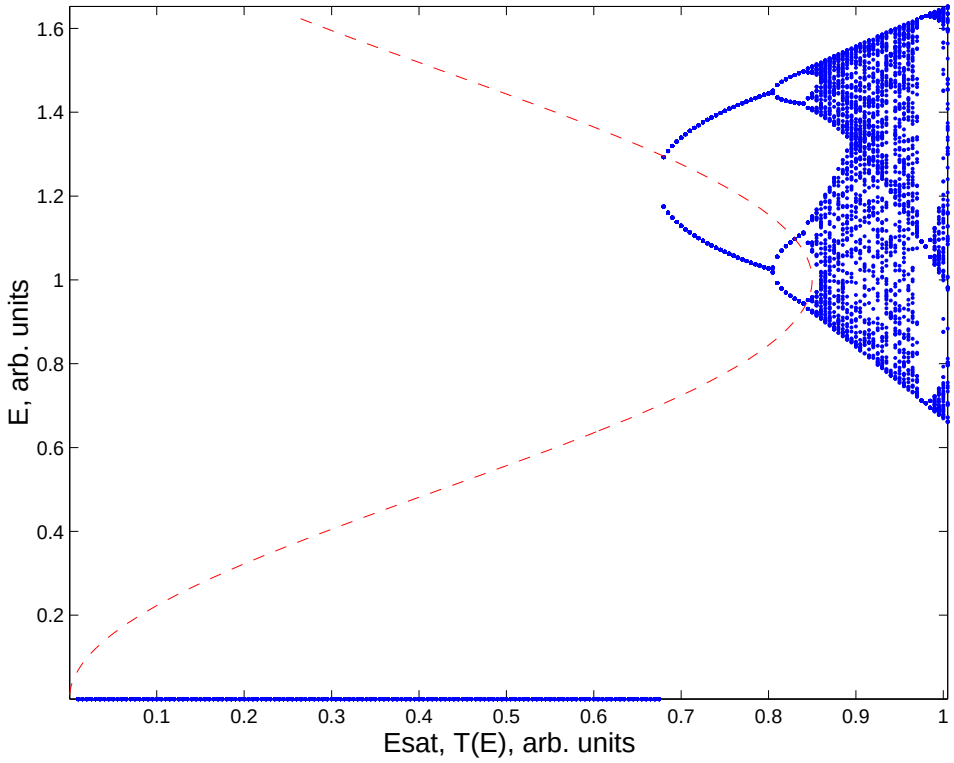

Figure 6.10: The bifurcation diagram for a modulation depth of 0.85. The final state of pulse energy (E) is plotted as a function of the gain saturation energy. Super-imposed on the bifurcation diagram is the transmittance corresponding to the pulse energy of the vertical axis for comparison.

studied extensively. The universal scaling results of Feigenbaum have been shown to apply regardless of the map shape. However, they need not necessarily apply to our case since the transmittance function is not unimodal.

6.5 Experimental Observation of Period-doubling Route to Double-pulsing

The predictions of the previous section are based on a rather basic model. For experimental verification, we have built a fiber laser similar to that of Ref. [13]. The intra-cavity dispersion was set to -0.02 ps^2 for soliton-like operation at a repetition rate of 40 MHz and the length of the Yb fiber was ~ 23 cm.

NPE rejection port and a reflection from one of the gratings were used to monitor the pulses. The pulse train coming out of these ports was monitored at these ports. Since the detector response is much longer than the pulse duration. The combination of the pulse train measurement and long-range autocorrelations demonstrated whether the laser was exhibiting single- or multiple-pulsing.

Pump power delivered to the gain fiber served as the experimentally-variable parameter. For low pump powers, mode-locking does not self-start and the laser remains in continuous-wave (cw) mode. As the pump power is increased beyond 160 mW, mode-locking is achieved. A stable, single pulse circulates the cavity as evidenced by the pulse train and auto-correlation measurements. As the pump power is increased to over 200 mW, the expected period-doubling sequence begins.

The pulse trains obtained both from the NPE rejection port and the grating reflection reveal that the pulse energy alternates between two distinct values. As the pump power is increased, another bifurcation takes place, resulting in period-

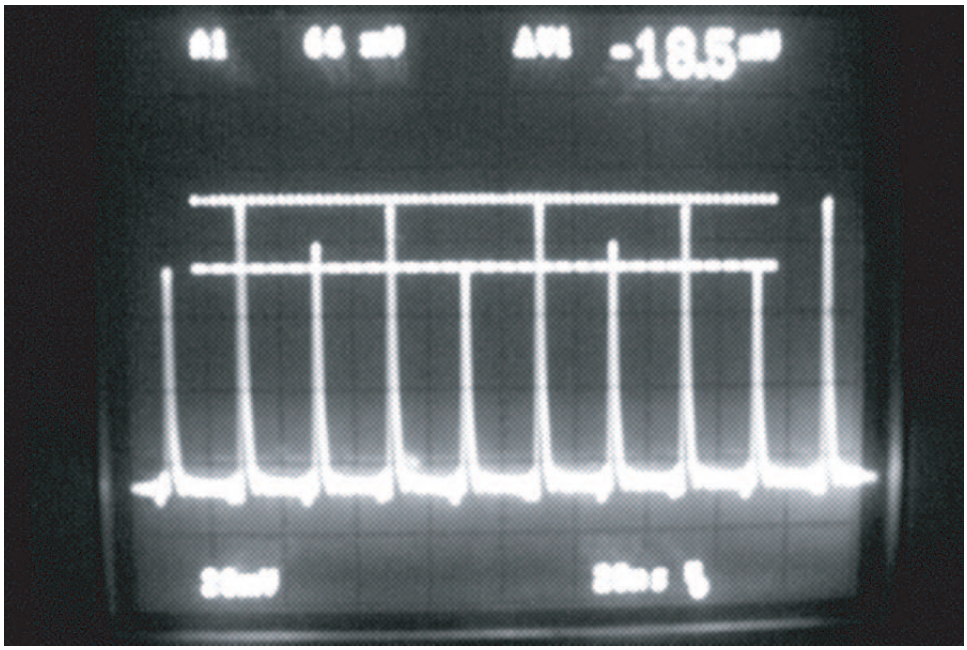

Figure 6.11: The pulse train recorded from the NPE rejection port showing the laser in stable, single-pulse mode-locked operation with a periodicity of $4T_R$.

icity of $4T_R$ (Fig. 6.11). At higher powers, it is possible to observe periodicities up to 16, but the bifurcations happen following smaller and smaller increases in the pump power, as theoretically expected. For high-periodicity operation, trigger of the oscilloscope by the pulse train becomes increasingly difficult.

The experimental period-doubling progression concludes unexpectedly: Instead of plunging into chaos and remaining in chaos, the pulse breaks up into two pulses. The energy content of each pulse is now reduced roughly to half, corresponding to a pulse energy below that of the first period-doubling bifurcation. Hence, the laser exhibits stable operation with two pulses circulating in the cavity and with a periodicity corresponding to T_R.

A bifurcation diagram showing the steady-state pulse energies for increasing pump power is presented in Fig. 6.12. It should be emphasized that the period-

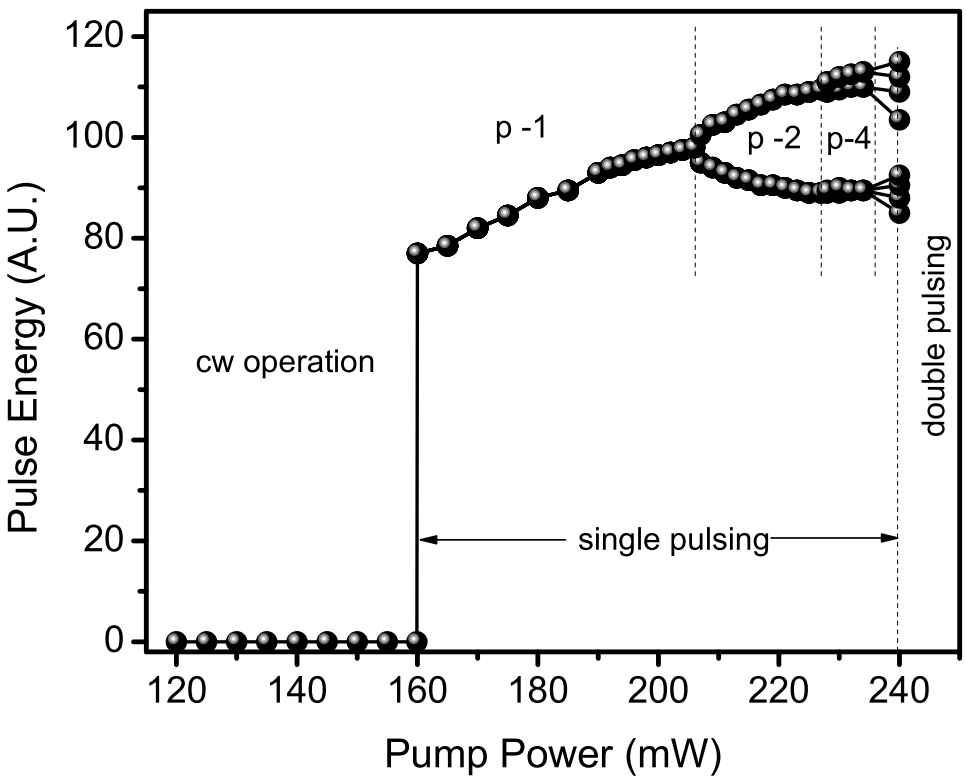

Figure 6.12: The experimentally-measured bifurcation diagram for weakly-stretched pulse fiber laser with anomalous intra-cavity dispersion.

doubling transition is repeatedly observable and no reduction in the laser's stability is observed even for high-periodicity operation.

Observations of period-doubling in short-pulsed lasers have been reported previously by several groups, however in most of these cases the underlying nature of the problem was vastly different. In the case of lasers with additive pulse mode-locking, the mechanism resulting in the period-doubling is similar, however the pulse shaping in those systems were not dominated by strong soliton dynamics [14]. The only experimental observation to our knowledge in a system where soliton dynamics dominate is Ref. [15]. However, in that study the authors have merely observed double and triple period operation and have not analyzed any

further.

6.6 Period-doubling Route to Multiple-pulsing

The experimental observation of transition to double-pulsing instead of chaos has an intuitive interpretation. As instability takes over the pulse at the end of the period-doubling progression, the pulse gets nearly destroyed. Thus, the situation resembles the initial states of pulse formation from intra-cavity noise. There are multiple pulse candidates. However, since the intra-cavity energy is large enough to drive one pulse beyond the first peak of NPE transmission, it follows that if that energy is distributed equally to two pulses. Each pulse would be placed in the vicinity of the first transmission peak of NPE. This is precisely what happens, and a two-pulse solution emerges. In other words, the system is able to relax into a stable state by exploiting its extra degrees of freedom corresponding to the temporal distribution of the field. Such a scenario is clearly impossible in a 1 dimensional system.

In this section, the previously-described model is generalized to account for this scenario. To this end, we allow for two-soliton solutions with pulse energies of $E_{1,n}$ and $E_{2,n}$, respectively, during the n$^{\text{th}}$ roundtrip. The gain saturates with the total intra-cavity energy, $E_{1,n} + E_{2,n}$. We obtain the following coupled difference equations

$$\begin{aligned} E_{1,n+1} &= \frac{1}{2}\frac{g_{net,0}}{1+(E_{1,n}+E_{2,n})/E_{sat}}(1-q'\cos(\pi E_{1,n}+\phi_0))E_{1,n}, \\ E_{2,n+1} &= \frac{1}{2}\frac{g_{net,0}}{1+(E_{2,n}+E_{1,n})/E_{sat}}(1-q'\cos(\pi E_{2,n}+\phi_0))E_{2,n}. \end{aligned} \tag{6.18}$$

We numerically solve the above equations for $q' = 0.60$ and $g_{net,0} = 3.50$

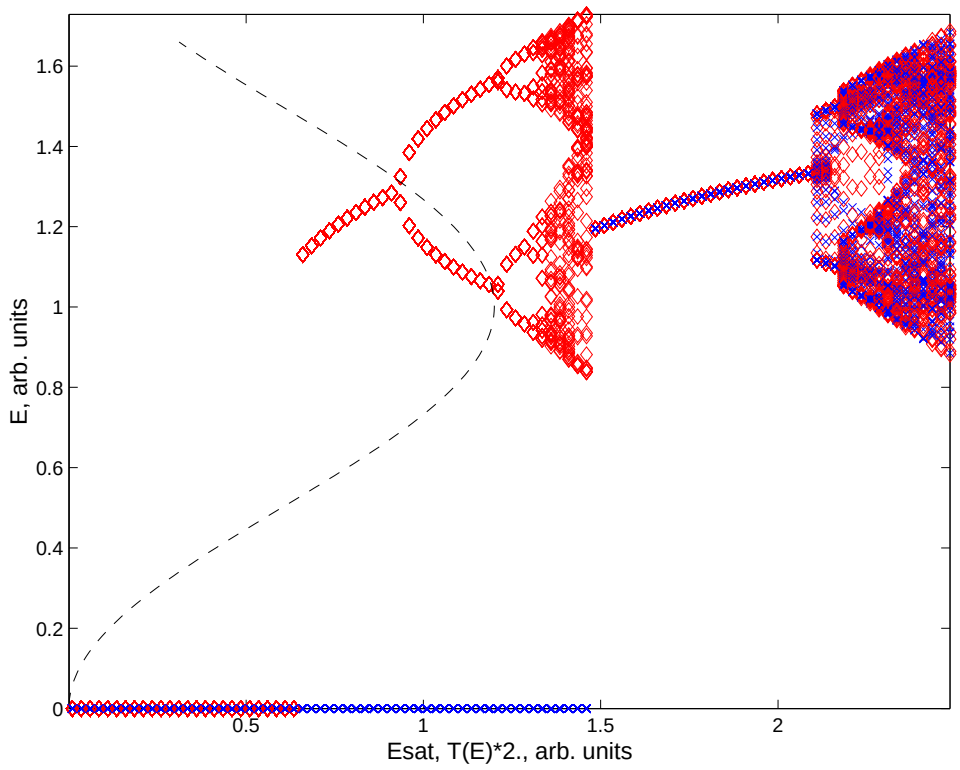

Figure 6.13: The bifurcation diagram for a modulation depth of 0.60, showing transition to double-pulsing instead of chaos. Super-imposed on the bifurcation diagram is the transmittance corresponding to the pulse energy of the vertical axis for comparison.

(Fig. 6.13) The initial pulse energies are set to different values to artificially break the symmetry which would be broken by noise in a real laser. For these conditions, the solution of the equations reveal that for low E_{sat} the system supports only one pulse. At $E_{sat} = 0.91$, a period-doubling bifurcation occurs. Additional period-doubling bifurcations take place, single-pulse solution retains its stability up to $E_{sat} = 1.47$. At this point, the second pulse can be supported stably, and it assumes an energy equal to that of the other pulse. The double-pulsed, period-1 solution retains its stability until an abrupt transition to chaos at $E_{sat} = 2.1$. Of course, this transition to chaos could also be eliminated if additional pulses are allowed to exist in the model.

6.7 Conclusion

In conclusion, we have derived a basic theory of mode-locking for fiber lasers dominated by soliton dynamics for the practically-relevant situation of non-monotonically saturating absorbers. In contrast to previous similar treatments, we do not make the assumption of small changes per roundtrip. Indeed, the contrary is obtained which leads to difference equations, instead of the usual differential equation formalism used to model mode-locking.

The basic theory reproduces several main features of mode-locked operation, such as the existence of a mode-locking threshold, the contraction of accessible phase space for small modulation depths of the SA. In addition, a period-doubling instability of the single-pulse solution is predicted as the pulse energy increases to overdrive the SA mechanism. A straight-forward generalization of the model to account for the possibility of multiple-pulses within the cavity predicts that the instability reached by the period-doubling progression is followed by a stable,

multiple-pulsed solution.

We have experimentally observed the period-doubling route at the end of which the laser assumes a two-pulse, period-1 solution. It is worth emphasizing that the experimental results are extremely repeatable, and we do not observe any reduction in stability even during high-periodicity operation.

A significant feature of these results is that, in contrast to the expected conclusion of the period-doubling route, the fiber laser does not plunge into chaos, but instead exhibits a regular two-pulse, period-1 solution. This is possible due to the existence of large (indeed, infinite) reservoir of extra degrees of freedom.

However, the main significance of the observation of a period-doubling route to multiple-pulsing in a femtosecond fiber laser is that the system under scrutiny is described by (coupled) partial difference equation(s), *i.e.* possessing infinitely-many degrees of freedom. Yet, this system admits soliton-like solution, which is remarkable fact by itself, that virtually consume all the degrees of freedom (corresponding to the pulse shape), except for a few, mainly the energy (or amplitude) of the soliton. This remaining degree of freedom can then be subjected to wild variations, behaving like a one-dimensional system, exhibiting the well-known period-doubling route to instability without disturbing the rest of the (infinitely-many) degrees of freedom held by the soliton dynamics. The system retains its stability for macroscopic time periods ($> 10^{12}\ T_R$).

The extraordinary stability and the repeatability of the experimental observation of interesting dynamics in short-pulsed fiber lasers strongly suggests that fiber laser can be invaluable tools in the experimental study of complex, nonlinear dynamical systems.

Finally, we would like to remark on the emergence of self-similarity in these

dynamics, as in any period-doubling transition, although we haven't focused our attention to that feature in this study.

BIBLIOGRAPHY

[1] L. E. Nelson, D. J. Jones, K. Tamura, and E. P. Ippen, Appl. Phys. B **65**, 277 (1997).

[2] M. Hofer, M. E. Fermann, F. Harberl, M. H. Ober, and A. J. Schmidt, Opt. Lett. **16**, 502 (1991).

[3] N. J. Doran and D. Wood, Opt. Lett. **13**, 56 (1988).

[4] H. A. Haus, J. Appl. Phys. **46**, 3049 (1975).

[5] F. Ö. Ilday, J. R. Buckley, H. Lim, F. W. Wise, and W. G. Clark, Opt. Lett. **28** 1635 (2003).

[6] H. A. Haus, K. Tamura, L. E. Nelson, and E. P. Ippen, IEEE J. Quantum Electron. **31** 591 (1995).

[7] F. X. Kärtner, I. D. Jung, U. Keller, IEEE J. Select. Top. Quantum Electron. **2** 540 (1996).

[8] H. G. Winful, Appl. Phys. Lett. **47**, 213 (1985).

[9] For example, see S. M. J. Kelly, "Characteristic side-band instability of periodically amplified average soliton," Elec. Lett. **28**, 806-807 (1992).

[10] S. Namiki, E. P. Ippen, H. A. Haus, and C. X. Yu, J. Opt. Soc. Am. B **14** 2099 (1997).

[11] T. R. Schibli, E. R. Thoen, F. X. Kärtner, and E. P. Ippen, Appl. Phys. B **70**, S41 (2000).

[12] For example, see R. M. May, Nature **261**, 459 (1976), M. J. Feigenbaum, J. Stat. Phys. **19**, 25 (1978), and M. J. Feigenbaum, Los Alamos Sci. **1**, 4 (1980).

[13] H. Lim, F. Ö. Ilday, and F. W. Wise, Opt. Lett. **28**, 660 (2003).

[14] For example, see G. Sucha, S. R. Bolton, S. Weiss, and D. S. Chemla, Opt. Lett. **20**, 1794 (1995).

[15] K. Tamura, C. R. Doerr, H. A. Haus, and E. P. Ippen, IEEE Phot. Tech. Lett. **6**, 697 (1994).

Chapter 7

Conclusion

In this thesis, we have presented studies spanning a broad range, from immediately-applicable improvements in fiber laser performance to fundamental studies of the dynamical systems.

With regards to improving the performance of fiber lasers, three new concepts have been proposed, nonlinearity management, an integrated, all-fiber oscillator-amplifier combination for energy-scaling, and self-similar pulse formation. The benefits of the latter two have been experimentally demonstrated, each delivering an order of magnitude improvement in peak powers and promising at least another order of magnitude with further development. It is not difficult to envisage lasers incorporating all three of these separate but compatible approaches for dramatic improvements in pulse energy. We expect the approaches described here to have a significant impact in the development of high-performance and user-friendly sources of femtosecond pulses.

In the course of studying limitation to pulse energy from saturable absorber mechanisms, fiber oscillators have been shown to exhibit deep dynamical properties. Considering the relative ease at which experiments can be conducted with fiber oscillators and the richness of the dynamical behavior accessible with simple modifications of the oscillator, we propose femtosecond fiber oscillators as an attractive experimental platform for studying complex phenomena.

Furthermore, we expect that the simple, but powerful approach developed in Chapter 6 to be useful in understanding the pulse generation in short-pulsed oscillators since the theory attempts to cover the previously-neglected regime of large

variations within each roundtrip.

7.1 Topics for Future Studies

The studies described in this thesis suggest many interesting directions to pursue for the future. In this section, a selected group of them are briefly discussed.

- Further studies for exploiting the self-similar pulse shaping approach are likely to result in drastically-improved pulse energies. As described previously, up to 1 μJ pulses can theoretically be obtained directly from a fiber laser. There is a challenging limitation imposed by the NPE, as investigated in detail in Chapter 6. With improved understanding of this mechanism, it may be possible get around this limitation, either by suppressing the instability or with a different mechanism for fast SA action.

  Our theoretical studies indicate that by incorporating a nonlinear loss or gain element within the NPE scheme or inside a NOLM, the over-driving pulse energy can be increased by several times without effecting the transmittance response at low energies, which is essential for self-starting operation [1].

  The brute-force solution to the problem of overdriving the SA, a fast mechanism such as NPE or a NOLM can be set to a large overdriving energy. The reduction in their self-starting capability can be remedied by the introduction of a slow, monotonic SA, such a semiconductor structure. Such combinations have been previously utilized successfully(for example, Ref. [2, 3, 4]), but high-pulse energy operation is yet to be reported.

- In a similar direction, a self-similar laser constructed with double-clad Yb-doped fiber for high power operation can incorporate a narrow bandpass

filter. The inclusion of a filter can force the laser to regenerate substantial amount of bandwidth within each roundtrip. Preliminary experimental and numerical studies indicate a possibility of improving the maximum pulse energy that can be extracted.

- The concept of self-similarity and wave-breaking-free operation are by no means unique to Yb-fiber oscillator s at 1 μm. By following a similar recipe, an Er-fiber laser with self-similar pulse generation can be made for improved pulse energy and ease of mode-locking at the important wavelength of 1550 nm.

- The requirement to avoid nonlinearity in the presence of anomalous dispersion currently forces these lasers to incorporate bulk optical elements to obtain anomalous dispersion. However, hollow-core photonic-crystals fiber based on the creation of a photonic band-gap have been demonstrated to provide anomalous dispersion. Thus, an all-fiber laser, incorporating such a fiber for anomalous dispersion can be constructed in the near future.

- Another possible approach to the generation of extremely high-energy pulses from a fiber laser is motivated by the theoretical observance of stable, few-periodicity solutions beyond instabilities that cause multiple-pulsing. Ordinarily, these windows of periodicity are not accessible as the pulse energy gradually increases during initial pulse formation. However, if a high-energy pulse is launched magically into the system, it should remain stable. This observation suggests the following scenario: A "master" fiber oscillator generating pulse energies in order of few nJ can be amplified by an order of magnitude. A pulse can then be selectively coupled into a "slave" fiber os-

cillator. If the launched pulse is adjusted to correspond to a window of periodicity for the slave oscillator, stable pulse formation at very high pulse energy may be possible.

- A particularly interesting direction for future studies is the construction of a fiber amplifier at 1 mJ energy level. Through the use of chirped pulse amplification (CPA) [10], pulse energies in the mJ range have been obtained. However, these systems are rather complicated, incorporate single-mode operation of highly multi-mode fiber, and the pulse quality remains low. A simple fiber amplifier would be highly-desirable. The use of large mode area photonic crystal fibers [5] along with the nonlinearity management [6] concept, and suppression of Raman-shifts with cascaded quadratic processes [7] should render such an approach feasible.

Many additions to the list are possible. Fiber lasers are beginning to emerge as practical alternatives to bulk solid state lasers with competing performance. We believe that in the near future, the performance of fiber laser will surpass bulk solid state lasers in various aspects. In addition, the rich nonlinear dynamics of the pulse propagation and formation may position fiber lasers to be an interesting experimental platform for the nonlinear dynamics community.

BIBLIOGRAPHY

[1] F. Ö. Ilday and F. W. Wise, in preparation.

[2] F. Ö. Ilday, F. W. Wise, and T. Sosnowski, Opt. Lett. **27**, 1531 (2002).

[3] M. Hofer, M. E. Fermann, L. Goldberg, IEEE Photon. Tech. Lett. **10**, 1247 (1998).

[4] M. Guina, N. Xiang, A. Vainionpää, O. G. Okhotnikov, T. Sajavaara, J. Keinonen, Opt. Lett. **26**, 1809 (2001).

[5] J. Limpert, T. Schreiber, S. Nolte, J. Zellmer, A. Tünnermann, R. Iliev, F. Lederer, K. Broeng, G. Vienne, A. Petersson, and C. Jakobsen, Opt. Express **11** 818 (2003).

[6] F. Ö. Ilday, and F. W. Wise, J. Opt. Soc. Am. B **19**, 470 (2002).

[7] F. Ö. Ilday, K. Beckwitt, Y.-F. Chen, H. Lim, and F. W. Wise, submitted to J. Opt. Soc. Am. B.

Appendix A

Numerical Techniques

Numerical simulations of pulse generation and propagation has formed a major component of this thesis work. These simulations have been performed to study many different phenomena under disparately different physical conditions. As a result, the simulations have never converged to standard form. To the contrary, various subcomponents of the codes have been in a state of constant flux and evolution. The formation of a master code that is able to address all of the phenomena previously studied is not practical due to the lengthy nature of the simulations. Thus, in many instances, it was prudent to preserve only the necessary components in order to maximize the code running time.

Here, we present a sample code that entails the most commonly-used functionalities. The simulations of the pulse propagation and generation have been performed using FORTRAN 77 programming language on personal computers running Linux (Redhat Distributions 6.x to 8.0). The original code was written in the MATLAB programming environment in order to utilize its high-level language. However, it was recognized that the use of high-level commands can be minimized while the speed improvement gained from a rudimentary language such as FORTRAN is impressive. Overall, a speed improvement of approximately 30-fold was obtained with FORTRAN over MATLAB.

Operationally, the system works as follows: The main code generates raw data, storing the electric field information at various stages of the pulse propagation as determined by the user. As the raw data is stored into data files at various intervals (e.g., at the end of each pulse roundtrip for an oscillator simulation), it

can be analyzed using additional tools.

In addition to generating the raw electric-field data, the main code is set to display on screen and log into a data file various information about the optical field. This information typically includes the pulse energy, peak power, pulse width and occasionally specific information such as the polarization angle of the field or the transmittance coefficient of a saturable absorber. Depending on the phenomena these various bits of information are invaluable in informing the user of how the simulation progresses. Based on these indicators, the simulation may be concluded or restarted. In many cases, the code is set to recognize that the field has converged and to halt, based on these indicators. A typical code is provided as an example below.

The main tools for analysis of the raw data were written MATLAB and later adapted to OCTAVE (a freely available MATLAB port) programming environments since these programs combine sophisticated programming and scripting features with high-level graphical display capabilities. This way, in addition to calculating the temporal and spectral intensity and phase profiles, various pulse parameters can be deduced, autocorrelation traces can be calculated. The resulting data can be exported in text format for additional analysis or in various graphical formats. A typical code is provided as example below.

A.1 Sample FORTRAN Program for Oscillator Simulations

The sample program provided below is configured to simulate pulse generation, self-initiated from intra-cavity noise, in a stretched-pulse Er-doped fiber laser operating

at 1550 nm.

```
************************************************************************
*                                                                      *
*     OSCILLATOR SIMULATOR                                             *
*     By F. Omer Ilday                                                 *
*                                                                      *
************************************************************************
      program main
      parameter (tres = 4096, maxpage=4, totalpages=72)
      DIMENSION Elast(tres), Elast1(tres), Elast2(tres)
      DIMENSION Epage(tres,totalpages)
      DIMENSION criteria(5)
      double complex Elast, Elast1, Elast2, Epage
      real criteria
      character*4 no
      character*9 filename
      integer d1, d2, d3, d4, dummy
      integer stepno, zres, totalsteps, totalpasses, To, pageno
      integer i, t, pass, page, fres, saveevery
      double precision L_1, L2d_1, L3d_1, Lnl_1, Lg_1, Esat_1, g2_1
      double precision L_2, L2d_2, L3d_2, Lnl_2, Lg_2, Esat_2, g2_2
      double precision L_3, L2d_3, L3d_3, Lnl_3, Lg_3, Esat_3, g2_3
      double precision L_4, L2d_4, L3d_4, Lnl_4, Lg_4, Esat_4, g2_4
      double precision L_5, L2d_5, L3d_5, Lnl_5, Lg_5, Esat_5, g2_5
      double precision dz, Ereal, Eimag, Isat, rat, Raman
      double precision conv, Treal, k2, k3, n2, Power
      double precision Lambda, Aeff, Gamma
      double precision Energy, Dtot, Ltot
      real Ipeak, Ip_dummy, Iglobal, Icenter
      totalpasses = 10000
      zres = 32
      saveevery = 10
      totalsteps = maxpage*zres
      To = 4
      dz = 1./totalsteps
C     A functional shape (such a super-Gaussian) in the spectral domain
C     can be defined as the startup condition:
C
C      do t = 1, tres/2+1
C        Elast(t) = 10.0*exp(-0.0002*(t-1.)**4/To**4)
C     &        *(0.+1.*sin((t-1.)/40.))
C     &        *exp((0,1)*2*3.14*(t-1)*tres*3)
C      enddo
C
C      do t = tres/2+2, tres
C        Elast(t) = 10.0*exp(-0.0002*(t-1.-tres)**4/To**4)
C     &        *(0.-1.*sin((t-1.-tres)/40.0))
C     &        *exp((0,1)*2*3.14*(t-1-tres)*tres*3)
C      enddo
C
C      fres=int(tres)
C      CALL dfour1(Elast,fres,-1)
```

```
C
C      DO t=1,fres
C         Elast(t) = Elast(t)/(tres*1.0)
C      ENDDO
C     Starting condition as defined in the time domain:
      DO t = 1, tres
C        Elast(t) = 1./cosh(-(t-tres/2.)/To)
C        Elast(t) = 1.*exp(-(t-6.*tres/16.)**2/To**2/2.)
C     &        + 1.*exp(-(t-10.*tres/16.)**2/To**2/2.)
C     &        + 0.*exp(-(t-12.*tres/16.)**2/To**2/2.)
C        Elast(t) = 1./sqrt(50.)/cosh(-(t-tres/2.)/To/50.)
c        Elast(t) = 1./sqrt(100.)*exp(-(t-tres/2.)**2/(To*100)**2/2.)
        Elast(t) = (1.77*To + rand(t))/(tres+0.01)
      ENDDO
*******************************************************************************
C     Uncomment this section to start from a previously saved position:
      start = 0000
c      open (19,file='data2200',status='old')
c      DO t=1, tres
c         DO page = 1, 24
c            read (19,*) dummy, Ereal, Eimag
c         ENDDO
c         Elast(t) = (1,0)*Ereal + (0,1)*Eimag
c      ENDDO
c      close(19)
*******************************************************************************
C     Uncomment this section to save the starting condition to a file:
c      open (19,file='data0000',status='new')
c      DO t = 1, tres
C         DO page = 1, totalpages
c            Ereal = dreal(Elast(t))
c            Eimag = dimag(Elast(t))
C         ENDDO
c      ENDDO
c      close(19)
*******************************************************************************
C     GENERAL DEFINITIONS:
C     --------------------
C     Open file to record simulation parameters:
      open (19,file='parameters',status='new')
C     To/Tfwhm conversion factors for sechant and Gaussian pulse shapes:
C     conv = 1.763
C     for sech(t) pulse shape (soliton-like)
      conv = 1.665
C     for Gaussian pulse shape (DM-soliton-like)
      Treal = 100.0/conv
C     time scale: Treal is To in real units. So Treal*conv, is T_FWHM in fs.
      Power = 1500.0
C     power scale: Ipeak (W) = Ipeak * Power
      Lambda = 1028.0
C     Central wavelength of the spectrum in nm.
C     Raman Effect: Raman factor is Traman/Tscaling (Traman=5 fs, typically)
```

```
      Raman  = 5.0*To/(Treal*1.0)
C     Total dispersion parameter:
      Dtot = 0.0
C     Total cavity length parameter:
      Ltot = 0.0
C     Record the general parameters:
      write (19,*) 'zres =',zres, ' tres =',tres, ' To =', To,' conv =',
     &     conv, ' Treal =', Treal,' fs', ' Power =', Power,'W',
     &     ' Lambda =',Lambda,'nm ', ' Raman factor =',Raman
*******************************************************************************
C     FIBER PARAMETERS:
C     -----------------
C     SEGMENT 1:
C     ----------
      L_1   =  20.0
      Ltot  =  Ltot + L_1
      k2    =  22.4
      k3    =  0.10
      Dtot  =  Dtot + k2*L_1
      L2d_1 =  Treal**2/k2/10.0
      L3d_1 =  Treal**3/k3/10.0
      n2    =  2.3
      Aeff  =  30.0
      Gamma =  2.0*3.14/lambda*n2/Aeff/10.0
      Lnl_1 =  1.0/(power*Gamma)
C     All lengths are in cm (hence the 1/10.0 factors for Ld&Lnl).
C     k2:   GVD parameter(ps^2/km)(+ -> normal)
C     n2:   Kerr nonlinearity (10^-8 um^2/W)
C     Aeff: effective mode area (um^2)
      write(*,*) 'L_1   =',L_1,' cm'
      write(*,*) 'L2d_1  =',L2d_1,' cm'
      write(*,*) 'L3d_1  =',L3d_1,' cm'
      write(*,*) 'Lnl_1 =',Lnl_1,' cm'
      write(19,*)' L_1   =',L_1,' L2d_1  =',L2d_1,' L3d_1 =',L3d_1,
     &           ' Lnl_1 =',Lnl_1
C     Small signal gain
C     10dB gain -> 10^1 = exp(2.30*0.5), Lg = L/gain, here Lg = L/1.15
C     0.5 is needed since E, not I=E^2 is used.
      Lg_1   =  L_1/(1.15*3.0)
C     Gain saturation energy:
      Esat_1 =  To*4.0
C     Gain bandwidth:
      g2_1   = 800.0
C     g2(THz) = g2*delta_f, where delta_f = (To/Treal)/tres
      write(*,*) 'Lg_1  =',Lg_1,' cm'
      write(*,*) 'Esat_1=',Esat_1*Power*Treal/(To*1.0)/1000.0,' pJ'
      write(*,*) 'g2_1  =',g2_1*1000*(To/Treal)/(tres*1.0), ' THz'
      write(*,*) 'Gain bandwidth = ',
     &     Lambda**2/300.0*(g2_1*(To/Treal)/(tres*1.0)),' nm'
      write(19,*) 'Lg_1  =',Lg_1,' Esat_1 =',Esat_1,' g2_1 =',g2_1,' =',
     &     Lambda**2/300.0*(g2_1*(To/Treal)/(tres*1.0)),' nm'
      write(*,*) '----------------------------------------'
```

```
C     SEGMENT 2:
C     ----------
      L_2   =  410.0
      Ltot  =  Ltot + L_2
      k2    = -22.4
      k3    =  1.580
      Dtot  =  Dtot + k2*L_2
      L2d_2 =  Treal**2/k2/10.0
      L3d_2 =  Treal**3/k3/10.0
      n2    =  2.3
      Aeff  =  100000.0
      Gamma =  2.0*3.14/lambda*n2/Aeff/10.0
      Lnl_2 =  1.0/(power*Gamma)
C     All lengths are in cm (hence the 1/10.0 factors for Ld&Lnl).
C     k2:   GVD parameter(ps^2/km)(+ -> normal)
C     n2:   Kerr nonlinearity (10^-8 um^2/W)
C     Aeff: effective mode area (um^2)
      write(*,*) 'L_SMF2   =',L_2,' cm'
      write(*,*) 'Ld_SMF2  =',L2d_2,' cm'
      write(*,*) 'L3d_2  =',L3d_2,' cm'
      write(*,*) 'Lnl_SMF2 =',Lnl_2,' cm'
      write(19,*)'L_2   =',L_2,' Ld_2  =',L2d_2,' Lnl_2 =',Lnl_2
C     Small signal gain
C     10dB gain -> 10^1 = exp(2.30*0.5), Lg = L/gain, here Lg = L/1.15
C     0.5 is needed since E, not i=E^2 is used.
      Lg_2   =  L_2/(1.15*0.0001)
C     Gain saturation energy:
      Esat_2 =  To*1000.0
C     Gain bandwidth:
      g2_2   =  5000.0
      write(*,*) '----------------------------------------'
C     SEGMENT 3:
C     ----------
      L_3   =  420.0
      Ltot  =  Ltot + L_3
      k2    =  22.4
      k3    =  0.10
      Dtot  =  Dtot + k2*L_3
      L2d_3 =  Treal**2/k2/10.0
      L3d_3 =  Treal**3/k3/10.0
      n2    =  2.3
      Aeff  =  30.0
      Gamma =  2.0*3.14/lambda*n2/Aeff/10.0
      Lnl_3 =  1.0/(power*Gamma)
C     All lengths are in cm (hence the 1/10.0 factors for Ld&Lnl).
C     k2:   GVD parameter(ps^2/km)(+ -> normal)
C     n2:   Kerr nonlinearity (10^-8 um^2/W)
C     Aeff: effective mode area (um^2)
      write(*,*) 'L_3   =',L_3,' cm'
      write(*,*) 'L2d_3  =',L2d_3,' cm'
      write(*,*) 'L3d_3  =',L3d_3,' cm'
      write(*,*) 'Lnl_3 =',Lnl_3,' cm'
```

```
      write(19,*)' L_3   =',L_3,' L2d_3  =',L2d_3,' L3d_3 =',L3d_3,
     &           ' Lnl_3 =',Lnl_3
C     Small signal gain
C     10dB gain -> 10^1 = exp(2.30*0.5), Lg = L/gain, here Lg = L/1.15
C     0.5 is needed since E, not I=E^2 is used.
      Lg_3   =  L_3/(1.15*0.0001)
C     Gain saturation energy:
      Esat_3 =  To*1000.0
C     Gain bandwidth:
      g2_3   =  10000.0
C     g2(THz) = g2*delta_f, where delta_f = (To/Treal)/tres
C      write(*,*) 'Lg_3  =',Lg_3,' cm'
C      write(*,*) 'Esat_3=',Esat_3*Power*Treal/(To*1.0)/1000.0,' pJ'
C      write(*,*) 'g2_3  =',g2_1*1000*(To/Treal)/(tres*1.0), ' THz'
C      write(*,*) 'Gain bandwidth = ',
C     &     Lambda**2/300.0*(g2_3*(To/Treal)/(tres*1.0)),' nm'
      write(19,*) 'Lg_3  =',Lg_3,' Esat_3 =',Esat_3,' g2_3 =',g2_3
C      write(*,*) '----------------------------------------'
*********************************************************************************
C     Total dispersion print-out
      write (*,*) 'Total dispersion is ', Dtot/100000.0,' ps^2'
      write (19,*) 'Dtot =',Dtot/100000.0,' ps^2'
C     Cavity length
      write (*,*) 'Repetition rate is ', 20000.0/Ltot,' MHz'
C     Absorber saturation intensity:
      Isat = 1.00
      Iglobal = 0.0
      close(19)
C     Close parameters file.
C     Open file to record simulation statistics:
      open (18,file='statistics',status='new')
*********************************************************************************
C     CAVITY ROUND-TRIP LOOP
C     ----------------------
      DO pass = start + 1, totalpasses
      write (*,*) '----------------------------------------'
      write (*,*) 'Roundtrip = ', pass
      Iglobal = 0.0
C     Calculate energy:
C     -----------------
      Energy = 0.0
      Ipeak  = 0.0
      DO t=1,tres
         Energy = Energy + Elast(t)*conjg(Elast(t))
         Ip_dummy = Elast(t)*conjg(Elast(t))
         IF (Ip_dummy.GT.Ipeak) THEN
            Ipeak = Elast(t)*conjg(Elast(t))
         ENDIF
      ENDDO
      write (*,*) 'Total energy in is',
     &     Energy*Power*Treal/(To*1.0)/1000.0, ' pJ'
c      write (*,*) 'Peak power is', Ipeak*Power,' W'
```

```
      criteria(mod(pass,5)+1) = Energy
      write (*,*) criteria(1),criteria(2),criteria(3),
     &      criteria(4),criteria(5)
      IF ((ABS(criteria(5)-criteria(4))/criteria(5).LT.0.000001).AND.
     &    (ABS(criteria(4)-criteria(3))/criteria(4).LT.0.000001).AND.
     &    (ABS(criteria(3)-criteria(2))/criteria(3).LT.0.000001).AND.
     &    (ABS(criteria(2)-criteria(1))/criteria(2).LT.0.000001).AND.
     &    (mod(pass,saveevery).EQ.1)) THEN
          write(*,*) "THE FIELD HAS CONVERGED !!!"
          STOP
      ENDIF
*****************************************************************************
C     Propagation through SEGMENT 1:
C     ------------------------------
      write (*,*) 'Segment 1'
      dz = 1./totalsteps
      DO stepno = 1,totalsteps
          CALL Propagate(Elast, dz, L_1, L2d_1, L3d_1, Lnl_1,
     &         Lg_1, Esat_1, g2_1, Raman)
          IF (mod(stepno,zres).EQ.0) THEN
             pageno=stepno/zres
             DO t = 1,tres
                Epage(t,pageno) = Elast(t)
             ENDDO
          END IF
          Ipeak  = 0.0
          DO t=1,tres
             Ip_dummy = Elast(t)*conjg(Elast(t))
             IF (Ip_dummy.GT.Ipeak) THEN
                Ipeak = Elast(t)*conjg(Elast(t))
             ENDIF
          ENDDO
          IF (Ipeak.GT.Iglobal) THEN
             Iglobal = Ipeak
          ENDIF
      ENDDO
*****************************************************************************
C     Calculate energy:
C     -----------------
      Energy = 0.0
      Ipeak  = 0.0
      DO t=1,tres
         Energy = Energy + Elast(t)*conjg(Elast(t))
         Ip_dummy = Elast(t)*conjg(Elast(t))
         IF (Ip_dummy.GT.Ipeak) THEN
            Ipeak = Elast(t)*conjg(Elast(t))
         ENDIF
      ENDDO
      write (*,*) 'Total energy out is',
     &     Energy*Power*Treal/(To*1.0)/1000.0 , ' pJ'
c      write (*,*) 'Peak power is', Ipeak*Power,' W'
*****************************************************************************
```

```
C     OC section
C     ----------
c      DO t=1,tres
c         Elast(t) = Elast(t)*sqrt(0.3)
c      ENDDO
*************************************************************************
      write (*,*) Ipeak
      Icenter = Ipeak
C     Saturable absorber action:
C     --------------------------
      DO t=1,tres
         rat = abs(Elast(t))*abs(Elast(t))/Isat
         Elast1(t) = Elast(t)*sqrt(1.0 - 0.7/(1.0 + rat))
c         Elast1(t) = Elast(t)*sqrt(0.3+0.7*(sin(3.14/2.0*rat))**2)
         Epage(t,1) = Elast(t) - Elast1(t)
         Elast(t) = Elast1(t)
      ENDDO
*************************************************************************
C     OC section
C     ----------
      DO t=1,tres
         Elast(t) = Elast(t)*sqrt(0.12)
      ENDDO
*************************************************************************
C     Propagation through SEGMENT 2:
C     ------------------------------
      write (*,*) 'Segment 2a'
      dz = 1./maxpage
      DO stepno = 1,maxpage
          CALL Propagate(Elast, dz, L_2, L2d_2, L3d_2, Lnl_2,
     &         Lg_2, Esat_2, g2_2, Raman)
C          IF (mod(stepno,zres).EQ.0) THEN
            pageno=stepno + maxpage
            DO t = 1,tres
               Epage(t,pageno) = Elast(t)
            ENDDO
C           END IF
          Ipeak  = 0.0
          DO t=1,tres
             Ip_dummy = Elast(t)*conjg(Elast(t))
             IF (Ip_dummy.GT.Ipeak) THEN
                Ipeak = Elast(t)*conjg(Elast(t))
             ENDIF
          ENDDO
          IF (Ipeak.GT.Iglobal) THEN
             Iglobal = Ipeak
          ENDIF
      ENDDO
*************************************************************************
C     Propagation through SEGMENT 3:
C     ------------------------------
      write (*,*) 'Segment 3'
```

```
      dz = 1./totalsteps
      DO stepno = 1,totalsteps
          CALL Propagate(Elast, dz, L_3, L2d_3, L3d_3, Lnl_3,
     &         Lg_3, Esat_3, g2_3, Raman)
          IF (mod(stepno,2).EQ.0) THEN
             pageno=stepno/2 + maxpage*2
             DO t = 1,tres
                Epage(t,pageno) = Elast(t)
             ENDDO
          END IF
          Ipeak  = 0.0
          DO t=1,tres
             Ip_dummy = Elast(t)*conjg(Elast(t))
             IF (Ip_dummy.GT.Ipeak) THEN
                Ipeak = Elast(t)*conjg(Elast(t))
             ENDIF
          ENDDO
          IF (Ipeak.GT.Iglobal) THEN
             Iglobal = Ipeak
          ENDIF
      ENDDO
      write (*,*) 'Overall peak power is', Iglobal*Power,' W'
      write (18,*) pass, Icenter, Iglobal
*******************************************************************************
C     Save the results to a file:
C     ---------------------------
      IF (mod(pass,saveevery).EQ.0) THEN
         write (*,*) 'Saving rountrip number ', pass
         d1 = int(pass/1000)
         d2 = int(pass/100 - 10*d1)
         d3 = int(pass/10 - 100*d1 - 10*d2)
         d4 = int(pass - d1*1000 - d2*100 - d3*10)
         d1 = d1 + 48
         d2 = d2 + 48
         d3 = d3 + 48
         d4 = d4 + 48
         no = char(d1)//char(d2)//char(d3)//char(d4)
         filename = 'data' // no
         open (19,file=filename,status='new')
         DO t = 1, tres
            DO page = 1, totalpages
               Ereal = dreal(Epage(t,page))
               Eimag = dimag(Epage(t,page))
               write (19,*) t, Ereal,Eimag
            ENDDO
         ENDDO
         close(19)
      ENDIF
      ENDDO
      close(18)
      stop
      end
```

```
*********************************************************************
      SUBROUTINE Propagate(Elast, dz, L, L2d, L3d, Lnl,Lg,Esat,g2,Raman)
      parameter (tres = 4096)
      dimension Elast(tres)
      double precision dz, L, L2d, L3d, Lnl, Lg, Esat, g2, Raman
      double precision factor
      double complex Elast, zero
      integer t
      zero = 0.0
      CALL PropDS(Elast, L, L2d, L3d, dz/2, Lg, Esat, g2)
      CALL PropNL(Elast(1),L,Lnl,dz,Elast(3),Elast(2),Elast(tres),
     &     Elast(tres-1),Raman)
      CALL PropNL(Elast(2),L,Lnl,dz,Elast(4),Elast(3),Elast(1),
     &     Elast(tres),Raman)
      DO t = 3,tres-2
C     CALL EdgeFilter(factor,t)
C     Elast(t) = Elast(t)*factor
         CALL PropNL(Elast(t),L,Lnl,dz,Elast(t+2),Elast(t+1),Elast(t-1),
     &        Elast(t-2),Raman)
      ENDDO
      CALL PropNL(Elast(tres-1),L,Lnl,dz,Elast(1), Elast(tres),
     &     Elast(tres-2),Elast(tres-3),Raman)
      CALL PropNL(Elast(tres),L,Lnl,dz,Elast(2), Elast(1),
     &     Elast(tres-1),Elast(tres-2),Raman)
      CALL PropDS(Elast, L, L2d, L3d, dz/2, Lg, Esat, g2)
      return
      end
*********************************************************************
      SUBROUTINE PropDS(E, L, L2d, L3d, dz, Lg, Esat, g2)
      parameter (tres = 4096, To = 4)
      dimension E(tres), Ef(tres)
      double precision L, L2d, L3d, dz, Lg, Esat, g2, Energy
      double complex E, Ef
      integer fres, f
      fres = int(tres)
      CALL dfour1(E,fres,1)
      Energy = 0.0
C     Finite gain bandwidth is imposed here:
      DO f=1,(fres/2+1)
         Ef(f) = E(f)*exp( 2.*(0,1)*(3.141592654*(f-1)*To/fres*1.0)**2
     &        *L/L2d*dz
     &        - (0,1)/6.*(2*3.141592654*(f-1)*To/(fres*1.0))**3*L/L3d*dz
C     &        -(0,1)/24.*(2*3.141592654*(f-1)*To/(fres*1.0))**4*L/L4d*dz
C     &        -(0,1)/120.*(2*3.141592654*(f-1)*To/(fres*1.))**5*L/L5d*dz
     &  + (0,1)*((2*(f-1)/g2)-(0,1))
     &/(1+(2*(f-1)/g2)**2)/2.*dz - dz/2. )
         Energy = Energy + Ef(f)*conjg(Ef(f))
      ENDDO
      DO f=(fres/2+2),fres
         Ef(f) = E(f)*exp( 2.*(0,1)*(3.141592654*(f-1-fres)*To/fres)**2
     &        *L/L2d*dz
     &  - (0,1)/6.*(2*3.141592654*(f-1-fres)*To/(fres*1.0))**3*L/L3d*dz
```

```
C     &  - (0,1)/24.*(2*3.141592654*(f-1-fres)*To/(fres*1.0))**4*L/L4d*dz
C     &  - (0,1)/120.*(2*3.141592654*(f-1-fres)*To/(fres*1.))**5*L/L5d*dz
     &  + (0,1)*((2*(f-1-fres)/g2)-(0,1))
     &/(1+(2*(f-1-fres)/g2)**2)/2.*dz - dz/2.)
         Energy = Energy + Ef(f)*conjg(Ef(f))
      ENDDO
C     The saturating of gain is included in the form g = g0/(1+E/Esat).
C     There is a division by fres since the magnitude of I increases by
C     a factor of fres due to the FFT.
      DO f=1,fres
         E(f) = Ef(f)*exp(L/Lg*dz/(1.0 + (Energy/fres/Esat)))
      ENDDO
      CALL dfour1(E,fres,-1)
      DO f=1,fres

         E(f) = E(f)/fres
      ENDDO
      return
      end
**********************************************************************
      SUBROUTINE PropNL(E, L, Lnl, dz, Eup2, Eup, Edown, Edown2, Raman)
      double complex   E, Eup, Eup2, Edown, Edown2
      double precision L, Lnl, dz, Raman, Steep
      double complex   k1, k2, k3, k4
C     Adding a d/dt(|A|) term here to account for Raman. Taking derivative using
C     (f(x+h) - f(x-h))/2h, where h=1 (one t-component). BEWARE this method is
C     prone to numerical error. This is only a crude approximation
C     for smooth pulses.
C     dI is d/dt(|A|). Scaling is
      dI = (Eup*conjg(Eup) - Edown*conjg(Edown))/2.0
      Steep = 0.0
      k1=dz*(0,1)*L/Lnl*E*conjg(E)*E
     &     - dz*(0,1)*L/Lnl*Raman*
     &     (-Eup2*conjg(Eup2) + 8*Eup*conjg(Eup) - 8*Edown*conjg(Edown)
     &     + Edown2*conjg(Edown2))/12.0*E
C     &     - dz*L/Lnl*Steep/E*
C     &     (Eup**2*conjg(Eup) - Edown**2*conjg(Edown))/2*E
      k2=dz*(0,1)*L/Lnl*(E+k1/2.0)*conjg(E+k1/2.0)*(E+k1/2.0)
     &     - dz*(0,1)*L/Lnl*Raman*
     &     ( -(Eup2+k1/2.0)*conjg(Eup2+k1/2.0)
     &     + 8*(Eup+k1/2.0)*conjg(Eup+k1/2.0)
     &     - 8*(Edown+k1/2.0)*conjg(Edown+k1/2.0)
     &     + (Edown2+k1/2.0)*conjg(Edown2+k1/2.0))/12.0*(E+k1/2.0)
C     &     - dz*L/Lnl*Steep/(E+k1/2)*
C     &     ( (Eup+k1/2)**2*conjg(Eup+k1/2)
C     &     - (Edown+k1/2)**2*conjg(Edown+k1/2) )/2*(E+k1/2)
      k3=dz*(0,1)*L/Lnl*(E+k2/2.0)*conjg(E+k2/2.0)*(E+k2/2.0)
     &     - dz*(0,1)*L/Lnl*Raman*
     &     ( -(Eup2+k2/2.0)*conjg(Eup2+k2/2.0)
     &     + 8*(Eup+k2/2.0)*conjg(Eup+k2/2.0)
     &     - 8*(Edown+k2/2.0)*conjg(Edown+k2/2.0)
     &     + (Edown2+k2/2.0)*conjg(Edown2+k2/2.0))/12.0*(E+k2/2.0)
```

```
C     &     - dz*(0,1)*L/Lnl*Steep/(E+k2/2)*
C     &     ( (Eup+k2/2)**2*conjg(Eup+k2/2)
C     &     - (Edown+k2/2)**2*conjg(Edown+k2/2) )/2*(E+k2/2)
      k4=dz*(0,1)*L/Lnl*(E+k3)*conjg(E+k3)*(E+k3)
     &     - dz*(0,1)*L/Lnl*Raman*
     &     ( -(Eup2+k3)*conjg(Eup2+k3)
     &     + 8*(Eup+k3)*conjg(Eup+k3)
     &     - 8*(Edown+k3)*conjg(Edown+k3)
     &     + (Edown2+k3)*conjg(Edown2+k3))/12.0*(E+k3)
C     &     - dz*(0,1)*L/Lnl*Steep/(E+k3/2)*
C     &     ( (Eup+k3/2)**2*conjg(Eup+k3/2)
C     &     - (Edown+k3/2)**2*conjg(Edown+k3/2) )/2*(E+k3/2)
      E= E + k1/6. + k2/3. + k3/3. + k4/6.
      return
      end
**********************************************************************
      SUBROUTINE EdgeFilter(factor,t)
      parameter (tres = 4096)
      double precision factor, mask
      integer t
      mask=100.
      IF (t.GT.mask.AND.t.LT.(tres-mask+1)) THEN
            factor=1
         ELSEIF (t.LE.(mask+1)) THEN
            factor=exp(-(t-mask)**2/(mask**2/100.))
         ELSE
            factor=exp(-(tres-t-mask+1)**2/(mask**2/100.))
      END IF
C     t=1:(mask) and (tres-mask):(tres) attenuated very strongly w/ ga-mask.
      return
      end
**********************************************************************
      SUBROUTINE dfour1(data,nn,isign)
      INTEGER isign,nn
      DOUBLE PRECISION data(2*nn)
      INTEGER i,istep,j,m,mmax,n
      DOUBLE PRECISION tempi,tempr
      DOUBLE PRECISION theta,wi,wpi,wpr,wr,wtemp
      n=2*nn
      j=1
      do 11 i=1,n,2
        if(j.gt.i)then
          tempr=data(j)
          tempi=data(j+1)
          data(j)=data(i)
          data(j+1)=data(i+1)
          data(i)=tempr
          data(i+1)=tempi
        endif
        m=n/2
1       if ((m.ge.2).and.(j.gt.m)) then
          j=j-m
```

```
          m=m/2
        goto 1
        endif
        j=j+m
11    continue
      mmax=2
2     if (n.gt.mmax) then
        istep=2*mmax
        theta=6.28318530717959d0/(isign*mmax)
        wpr=-2.d0*sin(0.5d0*theta)**2
        wpi=sin(theta)
        wr=1.d0
        wi=0.d0
        do 13 m=1,mmax,2
          do 12 i=m,n,istep
            j=i+mmax
            tempr=wr*data(j)-wi*data(j+1)
            tempi=wr*data(j+1)+wi*data(j)
            data(j)=data(i)-tempr
            data(j+1)=data(i+1)-tempi
            data(i)=data(i)+tempr
            data(i+1)=data(i+1)+tempi
12        continue
          wtemp=wr
          wr=wr*wpr-wi*wpi+wr
          wi=wi*wpr+wtemp*wpi+wi
13      continue
        mmax=istep
      goto 2
      endif
      return
      END
```

A.2 MATLAB Routines for Data Visualization and Analysis

The sample codes presented below are representative of the MATLAB routines used for graphical analysis of the output of the main simulator code. The file "ld.m" is a routine for the simple but time-consuming task of loading the raw data into memory. The routine "plt.m" is used for analyzing the data and for producing plots of the temporal intensity profile, the temporal phase profile and the spectrum of the optical field at a previously-recorded position along the optical medium.

The "page" parameter specifies the position. Since it is generally desirable to run "plt.m" for different values for "page", the time is saved by loading the data using "ld.m" only once.

A.2.1 "LD.M": Routine for Loading the Data to Memory

```
global loadeddata
% This MATLAB routine loads the data to memory.
format compact
number = input('Enter data file number: ','s')
     isstr(number)
name = strcat('data',number);
loadeddata = load(name);
```

A.2.2 "PLT.M": Analysis and Visualization Routine

```
function[]= plt(page)
% This MATLAB routine calculates the basic pulse parameters and
% plots the temporal intensity and phase profiles and the spectrum.
global loadeddata
global tres
% Set the global paraters
tres    = 4096;    % Number of time bins to store data
maxpage = 72;      % Number of pages that store data
To      = 4.0;     % Number time bins corresponding to Tr
Tr      = 100;     % Basic temporal unit, in units of femtoseconds
conv    = 1.665;   % Conversion factor for Gaussian/Sech(t) pulse shapes
power   = 10000.0; % Power scaling, in units of watts.
lambda_c= 1032.0;  % Center wavelength of the spectrum.
% Convert data to E-field info:
E = zeros(tres,1);
for t = 1:tres;
    E(t,1) = loadeddata((t-1)*maxpage+page,2) + i*loadeddata((t-1)*maxpage+page,3);
end
E = shiftbyn(E',tres/2)';
t=1:tres;
% Set the axes:
% Set the time axis:
treal = (t-tres/2)*Tr/To/conv;
% scaling info: t-factor is
% delta_t = 85fs(real pulse width)/To(pulse width in sim)/1.665(Gauss)
% Set the frequency axis:
fr = 300000/lambda_c+(t-tres/2)*1000*(To*conv/Tr)/(tres*1.0);
% scaling info: delta_f is 1000/(delta_t)/tres
% Set the wavelength axis:
for x = 1:tres;
lambda(x) = 1000*300.0./fr(x);
```

```
end
Inten = abs(E).*abs(E)*power;
Phase = angle(E);
Spect=spectrum(E');
Inten = shiftbyn(Inten',tres/2)';
% Pulse parameters are calculated below:
Imax = 0.0;
for x = 1:tres;
if Inten(x) > Imax
Imax = Inten(x);
end
end
Ppeak = Imax*power
for x = 1:tres-1;
if (Inten(x) < Imax/2.0) & (Inten(x+1) >= Imax/2.0)
leftside = x;
end
if (Inten(x) > Imax/2.0) & (Inten(x+1) <= Imax/2.0)
rightside = x;
end
end
deltaT = (rightside - leftside)*Tr/To/conv/1000.0
Imax = 0.0;
for x = 1:tres;
if Spect(x) > Imax
Imax = Spect(x);
end
end
for x = 1:tres-1;
if (Spect(x) < Imax/2.0) & (Spect(x+1) >= Imax/2.0)
leftside = fr(x);
end
if (Spect(x) > Imax/2.0) & (Spect(x+1) <= Imax/2.0)
rightside = fr(x);
end
end
deltaFrequency = (rightside - leftside);
deltaLambda = deltaFrequency*lambda_c*lambda_c/300/1000
Energy = sum(Inten)*power*Tr/To/conv/1000.0
% Set below to if 1 to export the data to text files:
if 0
fid = fopen('inten.txt','w');
for x=1:tres;
fprintf(fid,'%5.4f %2.12f\n',treal(x),Inten(x));
end
fclose(fid);
fid = fopen('spec.txt','w');
for x=1:tres;
fprintf(fid,'%5.4f %2.12f\n',fr(x),Spect(x));
end
fclose(fid);
fid = fopen('phase.txt','w');
```

```
for x=1:tres;
fprintf(fid,'%5.4f %2.12f\n',treal(x),Phase(x));
end
fclose(fid);
end
% Calculate intensity autocorrelation
%
%signal_auto = convn(Inten.*Inten,Inten.*Inten);
%automax = max(signal_auto);
%signal_auto = signal_auto./automax;
%
%Inten = shiftbyn(Inten',3031);
%
%signal_iAC = iAC(Inten',1);
subplot(1,3,1)
plot(treal,Inten(:)), axis tight, grid on
title('Intensity Profile')
ylabel('Intensity (A. U.)')
xlabel('Time Delay (fs)')
subplot(1,3,2)
plot(treal,Phase(:)), grid on, axis tight
title('Phase Profile')
ylabel('Phase (rad)')
xlabel('Time Delay (fs)')
subplot(1,3,3)
plot(lambda,Spect(:)), grid on, axis tight
title('Spectrum')
ylabel('Intensity (A. U.)')
xlabel('Wavelength (nm)')
```

A.2.3 "AUTOCORR.M": Auto-correlation Routine

```
function [] = autocorrelation()
% This MATLAB routine calculates the time domain intensity profile,
% and the interferometric autocorrelation traces from a
% given spectrum.
% Number of time bins.
tres = 4096;
% Load the data
load fielddata.dat
field(:,1) = fielddata(:,2);
time(:,1)  = fielddata(:,1);
field=field';
% Calculate interferometric autocorrelation
signal_iAC = iAC(field,1);
subplot(2,1,1)
plot(time,field.^2), grid on, axis tight
subplot(2,1,2)
plot(time,signal_iAC), grid on, axis tight
% Export the data to a file in ASCII format.
fid = fopen('iAC.txt','w');
```

```
for x=1:tres;
fprintf(fid,'%5.4f %2.6f %2.6f\n',time(x),signal_iAC(1,x),signal_iAC(2,x));
end
fclose(fid);
```

A.2.4 "IAC.M": Routine for Correlation Calculation

```
function signal=iAC(field,k)
% This MATLAB routine calculates the interferometric autocorrelation of
% the input field
[d,n]=size(field);
halfn=floor(n/2);
acup=field*0;
aclo=field*0;
for j=1:(halfn)
  shifted=k*shiftbyn(field,j);
  fielddiff=field-shifted;
  fieldsum=field+shifted;
  acup(halfn+j)=sum(fieldsum.^4);
  aclo(halfn+j)=sum(fielddiff.^4);
  shifted=k*shiftbyn(field,-j);
  fielddiff=field-shifted;
  fieldsum=field+shifted;
  acup(halfn-j+1)=sum(fieldsum.^4);
  aclo(halfn-j+1)=sum(fielddiff.^4);
end
%acup(halfn)=sum((1+k)^4*field.^4);
%aclo(halfn)=sum((1-k)^4*field.^4);;
aclo=aclo/abs(acup(halfn))*8;
acup=acup/abs(acup(halfn))*8;
base = aclo(1);
%acup = acup - base;
%aclo = aclo - base;
signal=[acup-base; aclo-base];
```

Appendix B

A Practical Guide to Femtosecond Fiber Oscillators

In this section, the leading design criteria are summarized and the construction of a fiber oscillator is discussed. We estimate that around 20 oscillators and 10 amplifiers have been built during this thesis work, which have had several hundred versions in total. It is neither possible, nor necessary to recall the different designs and issues related to this body of experimental background. Many of the crucial aspects are common to all of these systems as will be discussed here. A Yb-doped fiber oscillator similar to the one described in Ref. [1] will serve as the model.

B.1 Building the Cavity

The construction of the cavity consists of two steps, formation of the fiber section and the bulk optics section. The schematics of the oscillator that is adopted as a model for the section is presented in Fig. B.1.

We begin with the fiber section. The important parameters are the total length of the fiber section and the length of the Yb fiber. Light is taken out of and coupled back into the fiber with the use of fiber collimators (collimator info goes here). Following the direction of pulse propagation, the fiber collimator at the end of the free-space propagation section is followed by a segment of SMF which connects to the 980/1030 nm WDM coupler (Lightel, put further info here). The pump lead of the WDM coupler is connected to the pump laser diode. The incoming pulse and the 980 nm pump light is combined at the WDM coupler which connects to the Yb

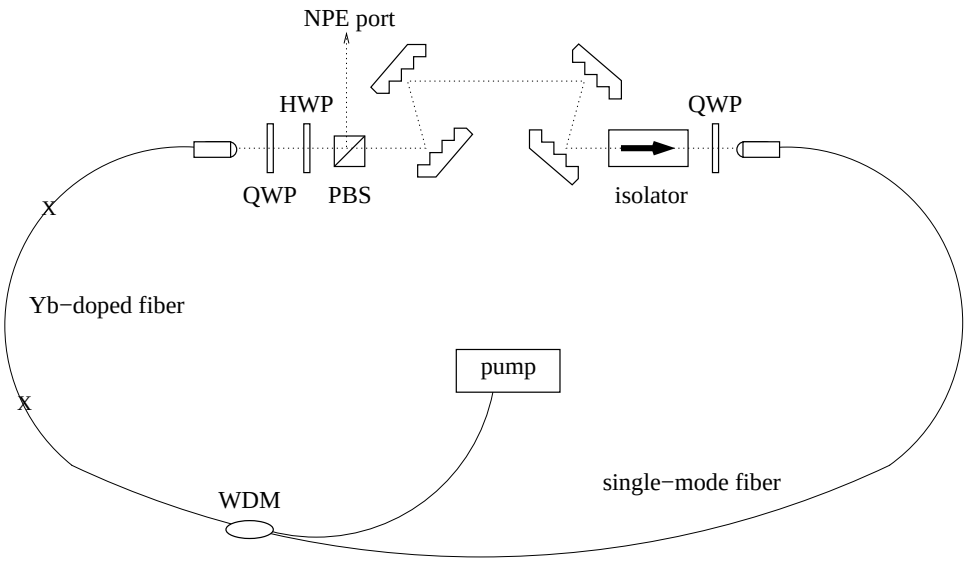

Figure B.1: Experimental setup. HWP: half-wave plate, QWP: quarter-wave plate, PBS: polarizing beam splitter.

fiber. The individual lengths of the collimator, WDM coupler fibers are relatively unimportant, as long as the total length is well-known and matches the desired value. Since all of the fiber-to-fiber connections are between standard SMF, very low splice losses are to be expected (0.01-0.03 dB). The length of the Yb fiber is more important due to its high doping level and should be within 20-24 cm for maximum efficiency. Following amplification in the Yb fiber, the pulses attain their maximum energy. Therefore, length of the lead fiber of the exit collimator should be absolutely minimized. Splicing of this particular Yb fiber to SMF is not easy and splice losses up to 0.12 dB should be expected.

The layout of the bulk optical components section is quite simple. A bird's eye view of an oscillator in our laboratory is presented in Fig. B.2. A quarter-waveplate converts the elliptical polarization out of the fiber to approximately linear polarization. A half-waveplate controls the alignment of the polarization

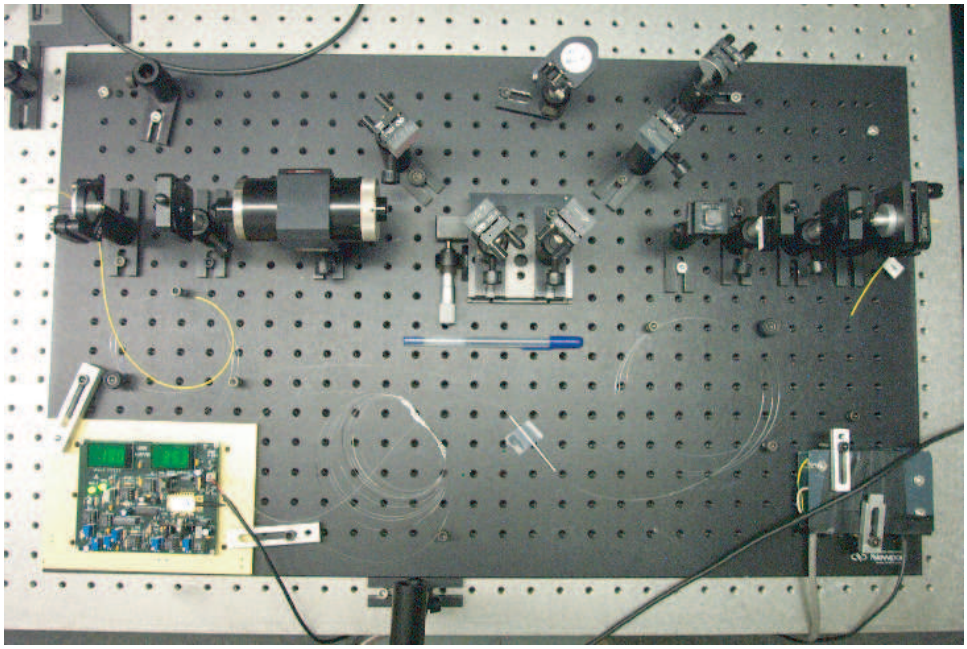

Figure B.2: Picture of the experimental setup.

axis with respect to the polarizing beamsplitter cube. The polarizing cube converts the nonlinear polarization rotation to amplitude modulation. The portion of the pulse diverted out of the cavity by the polarizing cube serves as the output port. An isolator is placed after the cube to ensure unidirectional operation. The grating section can be implemented using two pairs of gratings as in Fig. B.2 or using one folded pair to minimize the number of components and the space required. Finally, a quarter-waveplate placed before the fiber section converts the linear polarization to elliptical polarization. The alignment of the bulk optical components are quite easy, but some care is necessary in setting up the grating section to ensure that no spatial chirp is imparted on the beam.

B.2 Mode-locking the Oscillator

Once the construction of the cavity is completed and good cw operation is obtained, one can proceed to mode-locking the laser. As a first step the maximum cw power extracted from the polarizing cube should be determined by adjusting the waveplates. To initiate mode-locking, it is most useful to monitor the spectrum as the wave-plates are adjusted. Unfortunately, there is not reliable method to guide the search for the right combination of the wave-plate orientations. Typically, there are three wave-plates, hence they form a three dimensional phase space which is too large to search exhaustively. Due to this fact, in practice this search is almost completely random. A few indicators can be useful, though. If the cw-component(s) are virtually fixed at certain wavelength(s) as the waveplates are rotated in a particular area of the phase space, that is not a good indication. This empirical observation can be rationalized by arguing that mode-locked operation corresponds to the instability of cw-operation. A jumpy cw-spectrum can be argued to be an indication of of the onset of instability for cw operation.

B.3 A Summary of Design Considerations

The following guide may be helpful for the design of a fiber oscillator. A Yb fiber oscillator similar to those described in this thesis is assumed, however, most of the criteria should be generally applicable to fiber lasers.

- Unidirectional operation (ring cavity) is highly advisable due to ease of mode-locking [2].

- For given pump power, length of the fiber section cannot be chosen arbitrarily. If the fiber is too short, self-starting operation becomes unattainable.

This is due to two reasons: A shorter fiber section means reduced length of the nonlinear medium and a higher repetition rate which translates to lower energy storage in the cavity. In practice, mode-locking operation at repetition rates above 80 MHz is difficult to self-initiate.

- Similarly, if the fiber is too long, other problems emerge. Most notably, since the nonlinear medium is longer, and more energy is stored in the cavity, multiple-pulsing is likely to plague mode-locked operation. However, the simple scaling argument of maintaining the integral of pulse energy over the fiber length breaks down for very long cavities. In other words, arbitrarily low repetition rate operation of a fiber oscillator is not possible. Reliable, single-pulsed mode-locking becomes progressively more difficult for repetition rates below 20 MHz and it was not possible below 10 MHz in our studies. While the exact reason for this limit is under investigation, our working hypothesis is that residual birefringence of the fiber is interfering with the nonlinear polarization evolution which acts as the saturable absorber.

- As mentioned above, the residual birefringence of the fiber adversely effects mode-locked operation. To minimize birefringence, twists and turns should be avoided while laying down the fiber.

- For shortest pulse generation, net dispersion should be set to a small, negative value, $\beta_{net} = 0$ to -0.015 ps^2. The exact value for minimum pulse duration depends the details of the oscillator design. The shortest pulse duration obtained during this thesis study was 37 fs [3].

- Conditions for generation of the cleanest pulses also correspond to operation at small, net anomalous GVD, but in addition, it is advisable to minimize

the fiber length between the gain fiber and the extraction port.

- If desired, output coupling with a standard fiber-coupler is possible as has been demonstrated in the laser described in Chapter 3 and in Ref. [4]. This way, high-quality pulses can be obtained in fiber with the main drawback being reduced pulse energy. Output coupling ratios in excess of 10% run the risk of destabilizing mode-locked operation, although we have had success with up to 30% [5]. This method of output coupling is particularly suited to seeding a fiber amplifier.

- For the generation of highest pulse energies, it is advisable to operate with small, normal β_{net}, with an optimum value of $\beta_{net} \sim 0.005$ ps^2. As argued previously, ideally larger normal GVD should be better, however this is not possible at the present time. We attribute this to the limitations of artificial saturable absorber. If available, a slow semiconductor saturable absorber should be able to greatly reduce this limitation [1].

BIBLIOGRAPHY

[1] F. Ö. Ilday, J. R. Buckley, H. Lim, and F. W. Wise, Opt. Lett. **28**, 1365 (2003).

[2] K. Tamura, J Jacobson, E.P. Ippen, H.A. Haus, and J.G. Fujimoto, Opt. Lett. **18**, 220 (1993).

[3] F. Ö. Ilday, and F. W. Wise, in preparation.

[4] F. Ö. Ilday, H. Lim, J. R. Buckley, and F. W. Wise, Opt. Lett. **28**, 1362 (2003).

[5] F. Ö. Ilday, F. W. Wise, and T. Sosnowski, Opt. Lett. **27**, 1531 (2002).